STUDY OF THE HORIZONTAL-TO-VERTICAL SPECTRAL RATIO (HVSR) METHOD FOR CHARACTERIZATION OF DEEP SOILS IN THE MISSISSIPPI EMBAYMENT

A Thesis presented to the Faculty of the Graduate School
University of Missouri-Columbia

In Partial Fulfillment
of the Requirements for the Degree

Master of Science

---

by
RYAN P. GOETZ

Dr. Brent L. Rosenblad, Thesis Supervisor

DECEMBER 2009

The undersigned, appointed by the dean of the Graduate School, have examined the thesis entitled

STUDY OF THE HORIZONTAL-TO-VERTICAL SPECTRAL RATIO (HVSR) METHOD FOR CHARACTERIZATION OF DEEP SOILS IN THE MISSISSIPPI EMBAYMENT

Presented by Ryan P. Goetz,

A candidate for the degree of Masters of Science in Civil Engineering,

And hereby certify that, in their opinion, it is worthy of acceptance.

Professor Brent L. Rosenblad

Professor J. Erik Loehr, P.E.

Professor Francisco "Paco" Gomez

ACKNOWLEDGEMENTS

The first person I want to thank for my educational experience is Dr. Brent Rosenblad for being my advisor. He has been a great mentor and resource for teaching me the skills and thinking process to become a researcher. Dr. Rosenblad first sparked my interest in geotechnical engineering while I was an undergrad. His patience and guidance has enabled me to have success during my Master's program. The pursuit of perfection he expected will greatly benefit me as I enter the professional world.

I must thank the entire faculty and staff members in the department who have helped me over the years. Dr. Bowders' enthusiasm for geotechnical engineering and interest he takes in his students makes him "one of a kind". I thank Dr. Loehr for passing along his in-depth knowledge and experience of geotechnical engineering to me. Dr. Likos for teaching me to think on a micro-scale. All three professors were always willing to go above and beyond to lend guidance, as well as provide contacts or letters of recommendation.

I greatly appreciate Dr. Gomez for taking the time to participate on my thesis committee and give me his valuable input.

Dr. Van Arsdale at the University of Memphis, along with his graduate students, should also be thanked for information provided. The assistance from Dr. Lorraine Wolf at Auburn University and Dr. Paul Bodin at the University of Washington was much appreciated.

I also would like to thank all of my colleagues who have been there for me over the years. Jon Bailey's and Jianhua Li's assistance in the field made this study possible. Dr. Rick Coffman was always willing to take the time to answer technical or computer questions. Nathan Rose, Wyatt Jenkins, and Nabil Hasan provided valuable support either in the classroom or field. They have been good friends and always willing to help.

I would like to thank my parents, Larry and Vickie Goetz, and the rest of my family who have lent undying love and support to me for my life and school career. They have always been supportive and my biggest fans through everything. I am forever indebted to them for all they have done for me and for making me who I am. Finally, I would like to thank Michelle McCormick for her unbelievable understanding, support, and assistance. I sincerely appreciate each source of support.

TABLE OF CONTENTS

ACKNOWLEDGEMENTS ii

LIST OF FIGURES viii

LIST OF TABLES xiv

ABSTRACT xvii

1. INTRODUCTION 1

1.1 Overview 1

1.2 Problem Statement 3

1.3 Organization of Thesis 4

2. BACKGROUND AND REVIEW OF PREVIOUS STUDIES 6

2.1 Introduction 6

2.2 Influence of Local Soil Conditions on Earthquake Site Response 6

2.3 Overview of HVSR Method 8

2.3.1 Ambient Waves 9

2.3.2 Body and Surface Wave Interpretation 10

2.4 Past Studies 12

2.4.1 Worldwide Studies 12

2.4.2 Previous Shear Wave Velocity Studies in the Mississippi Embayment 16

2.5 Summary 23

3. MEASUREMENT LOCATIONS 25

3.1 Overview 25

3.2 Geology of the Upper Mississippi Embayment 26

3.3 Measurement Sites 31

3.3.1 Site Characteristics 31

3.4 Data Collection 47

3.5 Summary 49

4. METHODS 51

4.1 Introduction 51

4.2 Analytical Study of Simulated Velocity Profiles 51

4.2.1 Computer Programs 52

4.2.2 Simulated Shear Wave Profiles 56

4.2.3 Data Generation and Analysis 58

4.2.4 Average Velocity Calculation 61

4.3 Study of HVSR Processing Parameters 62

4.3.1 Processing of HVSR Data 62

4.4 Comparison of Experimental to Simulated Results for Sites in the Mississippi Embayment 68

4.4.1 Development of Site V_S Profiles for Simulation Studies 68

4.4.2 Examination of Fundamental Frequency Estimated from HVSR Frequency Peak 72

4.4.3 Average Velocity Comparison using HVSR Frequency Peaks 72

4.4.4 Examination of Second Frequency Peak in Experimental HVSR Data 73

4.5 Summary 73

5. RESULTS AND ANALYSIS 75

5.1 Introduction 75

5.2 Study of Variables Affecting HVSR Measurements 75

5.2.1 Effect of V_S Contrast 76

5.2.2 Poisson's Ratio 79

5.2.3 Summary of Findings from Simulation Study 80

5.3 Study of the Influence of Processing Parameters on HVSR Results 81

5.3.1 Window Length 82

5.3.2 Transients 83

5.3.3 Merging 86

5.3.4 Smoothing 87

5.3.5 Bandwidth of Smoothing Function 88

5.3.6 Tapering 89

5.3.7 Filter 90

5.3.8 Discussion of Results from the Influence of Processing Parameters 92

5.4 Comparison of Experimental and Simulated Results for Mississippi Embayment Sites 93

5.4.1 Introduction 93

5.4.2 Experimental HVSR Results 93

5.4.3 Simulated HVSR Results for Full Depth of the Profile 95

5.4.4 Simulated HVSR Results for Shallow Profiles 103

5.4.5 Discussion of Results from Comparison of Experimental and Simulated Data 107

5.5 Summary 110

6. CONCLUSION 111

6.1 Summary 111

6.2 Conclusions 112

6.3 Recommendations 114

A APPENDIX 116

B APPENDIX 122

C APPENDIX 126

D APPENDIX 127

REFERENCES 128

LIST OF FIGURES

Figure Page

Figure 2.1 Different methods for determining site frequency using ambient vibrations (Ibs-von eht and Wohlenberg 1999) 10

Figure 2.2 Two interpretations of the HVSR method in terms of (a) body waves and (b) surface waves showing (c) the transfer function for 1D, SH wave propagation and (d) the HVSR ratio for Rayleigh wave propagation. 12

Figure 2.3 Two-dimensional (2D) and 3D structures that were investigated in Guillier et al. (2006) (Guillier et al. 2006). 16

Figure 2.4 Reference V_S profile for the deep soils of the Mississippi embayment (Romero and Rix 2005). 18

Figure 2.5 Schematic showing the site response and transfer function for a single uniform layer over bedrock (Ibs-von Seht and Wohlenberg 1999). 20

Figure 2.6 Average shear wave velocity as a function of sediment thickness. Filled circles and shaded triangles represent data derived from Bodin et al. (2001) and Chen et al. (1996), respectively (Bodin et al. 2001). 21

Figure 2.7 Fundamental periods as a function of sediment thickness. T_0 is indicating the period of the first frequency peak while T_1 is indicating the period of the second frequency peak obtained from the HVSR method (Bodin et al. 2001). 23

Figure 3.1 Site locations of HVSR measurements in the Mississippi embayment. The lowland Holocene-age deposits and the upland Pleistocene-age deposits are represented by dark and light gray fill, respectively (Bailey 2008). 25

Figure 3.2 Elevation of Paleozoic basement relative to mean sea level in the upper Mississippi embayment (Romero and Rix 2005). 28

Figure 3.3 Idealized cross-section of Mississippi embayment profile near Memphis, Tennessee (Hashash and Park 2001). 28

Figure 3.4 Geologic column for the New Madrid seismic zone (Van Arsdale and TenBrink 2000). 29

Figure 3.5 Epicenters of earthquakes around the upper Mississippi embayment from 1974 to present. Locations and magnitudes taken from the Cooperative New Madrid Seismic Network catalog (Powell and Withers 2009). 30

Figure 3.6 Map of Site 1 (MORT) showing surrounding roadways (a) and a photograph of the placement of the three-component geophone at Site 1 (b). 33

Figure 3.7 Map of Site 2 (YARBRO) showing surrounding roadways (a) and a photograph of the placement of the three-component geophone at Site 2 (b). 34

Figure 3.8 Map of Site 3 (GNAR) showing surrounding roadways (a) and a photograph of the placement of the three-component geophone at Site 3 (b). 35

Figure 3.9 Map of Site 4 (Lepanto) showing surrounding roadways (a) and a photograph of the placement of the three-component geophone at Site 4 (b). 36

Figure 3.10 Map of Site 5 (Shelby Farms) showing surrounding roadways (a) and a photograph showing ground conditions at Site 5 (b). 37

Figure 3.11 Map of Site 6 (TNMT) showing surrounding roadways (a) and a photograph showing an overview of Site 6 (b). 38

Figure 3.12 Map of Site 7 (GLAT) showing surrounding roadways (a) and a photograph showing an overview of Site 7 (b). 39

Figure 3.13 Map of Site 8 (BRGM) showing surrounding roadways (a) and a photograph showing an overview of Site 8 (b). 40

Figure 3.14 Map of Site 9 (PENM) showing surrounding roadways (a) and a photograph showing an overview of Site 9 (b). 41

Figure 3.15 Map of Site 10 (EPRM) showing surrounding roadways (a) and a photograph showing an overview of Site 10 (b). 42

Figure 3.16 Map of Site 11 (MSAR) showing surrounding roadways (a) and a photograph showing an overview of Site 11 (b). 43

Figure 3.17 Shear wave velocity profiles derived from surface wave measurements (Bailey 2008), with corresponding soil lithology provided by Professor Van Arsdale at the University of Memphis, for Sites 1-5, (a) – (e) respectively..... 44

Figure 3.18 Shear wave velocity profiles derived from surface wave measurements (Bailey 2008), with corresponding soil lithology provided by Professor Van Arsdale at the University of Memphis, for Sites 6-11, (a) – (f) respectively. Legend for the eleven sites is shown in previous figure..... 45

Figure 3.19 Estimated soil lithology down to bedrock for Sites 1-11, (a) – (k) respectively, provided by Professor Van Arsdale at the University of Memphis..... 46

Figure 3.20 Preparing for the placement of the three-component geophone at Site 4..... 47

Figure 3.21 Data Physics Dynamic Signal Analyzer connected to the field laptop. 48

Figure 3.22 Monitoring the data collection from a vehicle for Sites 1-5 (a) and instrumented trailer used in data collection at Sites 6-11 (b)..... 48

Figure 3.23 Ambient noise recorded on vertical and two horizontal geophones at Site 9. 49

Figure 4.1 Shear wave velocity profile of a homogeneous layer over a halfspace of 2000 m/s (a) and resulting transfer function from SH waves (b). A HVSR curve from surface waves (c)..... 54

Figure 4.2 Shear wave velocity profile for Case 1 through 7, (a) through (g), respectively. $V_{S,AVG}$ for all profiles is 500 m/s..... 58

Figure 4.3 The different halfspace V_S values that were used in the V_S ratio study for Case 1..... 59

Figure 4.4 Values of V_P (dashed lines) used with the corresponding constant V_S value (solid line) for Case 1 to study the influence of Poisson's ratio. 61

Figure 4.5 The V_S profile of Site 1 measured from surface waves (Bailey 2008) (a) is combined with a reference profile (b) (Romero and Rix 2005) to produce an estimated site V_S profile from the ground surface to bedrock (c). 69

Figure 4.6 Estimated shear wave velocity profiles extended to bedrock for: Sites 1 through 11, (a) through (k) respectively. 70

Figure 4.7 Plot showing the comparison between the $V_{S,AVG}$ calculated from estimated full-depth V_S profiles to relationship for $V_{S,AVG}$ in the Mississippi embayment developed by Chen et al. (1996). 71

Figure 5.1 Peak frequencies for saturated conditions of Cases 1 through 7, (a) through (g), respectively. 77

Figure 5.2 Normalized velocities for Cases 1 through 7, (a) through (g), respectively.... 79

Figure 5.3 Changes in normalized velocity (calculated using f_{HVSR}) with changes in Poisson's ratio for all cases 1-7. 80

Figure 5.4 The four different values of window length: 50, 75, 100, and 200 seconds, (a) through (d), respectively, applied to Site 1. The windows used in the analysis are shaded in the figure. 82

Figure 5.5 The effect of changing the maximum STA/LTA ratio of 1.25, 1.5, 2, and 2.5, (a) through (d) respectively, on the time records for Site 2. The windows are shaded in the figure. 84

Figure 5.6 HVSR plots for Site 2 of the four maximum STA/LTA ratios of 1.25, 1.5, 2.0, and 2.5, (a) through (d). respectively 84

Figure 5.7 HVSR curves with fundamental frequencies peaks indentified for Sites 1 through 11 or (a) through (k), respectively. 94

Figure 5.8 Comparison of peak periods from experimental results from this study and relationship developed by Bodin et al. (2001) in the Mississippi embayment. 95

Figure 5.9 Calculated transfer function of SH waves (solid line) and HVSR plot from surface waves (broken line) for Site 1 using estimated V_S profile to bedrock. 96

Figure 5.10 Plot relating the experimentally measured first peak frequency to the simulated first peak frequency for each of the eleven sites. 97

Figure 5.11 Plot relating the experimentally measured second peak frequency to the simulated second peak frequency for each of the eleven sites. 98

Figure 5.12 Experimental V_S developed from the HVSR data. Also shown are V_S-sediment thickness relationships from Bodin et al. (2001) and Chen et al. (1996). .. 100

Figure 5.13 Shear wave velocities for "true" and estimated results as a function of sediment thickness for the eleven sites. Also shown are V_S-sediment thickness relationships from Bodin et al. (2001) and Chen et al. (1996). 101

Figure 5.14 The simulated and experimental V_S compared to the "true" V_S for the eleven sites (a) and the corresponding percent error (b). 103

Figure 5.15 Calculated transfer function of SH waves (solid line) and HVSR plot from surface waves (broken line) for Site 1 using shallow V_S profiles. 104

Figure 5.16 Comparison of simulated shallow profiles to measured frequency values for the eleven sites. 105

Figure 5.17 Period of experimental and SH simulated waves compared to depth of interfaces for the sand, gravel, Upper Claiborne, and Memphis Sand interfaces, (a)-(d) respectively. 106

Figure A.1 Image of Site 1 (MORT). 116

Figure A.2 Image of Site 2 (YARBRO). 117

Figure A.3 Image of Site 3 (GNAR). 117

Figure A.4 Image of Site 4 (LEPANTO). 118

Figure A.5 Image of Site 5 (SHELBY FARMS). 118

Figure A.6 Image of Site 6 (TNMT). 119

Figure A.7 Image of Site 7 (GLAT). 119

Figure A.8 Image of Site 8 (BRGM). 120

Figure A.9 Image of Site 9 (PENM). 120

Figure A.10 Image of Site 10 (EPRM). 121

Figure A.11 Image of Site 11 (MSAR). 121

Figure B.1 Time record from the single-station three-component sensor at Site 1. 122

Figure B.2 Time record from the single-station three-component sensor at Site 2. 122

Figure B.3 Time record from the single-station three-component sensor at Site 3. 122

Figure B.4 Time record from the single-station three-component sensor at Site 4. 123

Figure B.5 Time record from the single-station three-component sensor at Site 5. 123

Figure B.6 Time record from the single-station three-component sensor at Site 6. 123

Figure B.7 Time record from the single-station three-component sensor at Site 7. 124

Figure B.8 Time record from the single-station three-component sensor at Site 8. 124

Figure B.9 Time record from the single-station three-component sensor at Site 9. 124

Figure B.10 Time record from the single-station three-component sensor at Site 10. ... 125

Figure B.11 Time record from the single-station three-component sensor at Site 11. ... 125

Figure C.1 Three component spectrum for Sites 1-11 corresponding to (a)-(k), respectively. Vertical spectrum is represented by the thicker of the lines and HVSR frequency peaks are shown as dashed vertical lines…….. 126

LIST OF TABLES

Table Page

Table 2.1 Models developed for the Mississippi embayment and used to developed reference V_S profile (Romero and Rix 2005). 17

Table 3.1 Site coordinates and depth to bedrock at eleven measurement sites (* denotes CERI Station). 32

Table 3.2 The recording length used for experimental data collection at the eleven sites. 48

Table 4.1 Seven simulated V_S profile cases used in the analytical study. 57

Table 4.2 Halfspace V_S values that were used for each of the seven cases. 59

Table 4.3 Poisson's ratio values that were applied to all seven cases. 61

Table 4.4 Values of processing parameters used in this portion of the study. 63

Table 4.5 Default values of processing parameters. 63

Table 4.6 Recommended processing parameters and recording duration (SESAME 2004). 65

Table 4.7 Average shear wave velocities calculated from estimated V_S profiles using Eq. 4.9 for the eleven sites. 71

Table 4.8 Typical values used in DEEPSOIL and Mat-Disperse……..73

Table 5.1 First and second frequency peaks identified for different window lengths tested. ($^+$ indicates data were processed with less than the minimum recommended number of windows and "–" indicates that either no frequency peak could be identified or no windows could be developed using the window length parameter) 83

Table 5.2 First and second frequency peaks for different values of maximum threshold tested while holding minimum threshold at 0.5. (+ indicates data were processed with less than the minimum recommended number of windows and "–" indicates that either no frequency peak could be identified or no windows could be developed using this value of parameter) 85

Table 5.3 First and second frequency peaks for different values of minimum threshold tested while holding maximum threshold at 1.5. (+ indicates data were processed with less than the minimum recommended number of windows and "–" indicates that either no frequency peak could be identified or no windows could be developed using this value of parameter) 86

Table 5.4 First and second frequency peaks for different merging parameters tested. ("–" indicates that no frequency peak could be identified using this value of parameter) .. 87

Table 5.5 First and second frequency peaks for different smoothing parameters tested. ("–" indicates that no frequency peak could be identified using this value of parameter) 88

Table 5.6 First and second frequency peaks for different bandwidth parameters tested. ("–" indicates that no frequency peak could be identified using this value of parameter) 89

Table 5.7 First and second frequency peaks for different tapering parameters tested. ("–" indicates that no frequency peak could be identified using this value of parameter) .. 90

Table 5.8 First and second frequency peaks for different high pass filter parameters tested. (+ indicates data were processed with less than the minimum recommended number of windows and "–" indicates that no frequency peak could be identified using this value of parameter)..... 91

Table 5.9 First and second frequency peaks for different low pass filter parameters tested. (+ indicates data were processed with less than the minimum recommended number of windows and "–" indicates that no frequency peak could be identified using this value of parameter) 92

Table 5.10 Comparison of simulated to measured frequency values and corresponding percent errors for Sites 1 to 11. (^ indicates that no HVSR peak could be determined) 96

Table 5.11 Comparison of simulated to measured second frequency peak values and corresponding percent errors. ("–" indicates that no frequency peak could be identified) 98

Table 5.12 Shear wave velocities developed from surface wave V_S profiles with corresponding percent errors for the eleven sites. (^ indicates that no HVSR frequency peak could be determined) 102

Table 5.13 Shallow profile comparison of simulated to measured frequency peak results and corresponding percent errors. ("–" indicates that no frequency peak could be identified) 104

Table D.1 Table displaying the number of windows for each parameter that was used in the experimental processing of data. (Blocks having less than the minimum number of recommended windows are highlighted.) 127

STUDY OF THE HORIZONTAL-TO-VERTICAL SPECTRAL RATIO (HVSR) METHOD FOR CHARACTERIZATION OF DEEP SOILS IN THE MISSISSIPPI EMBAYMENT

Ryan P. Goetz

Dr. Brent L. Rosenblad, Thesis Supervisor

ABSTRACT

Soil deposits can significantly influence the amplitude and frequency content of surface ground motions during earthquakes. Estimating the fundamental frequency (f_0) of a site is often needed for improved planning and design for future earthquakes. A cost-effective method of obtaining an estimate of f_0 is the Horizontal-to-Vertical Spectral Ratio (HVSR) method (also termed Nakamura's method), which utilizes ambient energy recorded in the horizontal and vertical directions from a single, three-component sensor. In addition to estimating the fundamental frequency, average shear wave velocity ($V_{S,AVG}$) values have been estimated using the HVSR method and a simple approximate relationship relating $V_{S,AVG}$ to f_0 and the depth to bedrock. This procedure was performed by Bodin et al. (2001) to develop a relationship between $V_{S,AVG}$ and soil depths in the Mississippi embayment. However, this relationship predicts average velocity values that are about 25% higher than values predicted by another relationship developed using a different method (Chen et al. 1996). Although this inconsistency is known, the relationship of Bodin et al. (2001) is often cited as the best information on the velocity structure in the embayment. In addition, Bodin et al. (2001) identified a second

frequency peak of unknown origin in their HVSR plots. The objectives of this study are to answer these unresolved questions, specifically: (1) why the shear wave velocity relationships developed for the Mississippi embayment using the HVSR method are inconsistent with other findings, and (2) the origin of the second frequency peak observed in HVSR plots from the Mississippi embayment. To meet these objectives, the following three studies were performed: (1) a parametric study of site factors influencing the fundamental frequency and average velocity estimates from the HVSR method, (2) an investigation into the influence of the HVSR processing parameters using experimental data collected at eleven deep soil sites in the Mississippi embayment, and (3) comparison of experimental and simulated HVSR results for Mississippi embayment sites. With regard to the first objective, it was found that the HVSR method yielded reliable values of the fundamental site frequency for conditions of high velocity contrast between soil and rock and saturated soil conditions (conditions that are met in the Mississippi embayment). Also, it was shown that varying the HVSR processing parameters had a negligible impact on the HVSR frequency estimates. However, it was demonstrated that use of the approximate method to estimate $V_{S,AVG}$ systematically over-predicted the true $V_{S,AVG}$ values. With regard to the second objective, it was shown that the second frequency peak observed in the experimental HVSR plots can be attributed to either a higher-mode resonance of horizontally-polarized shear waves reflecting from the soil/bedrock boundary or local site resonance due to a shallow contrast in V_S within the soil deposit. Based on the findings of this study it is recommended that the V_S relationship for the

sediments of the Mississippi embayment developed by Chen et al. (1996) should be preferred to the Bodin et al. (2001) relationship.

1. INTRODUCTION

1.1 Overview

Soil deposits can significantly influence the amplitude and frequency content of surface ground motions during earthquakes. Estimating the fundamental frequency (lowest natural frequency) of a site is often needed for improved planning and design for future earthquakes; however, a thorough investigation of site frequencies requires knowledge of the shear wave velocity (V_S) profile, dynamic soil properties, and thickness of soil deposits. The use of borehole methods (such as downhole, cross-hole, and suspension logging tests) to determine V_S profiles may be cost prohibitive for characterizing large areas and deep soil deposits. Surface geophysical methods, such as the surface wave methods or refraction methods, can also be time consuming and expensive to perform and analyze.

A single station method (often termed Nakamura's method or the Horizontal-to-Vertical Spectral Ratio (HVSR) method) which utilizes ambient energy recorded in the horizontal and vertical directions, has found widespread use as a simple and relatively quick technique to estimate the small-strain fundamental frequency of a site. This approach has been used extensively around the world for microzonation studies of major cities (e.g. Bodin et al. 2001; Cara et al. 2007; Chen et al. 2009; Fäh et al. 2001; Guéguen et al. 2000; Kerh and Chu 2002; Konno and Ohmachi 1998; Panou et al. 2005; Souriau et al. 2007; Walling et al. 2009). By mapping the fundamental frequency around a city, it is

possible to infer local soil conditions (i.e. deep soft deposits versus shallow stiff deposits).

In addition to mapping changes in the site frequencies in a region, the HVSR method has been used in recent studies as an alternative tool to traditional geophysical exploration for estimating average shear wave velocity ($V_{S,AVG}$) values (Arai and Tokimatsu 1998; Arai and Tokimatsu 2004; Bodin et al. 2001; García-Jerez et al. 2007; Parolai et al. 2002; Tokeshi et al. 2008). The focus of this study is on the application of the HVSR method for characterizing the properties of the deep sediments in the Mississippi embayment of the central United States.

The Mississippi embayment is a region of deep soil deposits in the central United States that spans from the confluence of the Mississippi and Ohio rivers to the Gulf of Mexico. The upper Mississippi embayment encompasses the states of Missouri, Kentucky, Arkansas, Tennessee and overlies the New Madrid seismic zone (Cramer 2006). Soil depths in the embayment are as great as 1000 meters is some areas; however, V_S values are not well characterized below a depth of about 60 meters (Romero and Rix 2005). The V_S properties over the full depth of the embayment are of interest for seismic hazard studies, identifying earthquake locations, and understanding seismic wave propagation in these deep soils. A previous implementation of the HVSR method in the Mississippi embayment (Bodin et al. 2001) yielded very good experimental data; however, V_S values developed from the data were inconsistent with other studies. In this work, a systematic study of the HVSR method is performed using both synthetic and

experimental data to explain the inconsistent V_S results obtained by applying the HVSR method in the Mississippi embayment.

1.2 Problem Statement

Bodin et al. (2001) utilized the HVSR method to obtain the fundamental frequency for sites in the upper Mississippi embayment and Memphis metro area. Using known depths to bedrock at these sites, Bodin et al. (2001) calculated $V_{S,AVG}$ as a function of sediment thickness using a common method relating the $V_{S,AVG}$ to frequency and sediment thickness. The V_S values obtained by Bodin et al. (2001) were approximately 25% higher than values obtained using a different method (Chen et al. 1996). In addition, Bodin et al. (2001) observed a second frequency peak of unknown origin in the HVSR plots.

These unresolved issues of: (1) the $V_{S,AVG}$ value for the Mississippi embayment soils and (2) the origin of the second HVSR frequency peak are significant to future studies in the Mississippi embayment. Currently, the relationships developed by Bodin et al. (2001) are commonly used to represent the V_S properties of the embayment. For example, Powell and Withers (2009) stated: "information provided in Bodin et al. (2001) is presently our best estimate for the unconsolidated sediment thickness and velocity structure across the embayment." Also, although Bodin et al. (2001) attributed the second frequency peak to higher mode resonance at the sites, it is possible that the second frequency peak may be attributed by other sources.

The objectives of this study are to investigate: (1) why the HVSR method yields a higher estimate of shear wave velocity for the Mississippi embayment and (2) identify the origin of the second frequency peak observed in HVSR plots of the Mississippi embayment. With regard to the first objective, it is hypothesized that the higher velocity is erroneous and due either to a poor estimate of the site resonance from the HVSR method or to the use of the approximate method used to estimate $V_{S,AVG}$. With regard to the second objective, it is hypothesized that shallow impedance contrasts within the sediments may be the source of the second frequency peak.

These objectives will be met by performing three research tasks. The first task is a parametric study of factors influencing the HVSR frequency peak. The second task is to investigate the influence of HVSR processing parameters on the experimental results. Last, using V_S profiles at eleven experimental sites, experimental and simulated results will be compared to identify factors influencing the V_S estimate and the cause of the second frequency peak.

1.3 Organization of Thesis

This thesis is presented in six chapters. Chapter 2 presents background on the HVSR method and a review of previous relevant HVSR applications. The problem statement is also examined in greater depth in this chapter. Chapter 3 discusses the general geology of the upper Mississippi embayment, and characteristics of the eleven measurement sites. The methods used to achieve the research objectives along with the research tasks are described in Chapter 4. Chapter 5 presents the results of the data analyses and a

discussion of the findings. Lastly, Chapter 6 provides conclusions and recommendations for future studies.

2. BACKGROUND AND REVIEW OF PREVIOUS STUDIES

2.1 Introduction

In this chapter, background on the HVSR method and a brief review of previous HVSR applications are presented with emphasis on studies performed in the Mississippi embayment. The theory of the HVSR method is explained along with two interpretations of the origin of the HVSR frequency peaks. Previous work that used the HVSR method to obtain the $V_{S,AVG}$ as a function of depth of the Mississippi embayment sediments is discussed in detail. Inconsistencies between V_S values from the HVSR method and other methods are presented and possible explanations of a second frequency peak in HVSR plots from past Mississippi embayment studies are discussed.

2.2 Influence of Local Soil Conditions on Earthquake Site Response

Earthquake ground motions can be highly site-specific and are influenced by local soil properties (stiffness, thickness, and damping) which affect the amplitude, frequency content, and duration of strong ground motions. The estimation of frequency content is of particular interest since the frequency content of an earthquake motion will strongly influence the effects of the motion on structures. Characterization of the motion cannot be complete without consideration of the local site resonance (Kramer 1996). Knowledge of local site resonance allows for seismic risk mitigation in the design and construction of structures. A rigorous determination of local site response requires knowledge of the shear wave velocity (V_S) profile of the soil and rock, the bedrock depth,

and non-linear soil properties (modulus and damping). Typically a 1-D equivalent-linear analysis program (such as SHAKE or DEEPSOIL) is used to model horizontally polarized shear wave (SH) propagation and to calculate site response.

Over the past decades, V_S has become a key parameter for many analyses in soil dynamics and geotechnical earthquake engineering. For example, V_S measurements are a valuable index to determine susceptibility to liquefaction for shallow soils (Andrus and Stokoe 2000). Also, V_S values are used in the International Building Code (IBC) to determine site classification based on the $V_{S,AVG}$ for the top thirty meters of soil ($V_{S,30}$). In addition, knowledge of V_S properties is important in understanding wave propagation behavior and improving earthquake location identification. In the Mississippi embayment, soil depths as great as 1000 meters in some areas will influence the ground motions in the embayment (Hashash and Park 2001). Currently, the V_S properties in the embayment are fairly well characterized in the top sixty meters, but few studies have been performed to greater depths (Romero and Rix 2005). As described below, studies estimating the $V_{S,AVG}$ over the full depth of the embayment have yielded inconsistent results.

Traditional methods for measuring V_S involve intrusive and non-intrusive approaches. Intrusive borehole methods, such as downhole, crosshole, and suspension logging become cost prohibitive when performed to great depths and over large areas. Borehole methods are not practical to characterize the full-depth properties of the sediments in the Mississippi embayment, with depths to bedrock as great as 1000 meters. Common non-intrusive methods in geotechnical engineering include surface-wave based

methods and the seismic refraction method; however, these methods can be time consuming and difficult to apply quickly over a large area. Over the last decade, another non-intrusive approach, termed the Horizontal-to-Vertical Spectral Ratio method (HVSR or H/V) or Nakamura's method (Nakamura 1989), has become increasingly popular as a means to estimate the fundamental frequency of a site using only single-station measurements of ambient noise. It has been used extensively in microzonation studies, and in some cases to estimate $V_{S,AVG}$ values.

2.3 Overview of HVSR Method

Nogoshi and Igarashi (1971) furthered the study of microtremors (ambient vibrations) based on a previous study by Kanai and Tanaka (1961). Nakamura (1989) created a new method (HVSR) based solely on microtremors to estimate the fundamental frequency of a site. The HVSR method involves collecting ambient vibrations using a single-station, three-component sensor and dividing the horizontal spectrum by the vertical spectrum. This method assumes that, by dividing the horizontal spectrum by the vertical spectrum, source effects are negated. This division leaves only amplified frequency peaks due to site resonance (Lermo and Chavez-Garcia 1994).

The HVSR method has particular advantages over more traditional methods in urban areas where space is limited and large arrays cannot be placed. Also, the HVSR method is more cost effective and efficient than surface wave methods, which use a low-frequency vibrating source with multiple receivers. Further, in comparison with intrusive borehole methods, the HVSR procedure is significantly more cost-effective.

2.3.1 Ambient Waves

The earth vibrates almost constantly at periods ranging from milliseconds to days and amplitudes ranging from nanometers to meters (Kramer 1996). The vast majority of these vibrations are so weak that they cannot be detected without specialized measurement equipment. Ambient vibrations (often termed microtremors) are the summation of all ground motions that are not due to events of short duration, such as earthquakes or explosions (Steinwachs 1974). Ambient vibrations are produced by a variety of natural or man-made sources, such as waves on the coast, winds on trees or buildings, or traffic. Typically, vibrations at frequency ranges above 1 Hz are caused by man-made sources, and lower frequencies are caused by natural forces (Bonnefoy-Claudet et al. 2006b). Li (2008) showed that the main source of ambient waves above 1 Hz in the Mississippi embayment were major roadways and the Mississippi River.

There are two techniques for utilizing ambient vibrations for obtaining estimates of site frequency, as shown in Figure 2.1. The most ideal technique is to take recordings from a sediment site and compare the recordings to motions from a nearby rock outcrop reference site. This approach will produce the most accurate results. However, when working in a large embayment or valley, the distance to rock outcropping makes this method impractical due to the incoherency between the motions. The second approach is the aforementioned HVSR method, which does not require a rock outcropping and is therefore often used when a rock outcrop is not nearby.

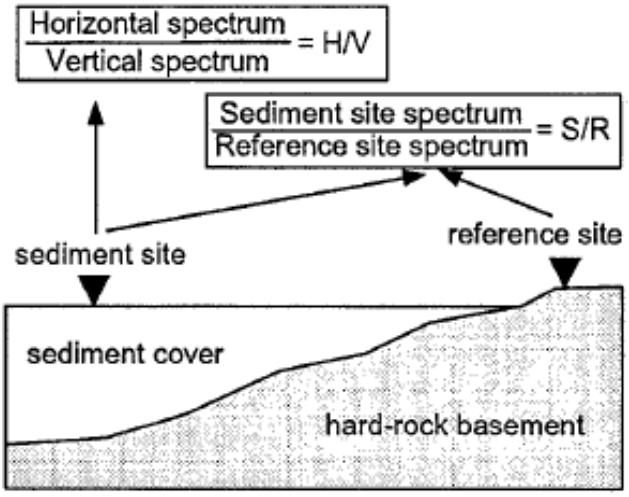

Figure 2.1 Different methods for determining site frequency using ambient vibrations (Ibs-von Seht and Wohlenberg 1999)

2.3.2 Body and Surface Wave Interpretation

The reason for the success of the HVSR method for identifying site frequency is still debated. There is disagreement among various researchers on the nature of the ambient waves. Some researchers (Herak 2008; Kudo 1995; Lachet and Bard 1994; Nakamura 2000) agree with Nakamura's (1989) qualitative explanation of body waves being the source of the ambient waves, while other researchers (Arai and Tokimatsu 2004; Arai and Tokimatsu 2005; Bonnefoy-Claudet et al. 2006a; Konno and Ohmachi 1998; Lermo and Chavez-Garcia 1994; Lunedei and Albarello 2009; Tokimatsu et al. 1992) suggest that Rayleigh or surface wave are the source. This disagreement leads to, what will be termed in this thesis, the *body* and *surface* wave interpretations of the HVSR frequency peak.

The *body wave* interpretation (See Figure 2.2a), assumes that ambient vibrations are composed primarily of body waves. Body waves consist of compression (p-waves) and shear (s-waves) waves, which can travel through the interior of the earth. When the

vertically propagating shear waves come in contact with the recording station, the two horizontal components are dominated by horizontally polarized shear waves (SH) while the vertical component is largely dominated by compression waves. When a fast Fourier transform (FFT) is applied to the noise measurements, a frequency peak in the two horizontal components (Figure 2.2c) is seen while there is no peak at the same frequency in the vertical component. Source effects, common to both the horizontal and vertical components, are minimized by taking the ratio of the horizontal to the vertical frequency spectra. By minimizing the source effects, the frequency peak of the fundamental frequency for the site is made more visible.

The *surface wave* interpretation (Figure 2.2b) assumes that Rayleigh and/or Love surface waves are the source of the ambient waves. Surface waves result from the interaction between body waves with the stress-free boundary at the surface and surficial layers of the earth (Kramer 1996). Surface waves have both horizontal and vertical particle motion and travel along the surface with amplitudes that decrease exponentially with depth. If a stiff boundary is encountered at depth, the amplitude of the vertical component of motions decreases to near zero for some frequencies and a "hole" in the spectrum occurs. The frequency at which this "hole" occurs is often very close to the fundamental mode of SH propagation for the soft layer, as shown in Figure 2.2d. This interpretation yields the interesting result that the frequency of body wave resonance (SH) can be estimated from measurements of purely surface wave motion. It has been noted by several researchers that ambient energy is often dominated by surface wave energy (Asten 2003; Fernandez and Rix 2008; Tokimatsu et al. 1992).

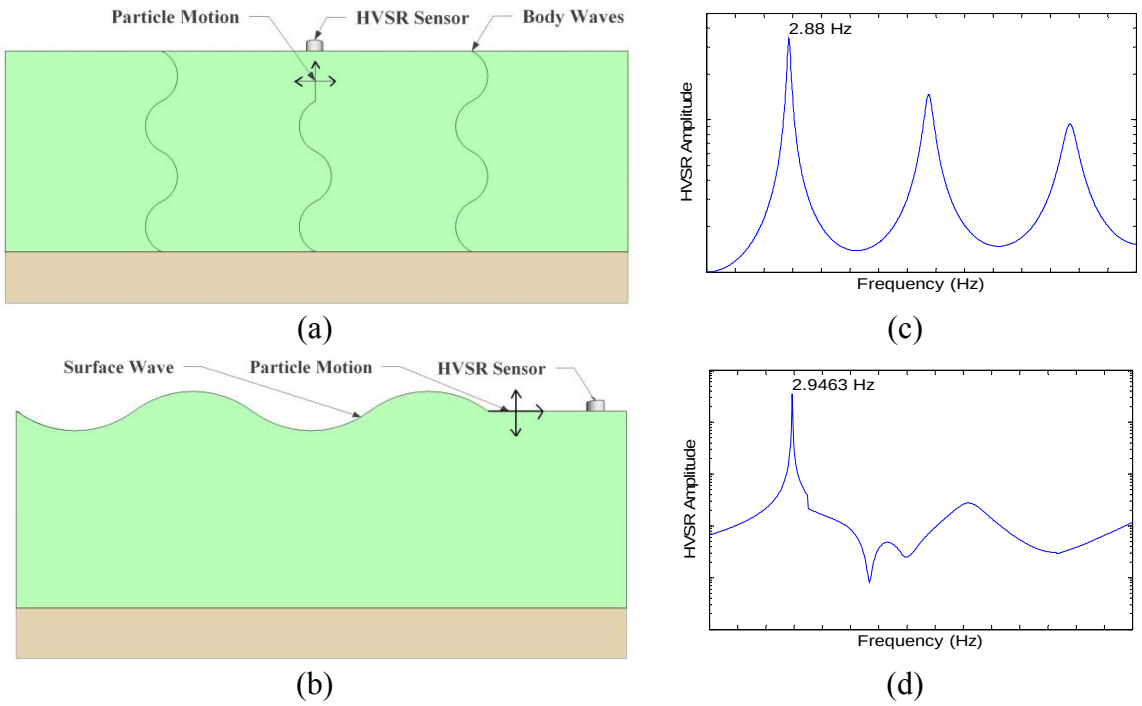

Figure 2.2 Two interpretations of the HVSR method in terms of (a) body waves and (b) surface waves showing (c) the transfer function for 1D, SH wave propagation and (d) the HVSR ratio for Rayleigh wave propagation.

2.4 Past Studies

2.4.1 Worldwide Studies

The HVSR method is used extensively for microzonation of cities, which is defined as the zonation with respect to ground motion characteristics taking into account source and site conditions (TC4-ISSMGE 1999). Selected examples of microzonation studies using the HVSR method are mentioned below. Past studies that have used the HVSR method to estimate $V_{S,AVG}$ are also discussed, with an emphasis on studies performed in the Mississippi embayment.

Microzonation: There are numerous examples of HVSR used in microtremor studies to estimate site frequency; a few examples are discussed here. Delgado et al. (2000) analyzed microtremors measured at 180 sites in the Segura river valley located in southeast Spain. The purpose of the study was to determine the distribution and thickness of soft soils, which can be applied to land-use planning and for civil engineering. The study concluded that the resonance frequency obtained from the HVSR ratios of microtremors allows the thickness of soft soils to be quickly and reliably determined and that the results demonstrate the utility of the HVSR method in the investigation of soft soils as it rapidly and accurately determines the resonance frequency of the soil at a low cost (Delgado et al. 2000).

Gosar (2007) studied the cause of extensive damage by two strong earthquakes that could not be explained by the epicentral distance or by changes in the radiation of seismic energy from the source. Free-field microtremor measurements were performed at 124 points in the Bovec basin of Slovenia, Europe. In addition, 20 buildings were surveyed with the microtremor method to determine the building fundamental frequencies. The HVSR method was performed to determine the fundamental frequency of the sediments. In addition, the main building frequencies were identified from microtremor measurements performed on different floors inside the buildings. By overlaying the frequency map of the soil deposits with the frequencies of buildings, an attempt was made to identify the areas of potential soil-structure resonance. The study concluded that microtremor investigations have proved an effective tool for assessment of local site response in cases of complex geological structure.

Walling et al. (2009) perform HVSR measurements in the eastern part of India at thirty-five locations in and around the Talchir Basin. The study concludes that the predominant frequency identifies quite well the characteristics of Talchir Basin and is in good agreement with synthetic ground motion modeling of the region.

Ibs-von Seht and Wohlenberg (1999) analyzed microtremor measurements at 102 sites in the western Lower Rhine embayment. Ibs-von Seht applied both the classical spectral ratio technique and the HVSR method (shown in Figure 2.1) to these sites discovering that both approaches revealed spectral ratios that were closely related to the calculated transfer functions of the subsoil. He also studied the effects of high-amplitude local noise sources. He found that the classical spectral ratio technique produced erroneous results, whereas the HVSR method results remained stable. This study concluded that the HVSR method can be a powerful tool to map sedimentary cover layers.

Application of HVSR Method to Estimate Vs: Parolai et al. (2002) analyzed noise measurements taken at 337 sites in the Cologne area of Germany for the purpose of deriving new relationships between the main resonance frequency, obtained by using the HVSR method, the thickness of soil deposits, and the V_S profile. This study developed a relationship between sediment thickness and the fundamental frequency peak in the HVSR spectral ratios and estimated the V_S distribution within the soil deposits and the $V_{S,AVG}$ depending on the thickness of the deposits.

Arai and Tokimatsu (1998) purposed to evaluate the local site response by using V_S profiles developed from an inversion of microtremor HVSR data using theoretical formulas. The inversion process consisted of using both Genetic Algorithms (GA) (Sen and Stoffa 1995) and a non-linear least-squares method. The study concluded that the inversion process successfully resulted in V_S profiles down to bedrock and the estimated results were in fairly good agreement with those of observed records. The paper concluded by stating that the HVSR method may be promising for the estimation of V_S profiles and local site response.

Effects of Geologic Structures on HVSR Method: Guillier et al. (2006) computed simulations of 2D and 3D structures in order to test the applicability of HVSR in providing qualitative and quantitative information on site features. The 2D and 3D structures that were investigated in this study are shown in Figure 2.3. This study concluded that:

> (1) The HVSR peak frequency decreases as the sediment thickness variation increases,
>
> (2) clear peaks are exhibited in the HVSR curves for the "flat" parts of the structures, whereas broad peaks or plateau-like shapes of low amplitude are revealed in the HVSR curves for structures with strong lateral sediment thickness variation (valley edges),
>
> (3) for 2D models, whenever it was possible to pick the HVSR peak frequencies, the HVSR peak frequencies agree within +/-20% of the theoretical 1D resonance frequencies in the flat parts of the structure and overestimates the theoretical 1D resonance frequency at the valley edge by around 15%, and
>
> (4) for 3D models, HVSR peak frequencies are close to the theoretical 1D resonance frequency at sites with gentle underground slopes, while HVSR peak frequencies strongly underestimate (up to 80%) the 1D resonance frequency at sites with steep underground slopes.

This study shows that the geologic structures have a major influence on HVSR measurements. While estimated frequencies of flat basic structures are in agreement with theoretical values, complicated 2D and 3D structures produce larger errors. This is significant in regards to this study because of the shape of the Mississippi embayment, shown in Chapter 3.

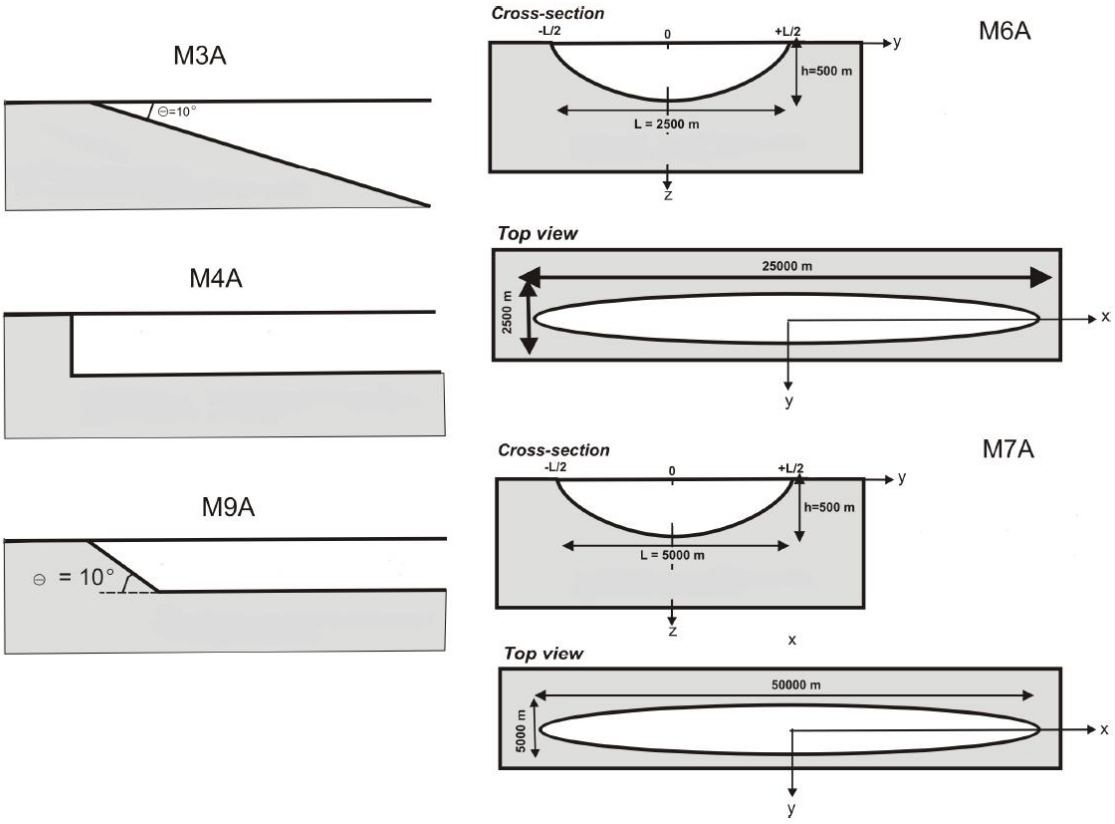

Figure 2.3 Two-dimensional (2D) and 3D structures that were investigated in Guillier et al. (2006) (Guillier et al. 2006).

2.4.2 Previous Shear Wave Velocity Studies in the Mississippi Embayment

The Mississippi embayment is a region of deep soil deposits in the central United States that spans from the confluence of the Mississippi and Ohio rivers to the Gulf of Mexico. The upper Mississippi embayment encompasses the states of Missouri,

Kentucky, Arkansas, Tennessee and overlies the New Madrid seismic zone, which is the most seismically active region east of the Rocky Mountains (Purser and Van Arsdale 1998). Soil deposits in the Mississippi embayment may be vulnerable to the amplification of ground motion due to the loose alluvial and erosional sediments commonly found throughout the embayment. In addition, ground failures such as liquefaction and flow slides are particularly prevalent in soft soils found along the floodplains of rivers (Romero and Rix 2001). The dominant frequency of ground motion amplification is related to the V_S profile, dynamic soil properties, and the depth to bedrock. Soil depths in the embayment are as great as 1000 meters in some areas. The V_S values are well characterized in the top sixty meters (Crone and Russ 1979; Ge et al. 2007; Liu et al. 1997; Luzietti et al. 1992; Romero and Rix 2001; Williams et al. 2003; Woolery and Street 2002), but poorly characterized at greater depths. Reference V_S profiles for the full depth of the embayment have been created, based on limited data (Dorman and Smalley 1994; Romero and Rix 2005).

Table 2.1 Models developed for the Mississippi embayment and used to developed reference V_S profile (Romero and Rix 2005).

Source	**Other Description**	**Type of data**
Kausel and Assimaki (2001)	MIT profile	Based on Memphis data
Herrmann and Akinci (1999)		Base on travel time
Mueller (2000)		Base on travel time
Hashash (1999)	New Madrid Test Well (NMTW)	Based on borehole test data
Hashash (1999)		Based on borehole test data
Hashash (1999)		Based on mini-sosie test
Wen (1999)		Based partly on Hashash profiles
Hwang (2000)	Memphis Soil Profile I	Based on SPT data
Hwang (2000)	Memphis Soil Profile II	Based on compiled SPT data
Hwang (2000)	Memphis Soil Profile III	Based on compiled SPT data

Romero and Rix (2005) generated a reference V_S profile for the deep soil deposits of the Mississippi embayment by combining measured V_S data for the top seventy meters (Romero and Rix 2001) with deeper information from multiple sources including: sonic logs, correlations, and models, as summarized in Table 2.1. A composite V_S profile was developed by computing the arithmetic mean of the combination of profiles. The reference V_S profile of Romero and Rix (2005) is shown in Figure 2.4.

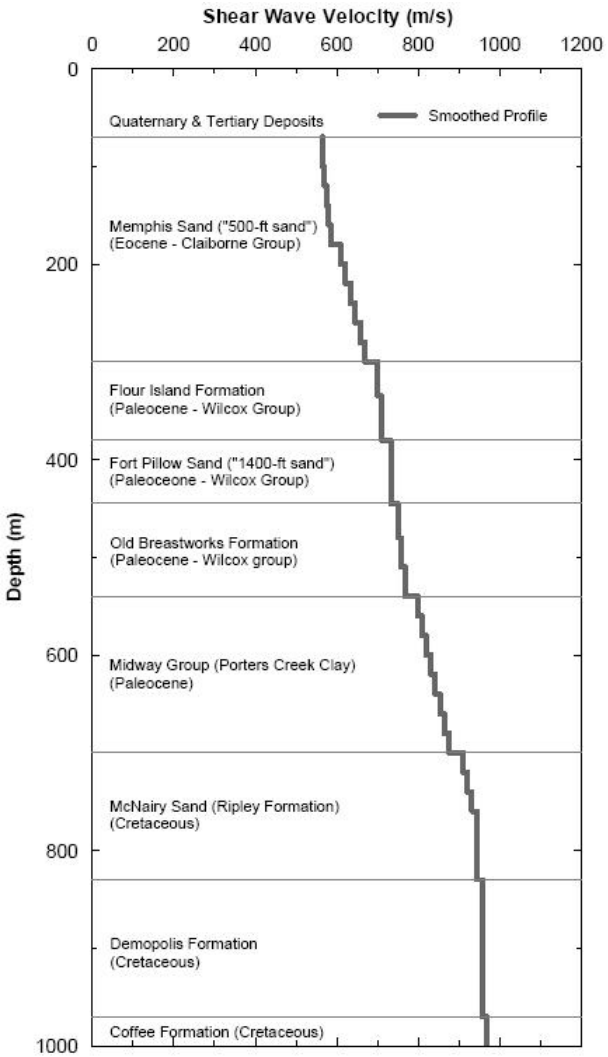

Figure 2.4 Reference V_S profile for the deep soils of the Mississippi embayment (Romero and Rix 2005).

Other studies have been performed to characterize the V_S profile down to bedrock, including Dorman and Smalley (1994) and Chen et al. (1996). Dorman and Smalley (1994) developed a V_S reference profile by using sonic log data to obtain the P-wave velocity (V_P) profile, from which the V_S profile was then derived. Chen et al. (1996) utilized measurements from forty, three-component Portable Array for Numerical Data Acquisition (PANDA) sensors positioned throughout the central New Madrid seismic zone (NMSZ). The thickness of sediments beneath each PANDA station was determined by linear interpolation from well-log data, and the $V_{P,AVG}$ for the sediments was determined from seismic refraction data. With the knowledge of those two parameters, the $V_{S,AVG}$ of the sediments beneath each PANDA station was determined based on the difference in arrival time of converted P-waves and S-waves from the bedrock. Chen et al. (1996) developed a relationship for V_S versus sediment thickness, shown later in this section in Figure 2.6.

The study most related to this research is HVSR measurements performed in the Mississippi embayment by Bodin et al. (2001). In this study, ambient ground motions were measured at more than 100 sites within and near Shelby County, Tennessee. Three-component geophones were placed at each site and measurements were recorded for 15 to 60 minutes. The HVSR method was used to estimate the fundamental frequency of each site and $V_{S,AVG}$ values estimated using a simple equivalent uniform layer approximation illustrated in Figure 2.5. This approximation relates the fundamental frequency, known sediment thickness, h, and $V_{S,AVG}$ through:

$$f_0 = \frac{n \cdot V_S}{4h}, \text{ where } n=1,3,5, \text{ etc} \quad (2.1)$$

Using this method, Bodin et al. (2001) developed a relationship for the $V_{S,AVG}$ of the Mississippi embayment as a function of sediment thickness.

$$V_{S,AVG_{"Est"}} = f_0 \cdot 4h \quad (2.2)$$

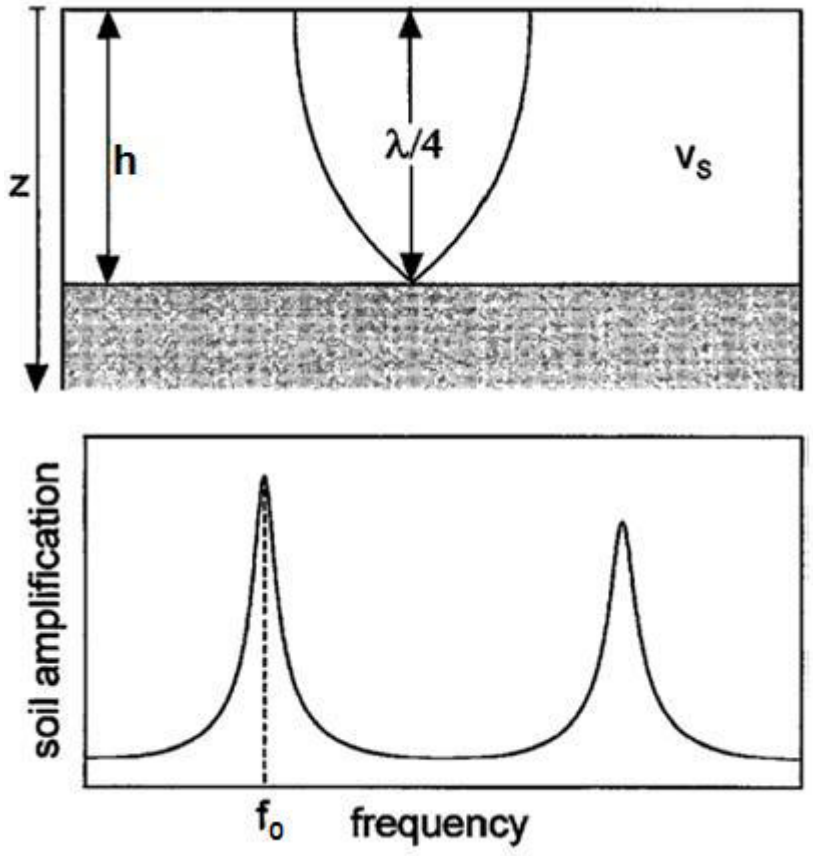

Figure 2.5 Schematic showing the site response and transfer function for a single uniform layer over bedrock (Ibs-von Seht and Wohlenberg 1999).

The results of Bodin et al. (2001) produced two unresolved questions. First the $V_{S,AVG}$ relationship was significantly higher than the relationship developed by Chen et

al. (1996). Secondly, a strong second frequency peak of unknown origin was observed at most sites. These issues are discussed in more detail below.

Average Vs Values: The $V_{S,AVG}$ values developed by Bodin et al. (2001) were approximately 25% higher when compared to values from Chen et al. (1996), which used a different approach, as mentioned earlier. A plot developed by Bodin et al. (2001) comparing the V_S relationship from both methods is shown in Figure 2.6.

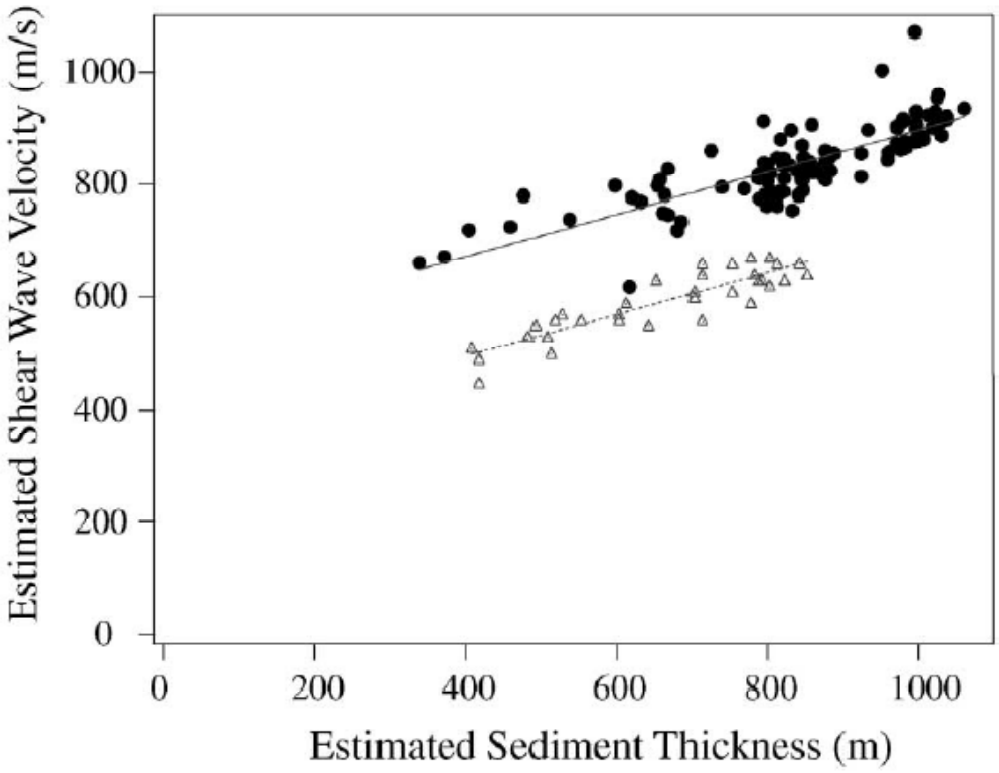

Figure 2.6 Average shear wave velocity as a function of sediment thickness. Filled circles and shaded triangles represent data derived from Bodin et al. (2001) and Chen et al. (1996), respectively (Bodin et al. 2001).

Since Bodin et al. (2001), additional work has been performed in the Mississippi embayment by Bailey (2008). Bailey (2008) utilized active-source surface wave measurements to derive V_S profiles in the top 200 to 250 m at eleven sites in the

Mississippi embayment. In addition, Bailey (2008) performed a preliminary analysis of HVSR data gathered at these sites using the same methodology as Bodin et al. (2001) and concluded that average shear wave velocities were consistent with Bodin et al. (2001). It should be noted that the consistency of results does not verify the validity of Bodin et al. (2001), only that the results are reproducible.

Second Frequency Peak of HVSR Plot: Bodin et al. (2001) also discusses a second frequency peak in the HVSR plot that was observed at many sites, as shown in terms of period (T) in Figure 2.7. Identifying a second frequency peak is significant because amplification of ground motion may also occur at frequencies higher than the fundamental mode even when thick sediments are present (Parolai et al. 2004).

Bodin et al. (2001) theorized that there were two possible explanations for the second frequency peak. The first explanation was that the second frequency peak was the first higher harmonic of the fundamental frequency of the site. From Eq. 2.1, this higher mode frequency would be expected to be at about three times the fundamental frequency, which is what was observed (see Figure 2.7). The other explanation given is that the second frequency peak is a resonance of a soft soil layer over a shallow stiffer layer.

Based on the consistent ratio of 3 observed between the periods, Bodin et al. (2001) interpreted the second frequency peak to be a higher mode of the fundamental frequency due to vertically propagating shear waves. However, Asten (2003), in reply to the Bodin et al. (2001) article, disagreed and argued that the second frequency peak could be interpreted in terms of Rayleigh-wave energy. The preliminary HVSR analysis of

experimental data performed by Bailey (2008) also produced a second frequency peak at most sites. The V_S profiles developed by Bailey (2008) from surface wave measurements identified several shallow stiffer interfaces that could possibly cause the second frequency peak. Bailey (2008) recommended further investigation into the sources of the observed second frequency peak.

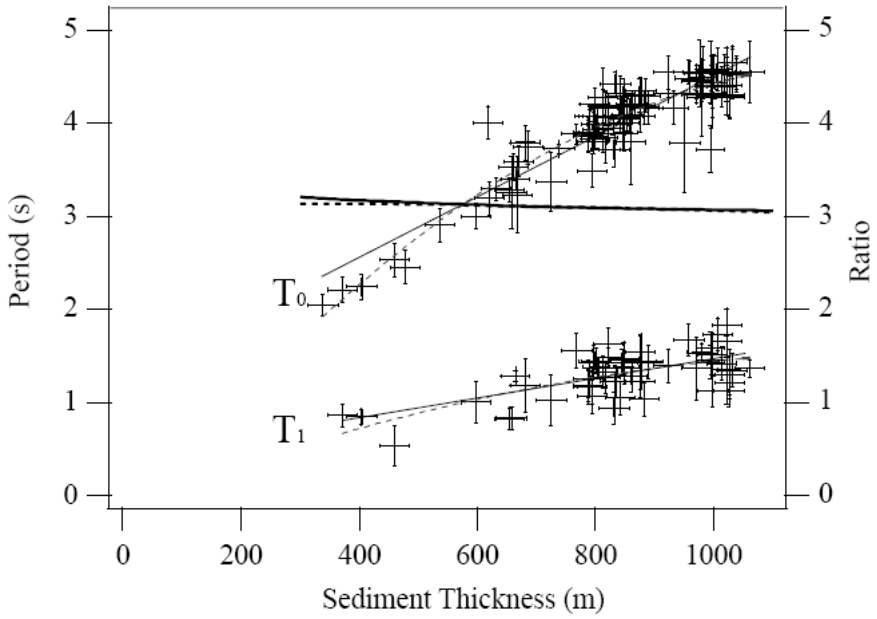

Figure 2.7 Fundamental periods as a function of sediment thickness. T_0 is indicating the period of the first frequency peak while T_1 is indicating the period of the second frequency peak obtained from the HVSR method (Bodin et al. 2001).

2.5 Summary

In this chapter, the theory of the HVSR method is presented along with previous applications of the HVSR method. The HVSR method is based on the analysis of ambient vibrations (microtremors) measured with a single-station, three-component sensor. By dividing the horizontal components by the vertical component, a frequency

peak is produced in some cases, which is used to estimate the fundamental frequency of site resonance.

Previous studies using the HVSR method for microzonation work were discussed. These studies generally showed the method to be a quick and effective approach for estimation of site resonance frequencies. A study showing that geologic structures can produce inaccuracies in the HVSR results was also discussed. Lastly, studies in the Mississippi embayment to estimate $V_{S,AVG}$ were discussed in detail. The HVSR measurements produced $V_{S,AVG}$ values that were, on average, 25% higher than values from other measurement methods in the region. In addition, a second strong frequency peak in the HVSR plot was observed in past studies.

3. MEASUREMENT LOCATIONS

3.1 Overview

Ambient vibration measurements for HVSR analyses were performed at eleven deep soil sites located in Missouri, Arkansas, and Tennessee. The locations of these sites are presented in Figure 3.1. Ten of the sites are located on lowland Holocene-age near surface deposits, while one site (Site 7) is located on upland Pleistocene-age near-surface deposits.

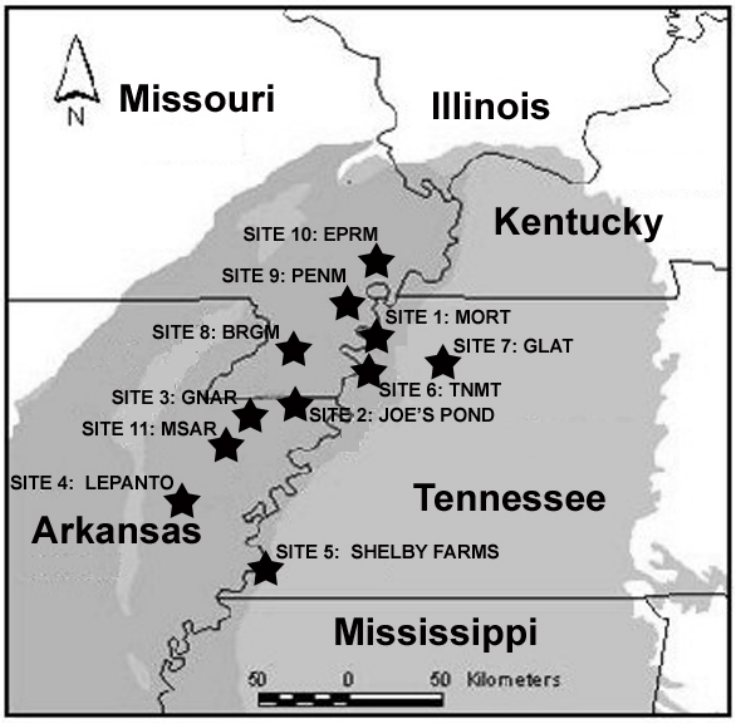

Figure 3.1 Site locations of HVSR measurements in the Mississippi embayment. The lowland Holocene-age deposits and the upland Pleistocene-age deposits are represented by dark and light gray, respectively (Bailey 2008).

The measurements were performed at sites where previous active-source surface wave measurements were conducted in May 2006 and May 2007 (Bailey 2008; Li 2008). These previous surface wave studies produced V_S profiles to depths of over 200 meters. The HVSR measurements were not performed during the initial May 2006 study for the first five sites. A return trip was made to Sites 1-5 in November 2007 for the purpose of collecting HVSR data. The HVSR measurements at the last six sites (Sites 6-11) were performed concurrently with the surface wave studies in May 2007.

Sites were selected based on the requirements of the surface wave studies, which included site access, variable subsurface conditions, and the ability to obtain requisite permits and permission. Most of the sites were located close to existing CERI seismic stations or locations of previous research studies. The sites were distributed around the Mississippi embayment to sample variable soil conditions (formation depths and thicknesses) and variable depths to bedrock.

3.2 Geology of the Upper Mississippi Embayment

The Mississippi embayment is a region of deep soil deposits in the central United States that spans from the confluence of the Mississippi and Ohio rivers to the Gulf of Mexico. The upper Mississippi embayment encompasses the states of Missouri, Kentucky, Arkansas, and Tennessee and has soil deposits as thick as 1000 meters near Memphis, TN, as shown in Figure 3.2. The upper embayment is bordered on the east and west by the Nashville Dome and the Ozark Uplift, respectively. The embayment is a syncline (Figure 3.3) with an axis that is nearly parallel to the Mississippi River. The

basement rock is the Knox Dolomite from the Paleozoic era which is overlain by deep deposits of gravel, sand, silt, clay, chalk, and lignite (Cushing et al. 1964). The general stratigraphy of the sediments in this region, as developed by Van Arsdale and TenBrink (2000), is presented in Figure 3.4.

The near-surface lithology is different on the eastern and western banks of the Mississippi River, with the divide following the bluffs along the eastern side of the river. The upland Pleistocene-age deposits (loess and upland gravel) are to the east of the Mississippi River bluffs, whereas the lowland Holocene-age river deposits (alluvium) are to the west (Van Arsdale and TenBrink 2000). The sites investigated in this study are shown along with the extent of the upland and lowland deposits in Figure 3.1.

Beneath the near-surface deposits is the Eocene-age Jackson Formation, which consists of fluvial/deltaic silty sand interbedded with clayey silt and lignite. Under the Jackson Formation is the Eocene Claiborne Group which is subdivided into the Cockfield Formation, Cook Mountain Formation, and the Memphis Sand Formation, in descending order. Silts and clays make up the majority of the Cockfield Formation and Cook Mountain Formation, whereas, the Memphis Sand Formation consists primarily of fluvial/deltaic sand. The underlying Paleocene Wilcox Group is composed of an upper section of mainly shale and a lower section of mostly sand, whereas the Paleocene Midway Group contains both marine clay and shale with subordinate sand and limestone beds. Beneath these formations is the Upper Cretaceous series consisting mostly of sand, clay, marl, and chalk that are mostly of marine origin (Cushing et al. 1964). Paleozoic

Knox Dolomite is the basement rock underlying all the sediments in the Mississippi embayment.

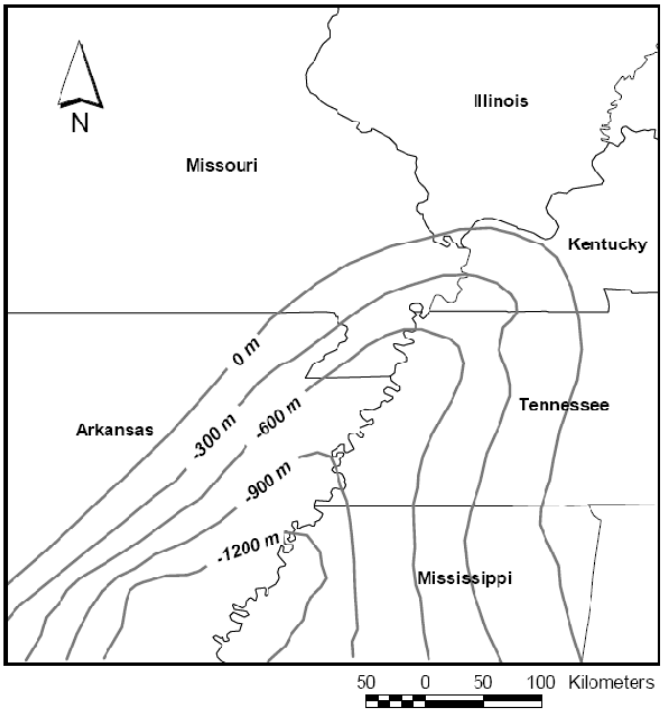

Figure 3.2 Elevation of Paleozoic basement relative to mean sea level in the upper Mississippi embayment (Romero and Rix 2005).

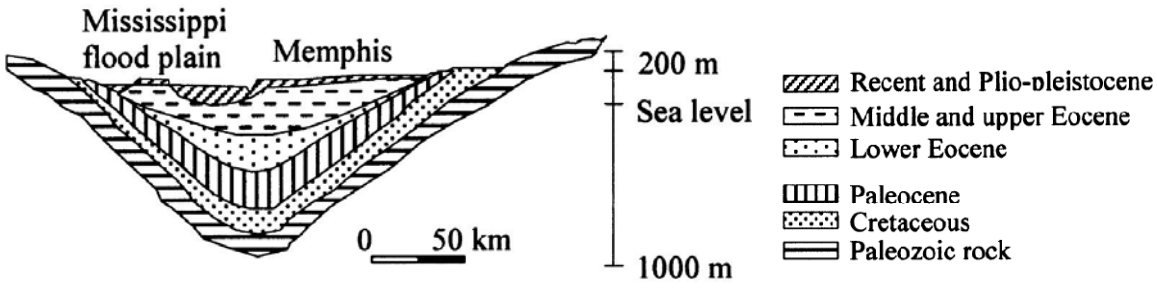

Figure 3.3 Idealized cross-section of Mississippi embayment profile near Memphis, Tennessee (Hashash and Park 2001).

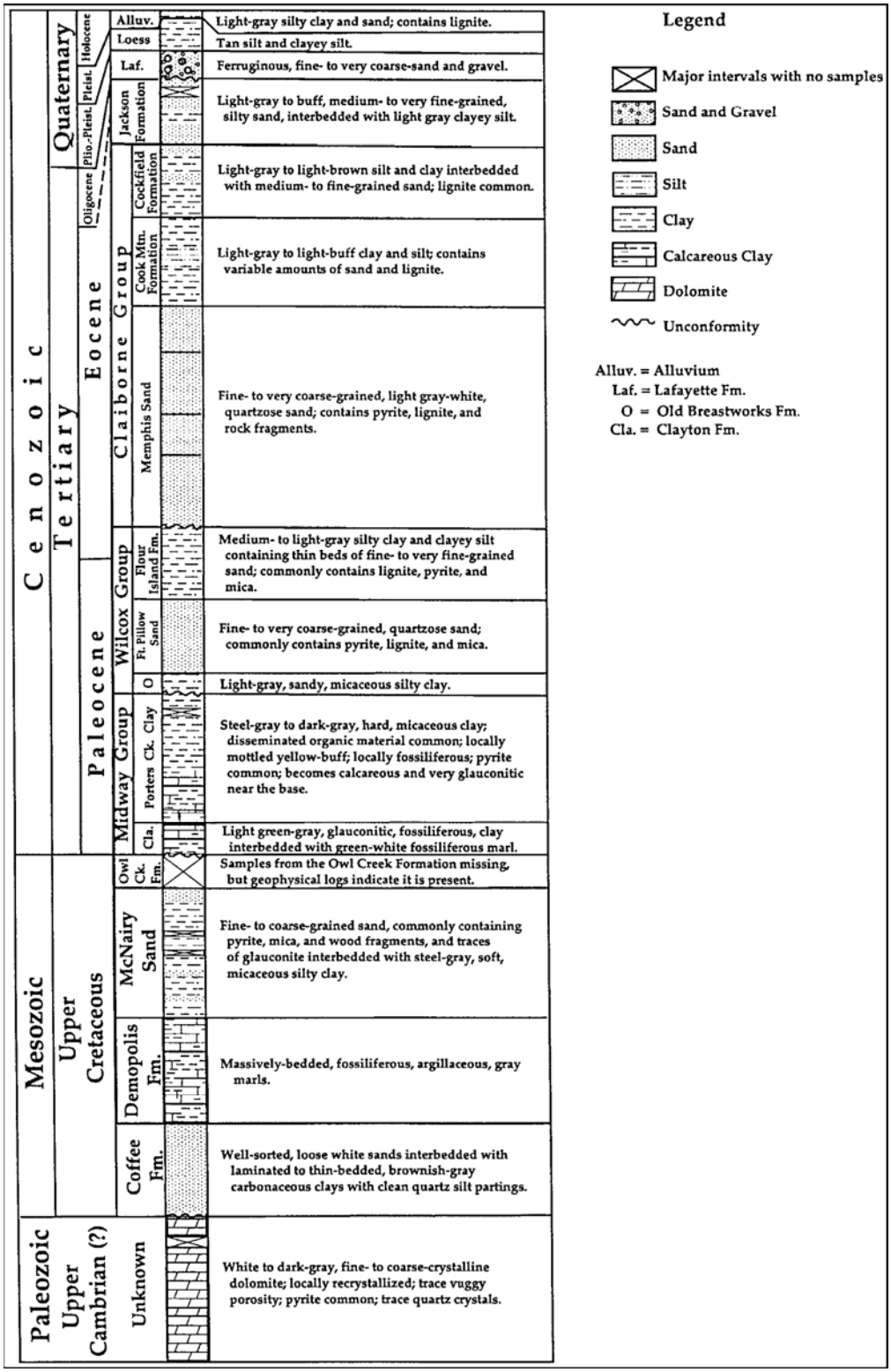

Figure 3.4 Geologic column for the New Madrid seismic zone (Van Arsdale and TenBrink 2000).

The New Madrid seismic zone (NMSZ) is in the northern section of the embayment and consists of a clustered pattern of earthquake epicenters between five and fifteen kilometers deep (Hashash and Park 2001), as shown in Figure 3.5. The NMSZ is considered to be the most seismically active zone in the eastern United States, where earthquakes are characterized as low probability, high consequence events (Hashash and Park 2001). Within the NMSZ, earthquakes with magnitudes greater than 6.0 have recurrence intervals of 70 to 140 years, while magnitude 7.0 and greater have intervals of 550 to 1100 years (Johnston and Nava 1985). These potentially large earthquakes could result in significant loss of life and property damage, especially in the Memphis metropolitan area. The deep soil deposits in this area will affect the frequency content and amplitude of ground motions. The majority of the eleven sites in this study are located directly above the NMSZ.

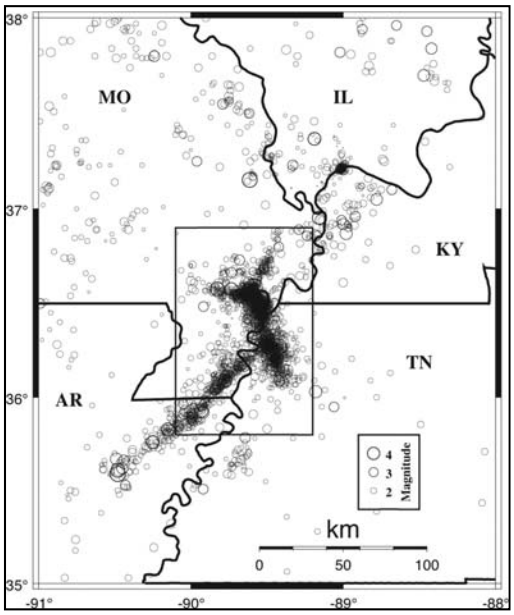

Figure 3.5 Epicenters of earthquakes around the upper Mississippi embayment from 1974 to present. Locations and magnitudes taken from the Cooperative New Madrid Seismic Network catalog (Powell and Withers 2009).

3.3 Measurement Sites

3.3.1 Site Characteristics

All of the sites examined in this study were located on deep soil deposits in the Mississippi embayment. The site coordinates, depths to bedrock, and the dates that the measurements were performed are presented in Table 3.1. A map of the region surrounding each site and a photo of the site are presented in Figures 3.6 through 3.16, for Sites 1 through 11, respectively.

With the exception of Site 5, which is located in Memphis, TN, all of the sites are located in rural areas, typically on privately owned farmland. Most of the nearby roadways are lightly travelled, although in most cases, major interstates were located within about twelve km of the sites (see Figure 3.6a to 3.16a). The estimated soil lithology at each site was provided by Professor Van Arsdale from the University of Memphis. Estimated depths to various formation tops were obtained for each of the sites by using interpolated values based on nearby geologic and geotechnical logs.

In addition, V_S profiles were determined to depths of 200 to 250 m at each site from active-source surface wave measurements by Bailey (2008). The V_S profiles were developed with no prior knowledge of the soil lithology for the sites. These V_S profiles are presented along with the corresponding soil lithology in Figure 3.17(a)-(e) for Sites 1-5 and Figure 3.18(a)-(f) for Sites 6-11. In addition, the estimated soil lithology provided by Professor Van Arsdale for the entire sediment depth of each site is shown in Figure 3.19.

There are several notable variations in the soil lithology between sites. At Site 5, the Memphis Sand is very shallow when compared to the other sites. In addition, Site 5 is one of two sites not located on the Mississippi River alluvial deposits; instead, it is located on Holocene-age, near-surface alluvial deposits of the Wolf River. Site 7 is also not located on the Mississippi River alluvial deposits and is the only site located on near-surface Pleistocene-age deposits. Site 10 is the shallowest site with bedrock at approximately 450 meters deep, and Site 11 is the deepest site with bedrock at a depth of roughly 847 meters.

Table 3.1 Site coordinates and depth to bedrock at eleven measurement sites (* denotes CERI Station).

Site	Name	Site Location	Measurement Performed On	Coordinates		Depth to Bedrock (Meters)
				Latitude	Longitude	
1	MORT*	Mooring, TN	11/1/07	36.324N	89.566W	703
2	YARBRO	Yarbro, AR	11/1/07	35.981N	89.915W	820
3	GNAR*	Gosnell, AR	11/1/07	35.960N	90.016W	783
4	LEPANTO	Lepanto, AR	11/1/07	35.614N	90.413W	794
5	SHELBY FARMS	Memphis, TN	11/1/07	35.136N	89.846W	840
6	TNMT*	Tennemo, TN	5/17/07	36.166N	89.579W	783
7	GLAT*	Glass, TN	5/18/07	36.269N	89.288W	751
8	BRGM*	Braggadocio, MO	5/19/07	36.205N	89.859W	714
9	PENM*	Portageville, MO	5/21/07	36.450N	89.628W	586
10	EPRM*	East Prairie, MO	5/22/07	36.717N	89.358W	451
11	MSAR*	Manila South, AR	5/23/07	35.784N	90.147W	847

(a)

(b)

Figure 3.6 Map of Site 1 (MORT) showing surrounding roadways (a) and a photograph of the placement of the three-component geophone at Site 1 (b).

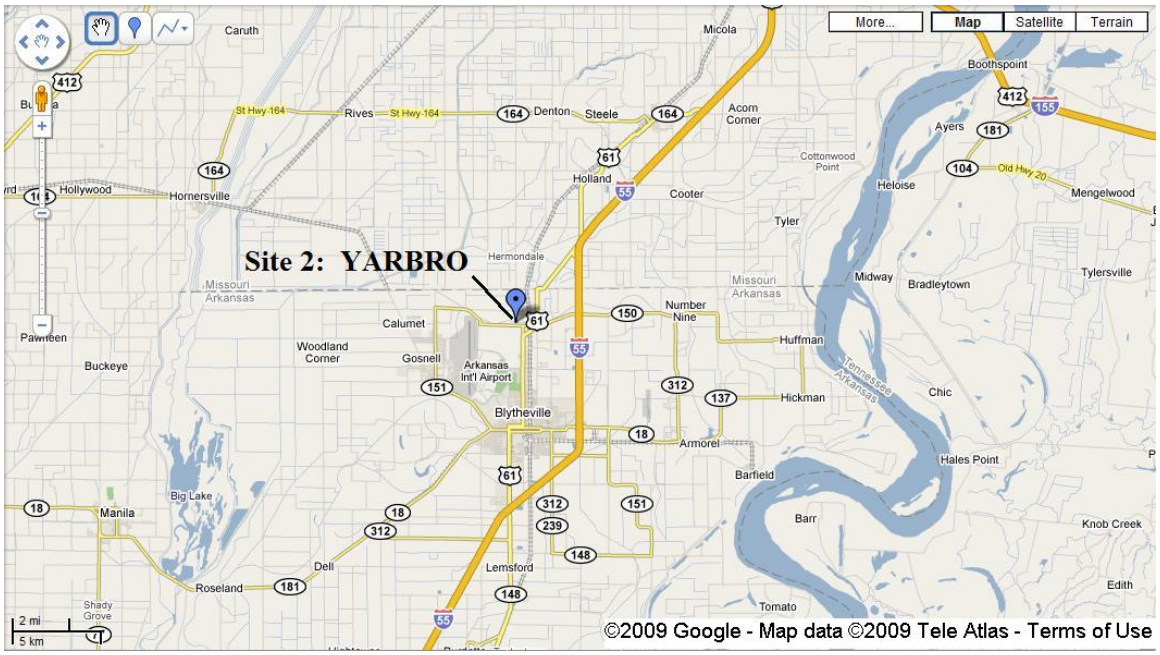

(a)

(b)

Figure 3.7 Map of Site 2 (YARBRO) showing surrounding roadways (a) and a photograph of the placement of the three-component geophone at Site 2 (b).

(a)

(b)

Figure 3.8 Map of Site 3 (GNAR) showing surrounding roadways (a) and a photograph of the placement of the three-component geophone at Site 3 (b).

(a)

(b)

Figure 3.9 Map of Site 4 (Lepanto) showing surrounding roadways (a) and a photograph of the placement of the three-component geophone at Site 4 (b).

(a)

(b)

Figure 3.10 Map of Site 5 (Shelby Farms) showing surrounding roadways (a) and a photograph showing ground conditions at Site 5 (b).

(a)

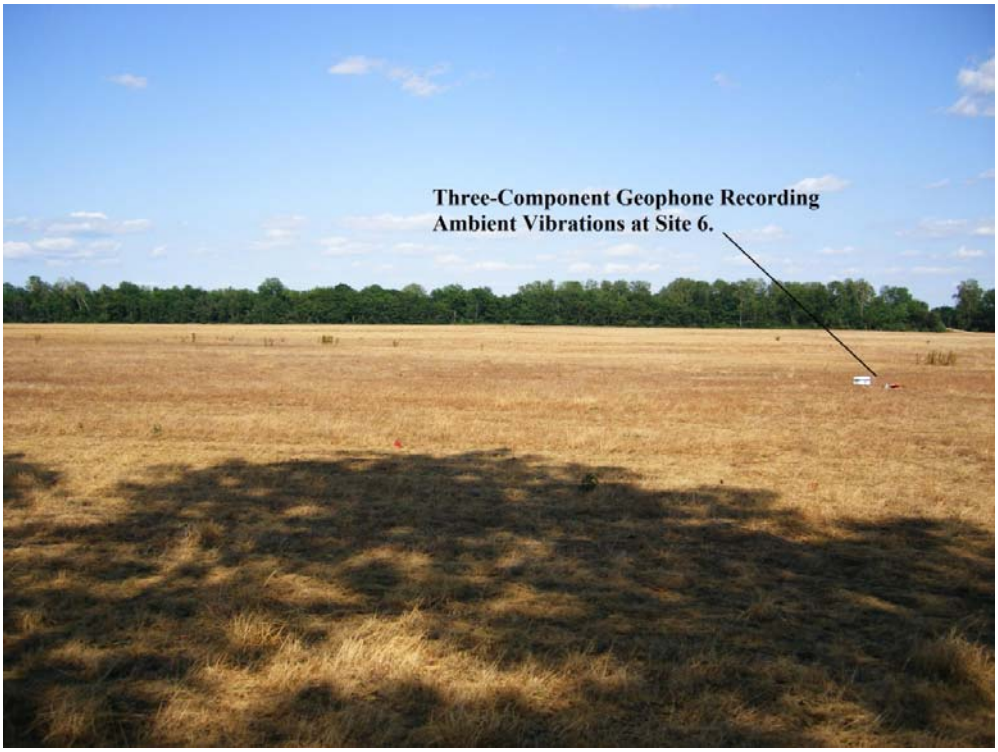

(b)

Figure 3.11 Map of Site 6 (TNMT) showing surrounding roadways (a) and a photograph showing an overview of Site 6 (b).

(a)

(b)

Figure 3.12 Map of Site 7 (GLAT) showing surrounding roadways (a) and a photograph showing an overview of Site 7 (b).

(a)

(b)

Figure 3.13 Map of Site 8 (BRGM) showing surrounding roadways (a) and a photograph showing an overview of Site 8 (b).

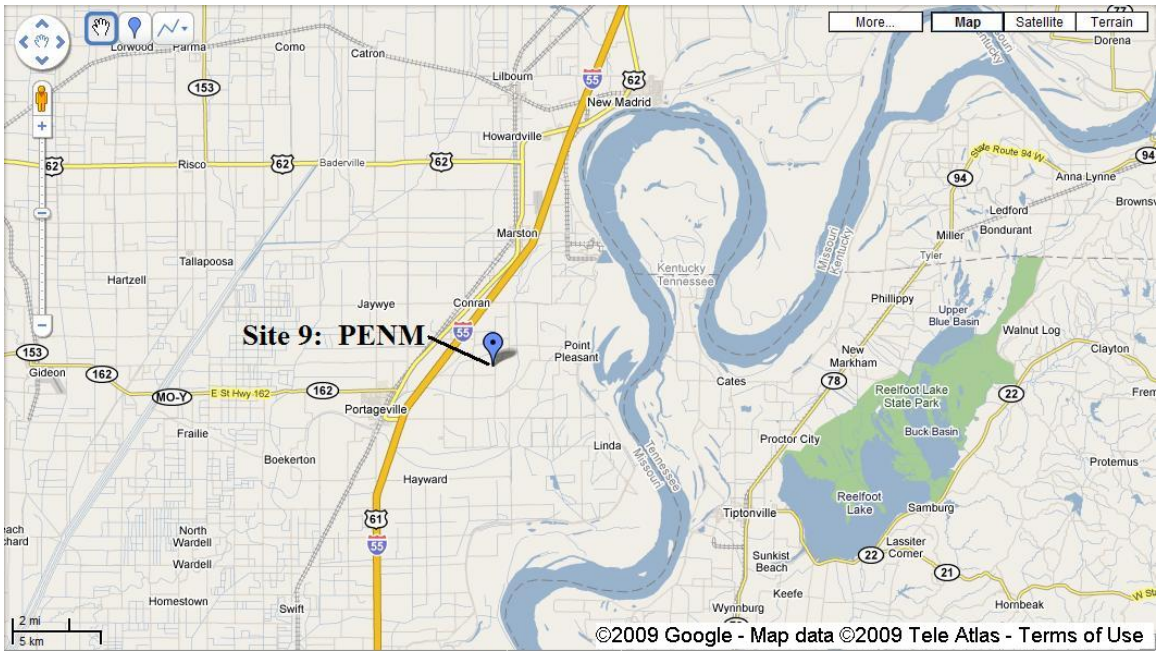

(a)

(b)

Figure 3.14 Map of Site 9 (PENM) showing surrounding roadways (a) and a photograph showing an overview of Site 9 (b).

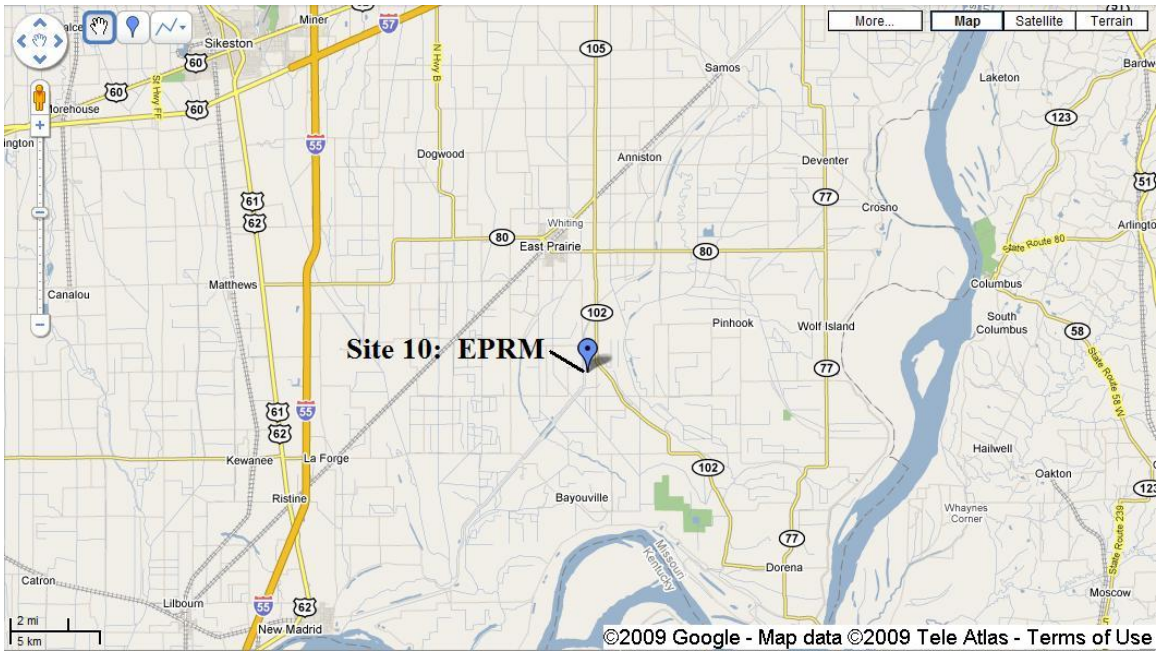

(a)

(b)

Figure 3.15 Map of Site 10 (EPRM) showing surrounding roadways (a) and a photograph showing an overview of Site 10 (b).

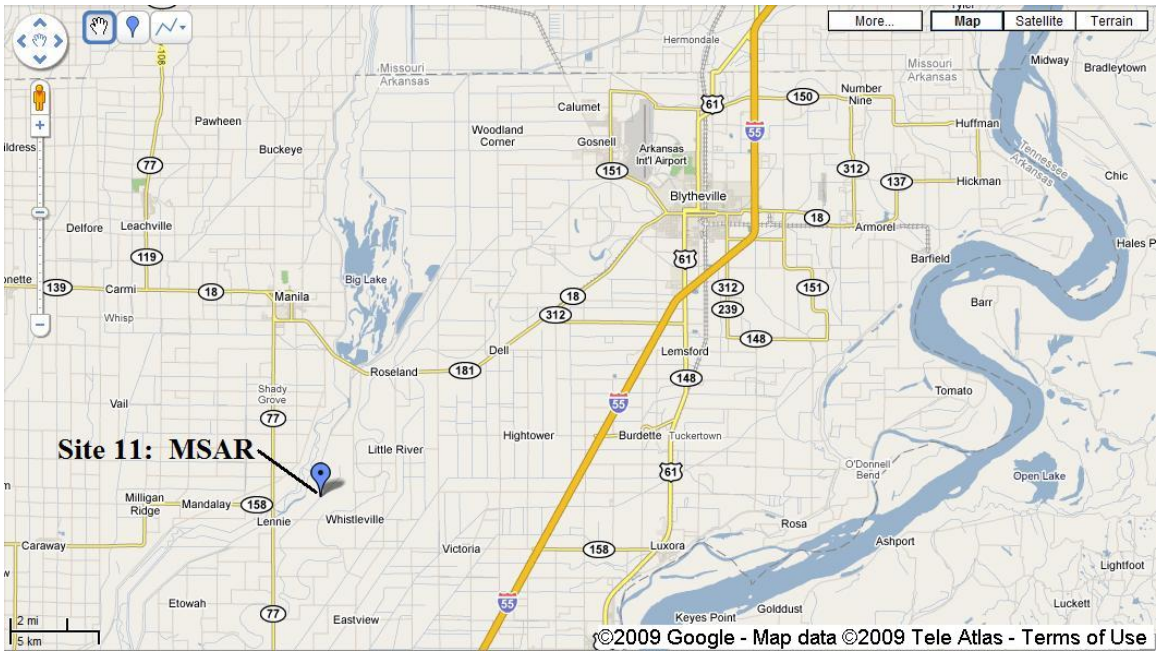

(a)

(b)

Figure 3.16 Map of Site 11 (MSAR) showing surrounding roadways (a) and a photograph showing an overview of Site 11 (b).

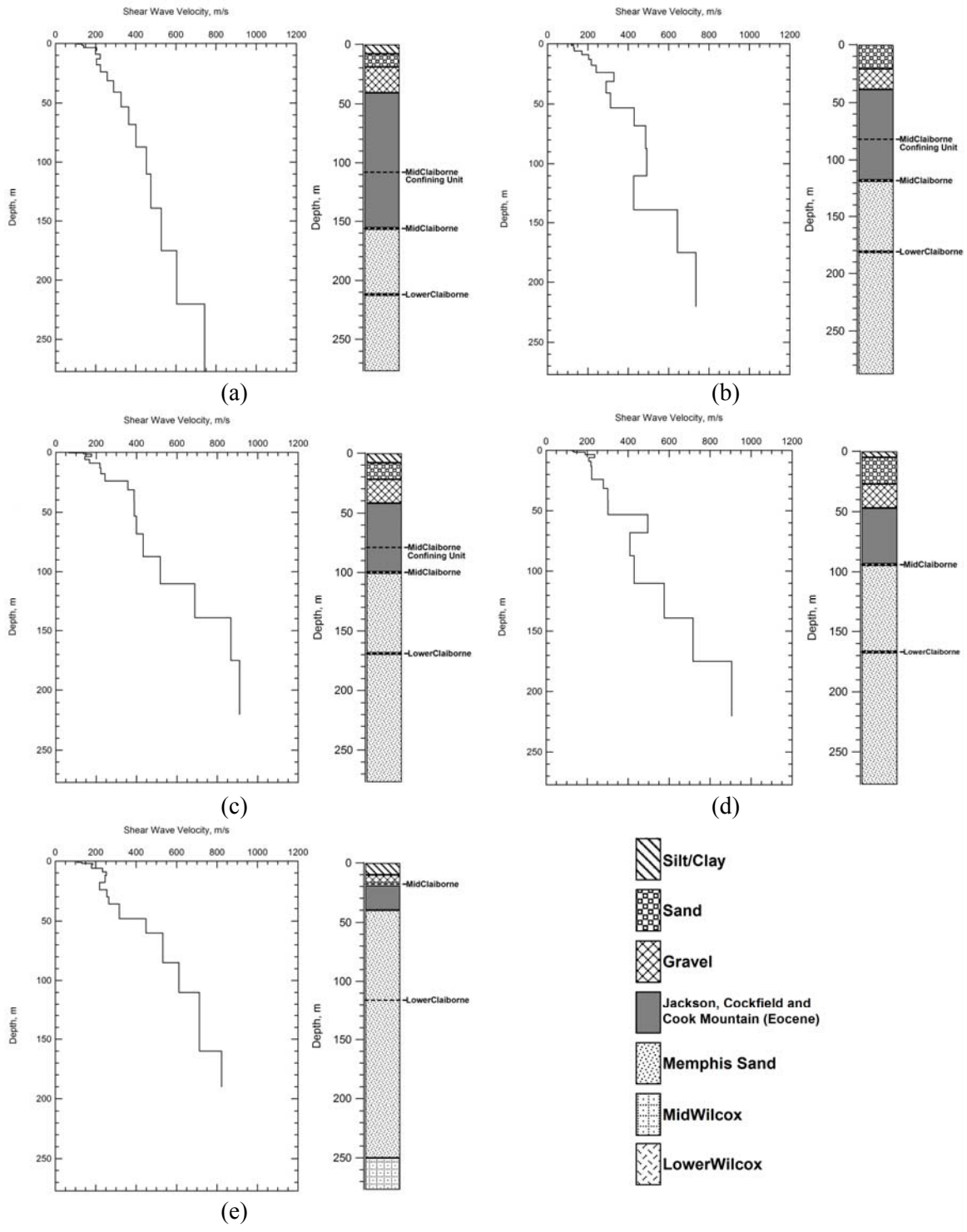

Figure 3.17 Shear wave velocity profiles derived from surface wave measurements (Bailey 2008), with corresponding soil lithology provided by Professor Van Arsdale at the University of Memphis, for Sites 1-5, (a) – (e) respectively.

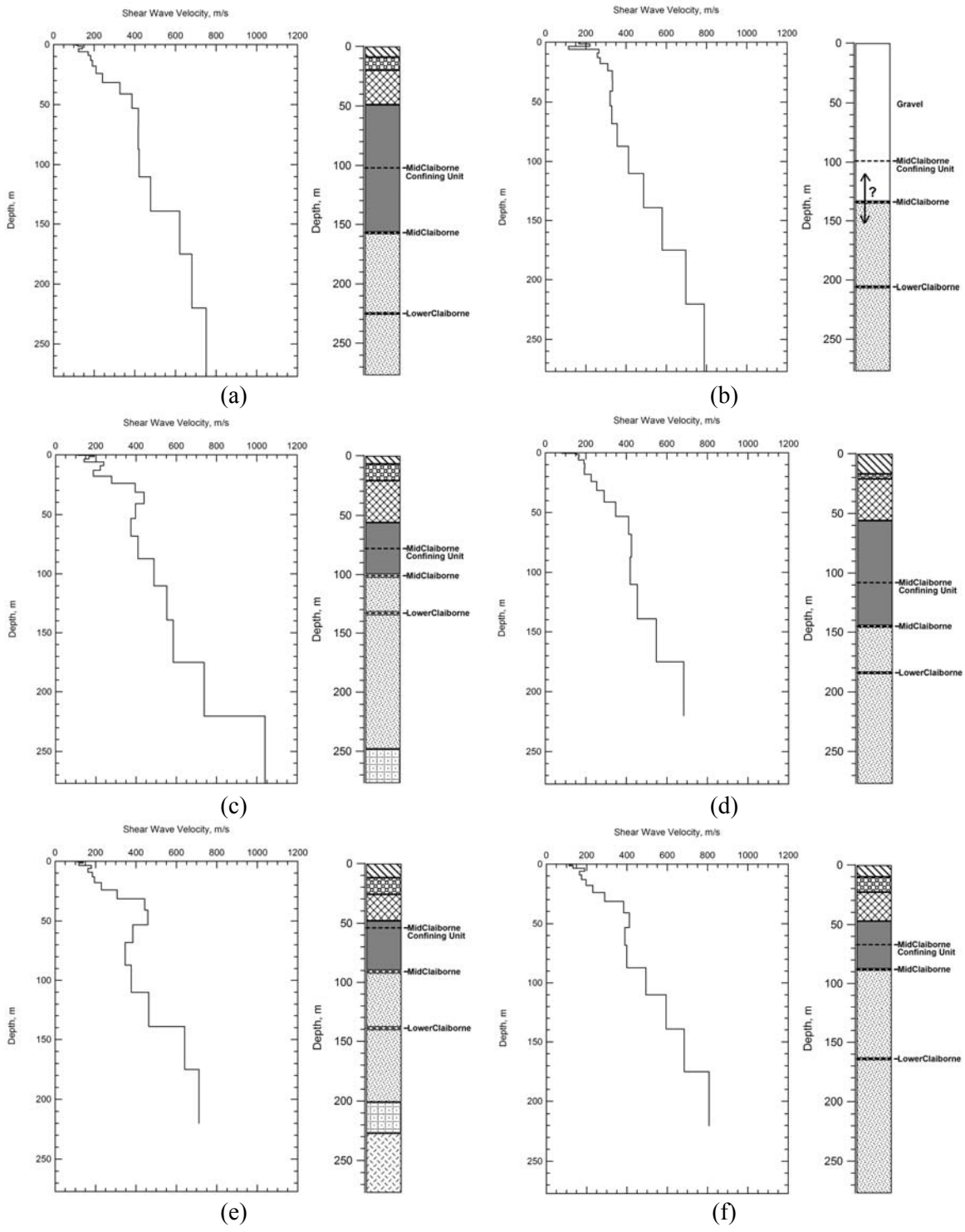

Figure 3.18 Shear wave velocity profiles derived from surface wave measurements (Bailey 2008), with corresponding soil lithology provided by Professor Van Arsdale at the University of Memphis, for Sites 6-11, (a) – (f) respectively. Legend for the eleven sites is shown in previous figure.

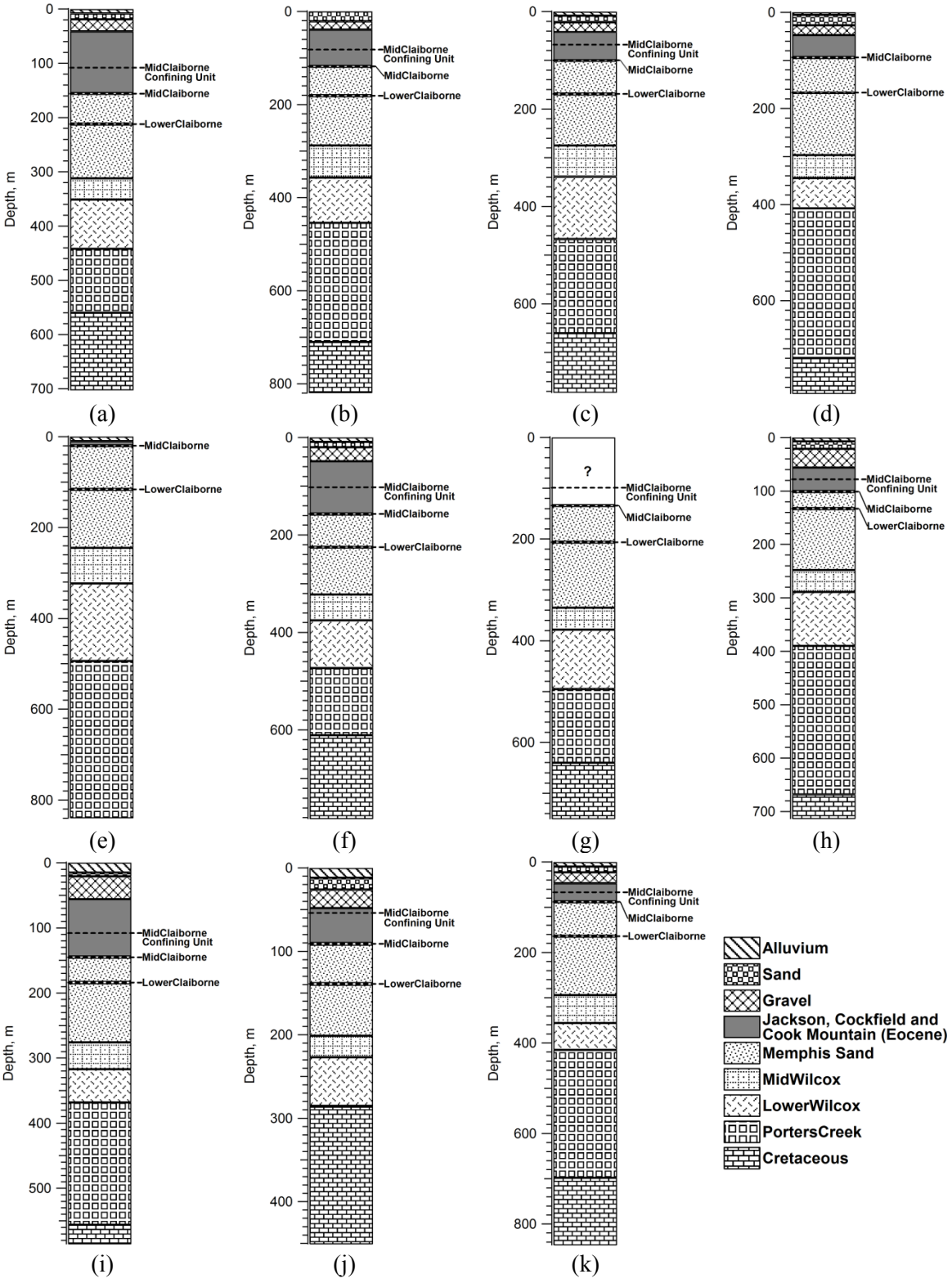

Figure 3.19 Estimated soil lithology down to bedrock for Sites 1-11, (a) – (k) respectively, provided by Professor Van Arsdale at the University of Memphis.

3.4 Data Collection

Data collection for the HVSR analyses was made using a Mark Product Inc. three-component seismometer (Model Number L-4-3D) with three 1-Hz geophones (one vertical and two horizontal). The three-component geophone was placed in the ground to a depth of about 10 cm to avoid adverse effects from wind vibrations. At one site (Site 2), it was not possible to bury the sensor, so it was placed directly on the surface. Figure 3.20 shows the author preparing a hole for placement of the three-component sensor. After placement in the hole, the sensor was leveled using a bull's-eye bubble level to ensure free movement of the geophone components.

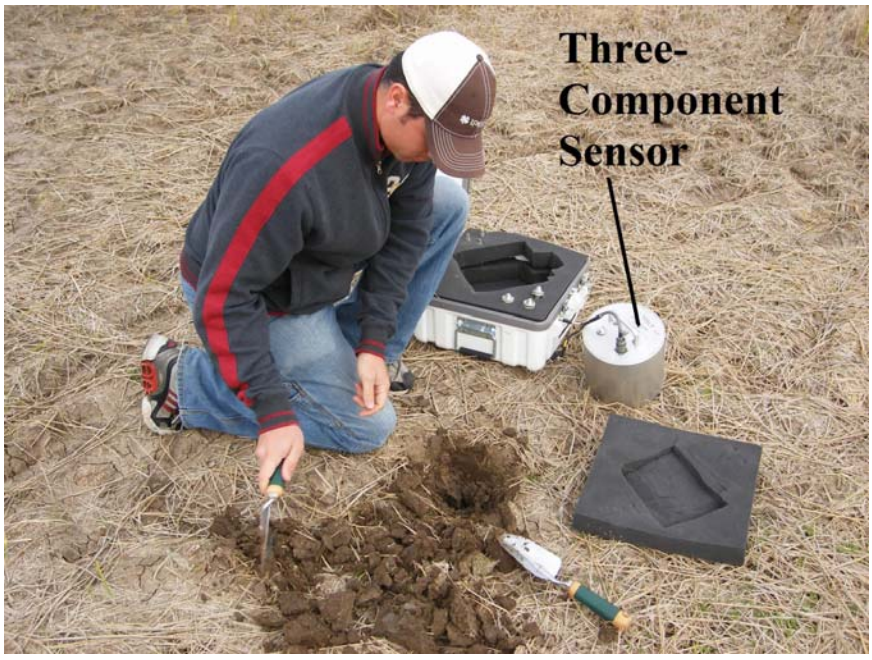

Figure 3.20 Preparing for the placement of the three-component geophone at Site 4.

After the geophones were placed and leveled, ambient noise was recorded for typically thirty to forty minutes at a sampling rate of 205 Hz for Sites 1-5 and 80 Hz for Sites 6-11, as shown in Table 3.2. For all but one site (Site 5), the data were collected in quiet rural environments with few nearby man-made sources of ambient energy. Care was taken to avoid other man-made noise such as walking and vehicle noise. The data

Table 3.2 The recording length used for experimental data collection at the eleven sites.

Site	Site Name	Sampling Frequency (Hz)	Recording Length (mins)
1	MORT	204.8	40
2	Yarbro	204.8	40
3	GNAR	204.8	40
4	Lepanto	204.8	40
5	Shelby Farms	204.8	40
6	TNMT	81.92	40
7	GLAT	80	25
8	BRGM	80	20
9	PENM	80	30
10	EPRM	80	25
11	MSAR	80	30

Figure 3.21 Data Physics Dynamic Signal Analyzer connected to the field laptop.

(a) (b)

Figure 3.22 Monitoring the data collection from a vehicle for Sites 1-5 (a) and instrumented trailer used in data collection at Sites 6-11 (b).

were collected using a Data Physics Dynamic Signal Analyzer (shown in Figure 3.21) operated in the throughput mode, as shown in Figure 3.22. Examples of ambient noise records (collected at Site 9) are presented in Figure 3.23. Data processing procedures are discussed in the next chapter.

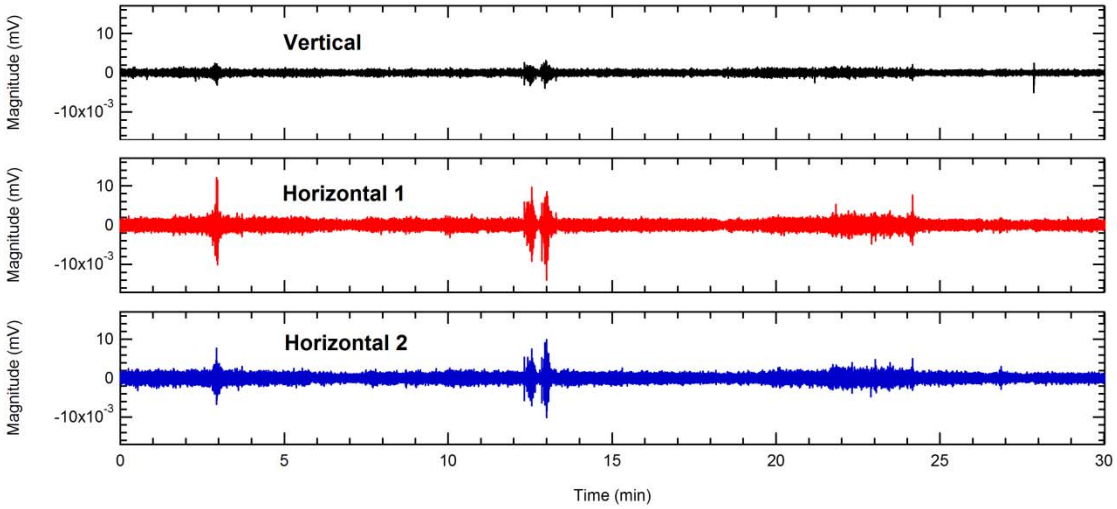

Figure 3.23 Ambient noise recorded on vertical and two horizontal geophones at Site 9.

3.5 Summary

Ambient noise records were recorded at eleven sites located in the upper Mississippi embayment. In this chapter, descriptions of the measured sites and an overview of the geology of the upper Mississippi embayment were presented. Site lithology was provided by Professor Van Arsdale for each of the sites using interpolated values based on nearby geologic and geotechnical logs. Sites included both rural and urban environments with sediment thickness ranging from approximately 450 to 850 m. The majority of the sites were on near-surface, Holocene-age Mississippi River alluvial deposits, with the exceptions of Site 5 (located on Wolf River alluvial deposits) and Site

7 (located on Pleistocene-age uplands). Data collection procedures using a single station, three-component sensor were also described. Recordings of ambient energy were performed for thirty to forty minutes at sampling frequencies of 80 to 205 Hz. Analyses and results are presented in subsequent chapters.

4. METHODS

4.1 Introduction

As previously mentioned, the primary objectives of this study are to: (1) explain why the V_S relationships from the HVSR method are inconsistent with other methods in the Mississippi embayment and (2) explain the origin of the second frequency peak observed in the experimental HVSR data recorded in the Mississippi embayment. To meet these objectives, both numerical simulations and experimental data analyses were performed. This work was separated into the following three studies: (1) analytical study of simulated V_S profiles (Section 4.2), (2) study of HVSR processing parameters (Section 4.3), and (3) comparison of experimental and simulated results for Mississippi embayment sites (Section 4.4). The methods used for each of these studies are described in this chapter.

4.2 Analytical Study of Simulated Velocity Profiles

In this portion of the research, body and surface wave propagation were simulated for a variety of V_S profile conditions to examine the parameters affecting site frequency and average velocity estimates from the HVSR analyses. Two computer programs were used to calculate body and surface wave motions for seven simulated soil profile conditions, as discussed below.

4.2.1 Computer Programs

Shear Wave Propagation: The computer program DEEPSOIL (Hashash et al. 2005) was used to calculate the transfer function between the bedrock and ground surface for vertically-propagating, horizontally-polarized shear waves (SH waves) propagating through the site stratigraphy. DEEPSOIL, developed at the Mid-America Earthquake Center, is a one-dimensional (1D) site response analysis program that can perform either equivalent-linear or true nonlinear analysis. For this study, a linear analysis was performed with strain-independent soil properties, due to the small-strain nature of the ambient noise measurements. The 1st and 2nd frequency peaks of the transfer function were used to identify small-strain site resonance frequencies for each site. These values represent the "true" site resonance frequencies that were compared to values developed from simulated HVSR analysis using surface wave propagation. The DEEPSOIL results were verified using EDUSHAKE (EduPro Civil Systems 2006), which is another 1D equivalent-linear analysis program to simulate SH waves in layered profiles.

In DEEPSOIL, the solution of the 1D wave propagation equation is presented in the frequency domain. As mentioned in Park and Hashash (2004), the frequency domain solution begins with the following 1D equation of motion for vertically-propagating shear waves through an unbounded medium:

$$\rho \frac{\partial^2 u}{\partial z^2} = \frac{\partial \tau}{\partial z} \tag{4.1}$$

where, ρ is density, τ is shear stress, u is displacement, and z is depth below the ground surface. The shear stress-shear strain soil behavior of a Kelvin-Voigt solid is expressed by:

$$\tau = G\gamma + \eta\frac{\partial\gamma}{\partial t} \tag{4.2}$$

where, G is shear modulus, γ is shear strain, and η is viscosity. Combining Eq. 4.1 and 4.2 results in the following relationship for vertically propagating shear waves traveling through soil:

$$\rho\frac{\partial^2 u}{\partial t^2} = G\frac{\partial^2 u}{\partial z^2} + \eta\frac{\partial^3 u}{\partial z^2 \partial t} \tag{4.3}$$

According to Schnabel et al. (1972), Eq. 4.3 can be solved for a harmonic wave propagating through a multilayered soil column by entering a local coordinate, Z, as the height of each layer in the site stratigraphy, and expressing the displacements at the top and bottom of the layer as:

$$\begin{aligned} &\text{Top:} && u(Z_m = 0,t) = u_m = (A_m + B_m)e^{i\omega t} \\ &\text{Bottom:} && u(Z_m = h_m,t) = u_{m+1} = \left(A_m e^{ik_m^* h_m} + B_m e^{-ik_m^* h_m}\right) e^{i\omega t} \end{aligned} \tag{4.4}$$

where, A_m and B_m are the amplitudes of the upward traveling wave, h_m is the thickness, $k_m^* = \frac{\omega}{(V_S)m(1+i\xi_m)}$, and ξ is the damping ratio for each layer. When the boundary conditions and compatibility requirements are applied, a repeating procedure for ensuing layers is established:

$$A_{m+1} = \frac{1}{2} A_m\left(1 + \alpha_m^*\right)e^{ik_m^* h_m} + \frac{1}{2} B_m\left(1 - \alpha_m^*\right)e^{-ik_m^* h_m}$$
$$B_{m+1} = \frac{1}{2} A_m\left(1 - \alpha_m^*\right)e^{ik_m^* h_m} + \frac{1}{2} B_m\left(1 + \alpha_m^*\right)e^{-ik_m^* h_m} \quad (4.5)$$

where, $\alpha_{m+1}^* = \frac{\rho_m (V_S)_m (1+i\xi_m)}{\rho_{m+1} (V_S)_{m+1}(1+i\xi_{m+1})}$ (Park and Hashash 2004). The transfer function between any two layers in the site stratigraphy is expressed as:

$$F_{ij}(\omega) = \frac{|u_i|}{|u_j|} = \frac{A_i(\omega) + B_i(\omega)}{A_j(\omega) + B_j(\omega)} \quad (4.6)$$

The transfer function provides the ability to determine which frequencies of the motions at the base of the column will be amplified in the soil column. An example transfer function, calculated with DEEPSOIL, for the case of a homogeneous layer over bedrock (Figure 4.1a) is shown in Figure 4.1b.

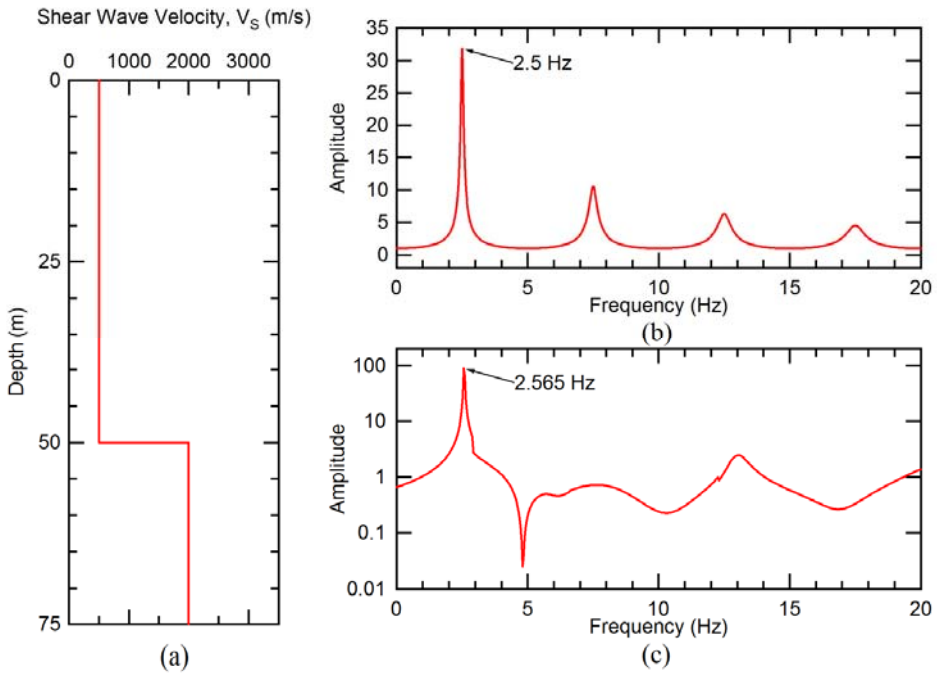

Figure 4.1 Shear wave velocity profile of a homogeneous layer (500 m/s) over a halfspace of 2000 m/s (a) and resulting transfer function from SH waves (b). A HVSR curve from surface waves (c).

Surface Wave Program – Mat Disperse: To simulate surface wave propagation, a publically-available MATLAB computer program call "Mat_Disperse," based on algorithms from Hisada (1994) and Lai and Rix (1998), was implemented in this study. Mat_Disperse is a set of Matlab m-files developed to solve the eigenvalue problem for Rayleigh waves in an elastic, vertically heterogeneous halfspace, and returns the Green's function of the two-dimensional Rayleigh wave displacement field (Lai and Rix 1998). The horizontal and vertical displacements are calculated from the superposition of several modes of propagation of the Rayleigh wave. To obtain the HVSR results needed for this study, the spectrum of horizontal displacements was divided by the vertical spectrum.

The vertical displacement at each sensor can be computed by superposing the contributions of all the Rayleigh modes of propagation when a harmonic unit point source is vertically applied on the free surface of the given layered system (Lai and Rix 1998). The displacement and amplitude of Rayleigh waves can be expressed as:

$$u(x,z,\omega) = \sum_{j=1}^{M} [A(x,z,\omega)]_j \exp\left[i\left(\omega \cdot t - k_j \cdot x - \pi/4\right)\right] \tag{4.7}$$

$$[A(x,z,\omega)]_j = \frac{F_0 \cdot r_2(z_s,k_j,\omega)}{4V_j \cdot U_j \cdot I_j \cdot \sqrt{2\pi x k_j}} \cdot r_1(z,k_j,\omega) \tag{4.8}$$

where, u is the displacement, M is the total number of modes, k_j is the wave number, ω is the angular frequency, z_s is the source depth, $[A(x,z,\omega)]_j$ is the modal amplitude of the modal displacement, F_0 is the amplitude of the vertical harmonic force, V_j is the modal phase, U_j is group velocities, I_j is the first energy integral, and $r_1(z,k_j,\omega)$ is the

displacement eigenvectors. Eq. 4.7 and 4.8 only account for contributions of Rayleigh wave propagation and neglect the influence of body waves (Lai and Rix 1998).

An example of an HVSR result for the same case of a homogenous layer over bedrock is presented in Figure 4.1c. This is often referred to as the *ellipticity* of the surface wave. The simulated HVSR frequency peak from surface waves (2.57 Hz) is very close to the SH wave resonance of 2.5 Hz, as shown in Figure 4.1. The comparison shown in Figure 4.1 demonstrates how the 1D fundamental frequency of the site (due to SH propagation) can be estimated from the HVSR of Rayleigh waves, in the absence of body waves.

The two possible interpretations for the origin of the HVSR frequency peak in experimental data, namely (1) ambient SH waves are dominant and produce amplifications at the site frequency or (2) surface waves dominate the ambient wave field and the frequency peak is produced by a decrease in energy of the vertical spectrum, are demonstrated in Figure 4.1. The agreement between Rayleigh wave ellipticity frequency peaks and the "true" site resonance was examined for several simulated site conditions, as described in the next section.

4.2.2 Simulated Shear Wave Velocity Profiles

Seven simulated soil profiles were examined in this study, as presented in Table 4.1 and Figure 4.2. Case 1 (Figure 4.2a) is the baseline case with a uniform, constant velocity layer. Cases 2 and 3 (Figure 4.2b and Figure 4.2c) are two-layer profiles with differing degrees of velocity contrast. Case 4 (Figure 4.2d) is a stiff-over-soft two-layer

profile. Cases 5 and 6 (Figure 4.2e and Figure 4.2f) are three-layer profiles with differing degrees of velocity contrast. Case 7 is a profile with a power function relationship for velocity change with depth (see Table 4.1). The exponent "n" was set equal to 0.25 (a common value used to represent V_S change with depth in normally-consolidated soils) and the coefficient "c" was set equal to 138.85 to obtain an average velocity of 500 m/s over the depth of the profile. Each of the seven profiles was created to have an average velocity of 500 m/s over the 50 m depth of the profile, as calculated using:

$$V_{S_{"True"}} = \frac{\sum h}{\sum \frac{h_i}{V_{S_i}}} \tag{4.9}$$

where, "h" is the total height of the profile, and "h_i" and "V_{Si}" are the height and shear wave velocity for each individual layer.

Data were generated and analyzed for these seven profiles for several different conditions as described below.

Table 4.1 Seven simulated V_S profile cases used in the analytical study.

Case	Number of Layers	Height of Profile (Meters)	Shear Wave Velocity (m/s)			$V_{S,AVG}$ (m/s)
			1st Layer	2nd Layer	3rd Layer	
1	1	50	500	-	-	500
2	2	50	400	667	-	500
3	2	50	458	550	-	500
4	2	50	700	457	-	500
5	3	50	400	537	600	500
6	3	50	364	500	800	500
7	25	50	Power Function: $V_S = c \cdot \bar{\sigma}^n$			500

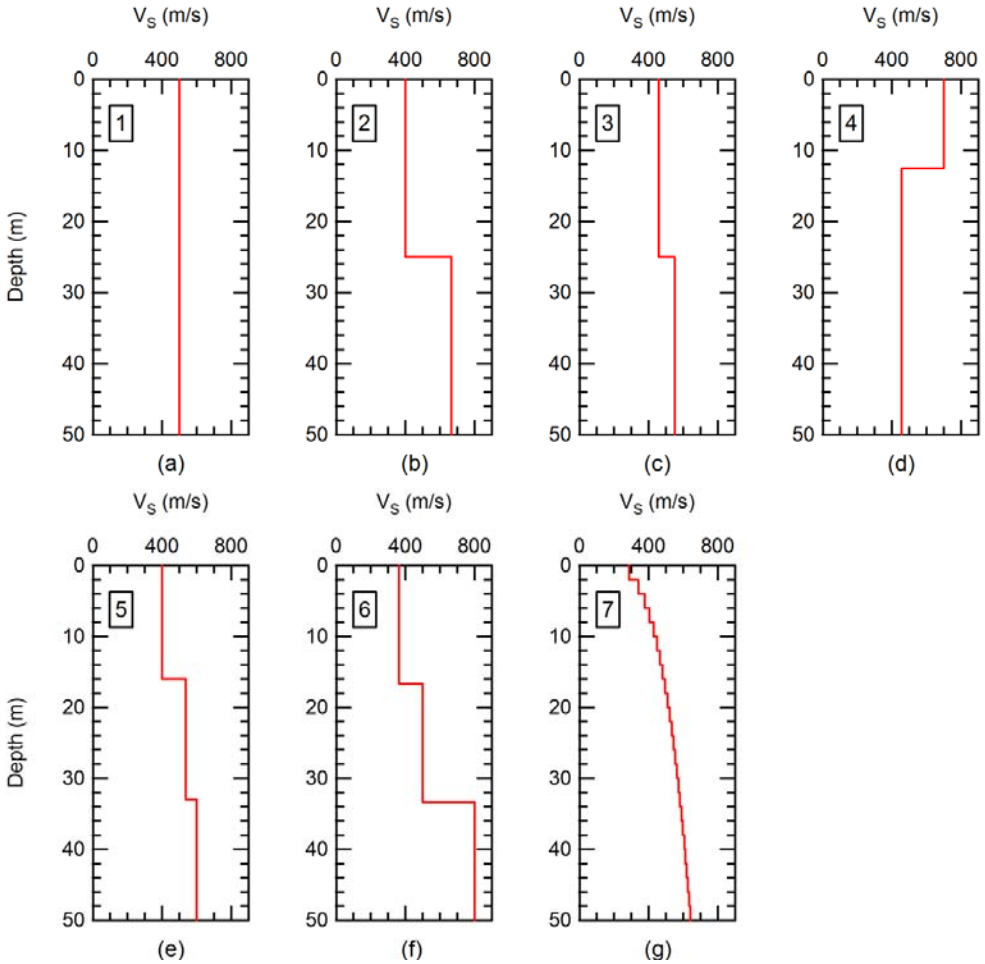

Figure 4.2 Shear wave velocity profile for Case 1 through 7, (a) through (g), respectively. ($V_{S,AVG}$ for all profiles is 500 m/s)

4.2.3 Data Generation and Analysis

Transfer functions and HVSR plots were generated by entering the soil V_S profile data for each of the cases mentioned above into the two computer programs described in Section 4.2.1. The parameters that were varied in this portion of the study were (1) shear wave velocity contrast between the soil and rock and (2) Poisson's ratio (ν) in the soil layer. Mass density values (1.8 g/cm^3 for the soil and 2.7 g/cm^3 for rock) and material

damping values (2% for both the soil and rock) were held constant through this portion of the study. The parameters that were varied are described below.

Shear Wave Velocity Contrast: The V_S contrast is defined here as the ratio of the halfspace V_S divided by the $V_{S,AVG}$ of the soil profile. For example, the V_S contrast ratio for Case 1 between the 500 m/s layer and the 2500 m/s halfspace is 5.

Table 4.2 Halfspace V_S values that were used for each of the seven cases.

Halfspace Shear Wave Velocities, V_S (m/s)	Seven Cases						
	1	**2**	**3**	**4**	**5**	**6**	**7**
800						X	
900						X	
1000	X	X	X	X	X	X	X
1062.5		X			X	X	
1125		X	X		X	X	X
1150	X						
1250		X	X	X	X	X	X
1300	X						
1375		X	X	X	X	X	X
1500	X	X	X	X	X	X	X
1625				X			
1650	X						
1750		X	X	X	X	X	X
1800	X						
1875		X		X	X	X	
1937.5					X	X	
1950					X	X	
2000	X	X	X	X	X	X	X
2250		X	X	X	X	X	
2300	X						
2400	X						
2500	X	X	X	X	X	X	X
3000	X	X	X	X	X	X	X

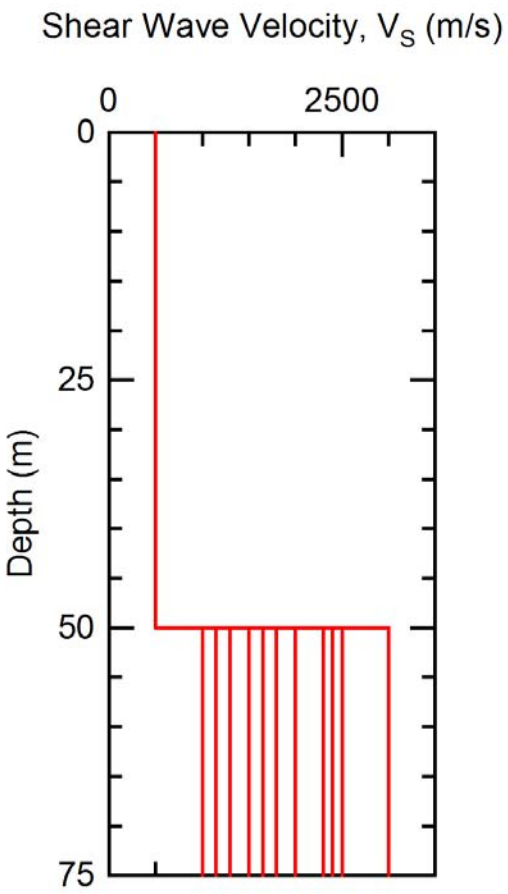

Figure 4.3 The different halfspace V_S values that were used in the V_S ratio study for Case 1.

The V_S ratio study was performed to examine the effect of varying the halfspace V_S values for the seven cases on the frequency estimates. Halfspace V_S values for the seven cases were varied from 800 m/s to 3000 m/s, corresponding to V_S ratios of 1.6 to 6, as shown for all seven cases in Table 4.2. Figure 4.3 shows the values used for Case 1. Poisson's ratio values were assigned to be consistent with a fully-submerged profile, assuming compression wave velocity (V_P) of 1500 m/s in the water. Frequency peaks from DEEPSOIL and Mat_ Disperse were compared. Results are presented and discussed in Section 5.2.1 of Chapter 5. In addition to the comparison of frequency values, average profile velocity values were calculated from the frequency peaks and compared to the true values, as discussed in Section 4.4.3.

Poisson's Ratio: For this part of the study, the consistency of the fundamental frequency estimates with varying Poisson's ratio (ν) was examined. Poisson's ratio in soil typically ranges from 0.2 to 0.33 for unsaturated conditions; however, when the soil is saturated (as is typical under the water table), ν can approach values near 0.5. Poisson's ratio can be directly related to V_P and V_S as:

$$\frac{V_P}{V_S} = \sqrt{\frac{2-2\nu}{1-2\nu}} \tag{4.10}$$

In this portion of the study, V_S was held constant and ν was varied from 0.2 to 0.49, as shown in Table 4.3. To isolate the influence of ν on the frequency peak, the halfspace V_S was held constant at a high value of 2000 m/s (V_S ratio of 4). Figure 4.4 shows the different V_P values that were examined for Case 1 correspond to ν values in Table 4.3.

The comparison between "true" and estimated values for site resonance as a function of ν is presented in Section 5.2.2 of Chapter 5.

Table 4.3 Poisson's ratio values that were applied to all seven cases.

Poisson's ratio, ν
0.2
0.25
0.3
0.33
0.35
0.4
0.4375
0.45
0.49

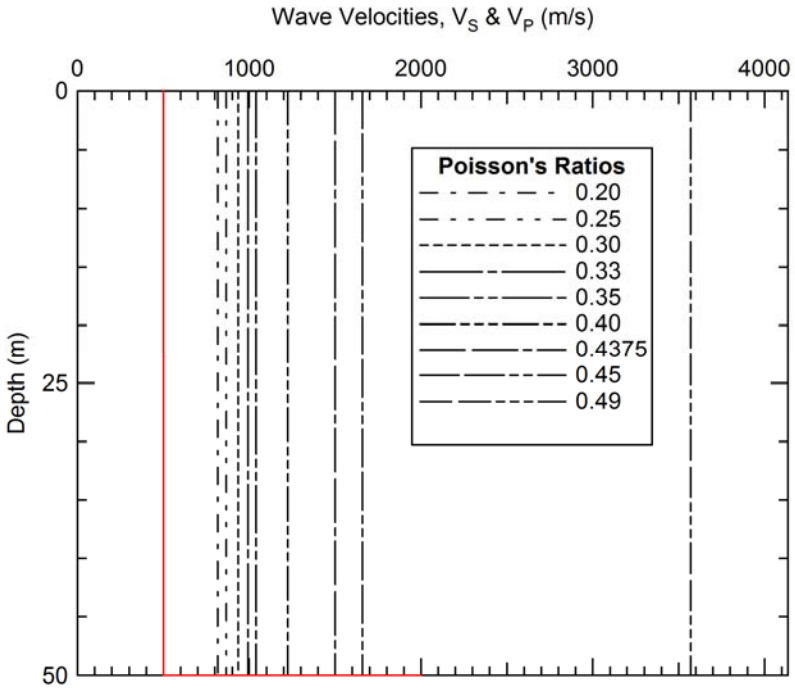

Figure 4.4 Values of V_P (dashed lines) used with the corresponding constant V_S value (solid line) for Case 1 to study the influence of Poisson's ratio.

4.2.4 Average Velocity Calculation

In addition to comparing the site frequency estimates, comparisons were made between the "true" $V_{S,AVG}$ of each profile:

$$V_{S,AVG_{"True"}} = \frac{\sum h}{\sum \frac{h_i}{V_{S_i}}} \tag{4.9}$$

(calculated directly from the known velocity values) and the "estimated" average velocity (from Section 2.4.2):

$$V_{S,AVG_{"Est"}} = f_0 \cdot 4h \tag{2.2}$$

calculated using the frequency values identified from the transfer function and HVSR plot. As discussed above, each of the simulated profiles was designed to have the same average velocity of 500 m/s (calculated using Eq. 4.9). The estimated velocity values were calculated for each case using Eq. 2.2 with the known depth of the soil (h = 50 m) and the fundamental frequency (f_0). The relationship shown in Eq. 2.2 is only exact for the case of a uniform velocity layer. However, it is commonly used for other V_S profile conditions and was used in the study performed by Bodin et al. (2001) to obtain the $V_{S,AVG}$ versus sediment thickness relationship.

4.3 Study of HVSR Processing Parameters

In this section, the influence of the data processing parameters on the experimental HVSR results was studied. The experimental data collection procedures were described in Section 3.4. A description of the HVSR processing procedure is presented in this section, along with detailed explanations of the parameters used in the data processing.

4.3.1 Processing of HVSR Data

The HVSR data processing is performed by breaking the ambient noise record into individual windows and performing a Fast Fourier Transform (FFT) to each window. The FFT transforms the noise record from the time domain into the frequency domain. The horizontal spectra are then merged and divided by the vertical spectrum, creating a horizontal to vertical spectral ratio (HVSR) for each window. The HVSR curves for each window are combined into an average HVSR curve. An ideal noise record would have no transients, which are often near-field, high-amplitude signals (caused by footsteps,

close traffic, etc) that can distort the results. Transients can be avoided in the data analyses by using automated window selection tools in the HVSR processing program.

Table 4.4 Values of processing parameters used in this portion of the study.

J-SESAME Parameters Tested								
Window Length (sec)	**Transient STA/LTA**		**Filter (Hz)**		**Merging**	**Smoothing**	**Bandwidth (Hz)**	**Tapering**
	Min	**Max**	**Low Pass**	**High Pass**				
50	0.25	1.25	15	0.25	Arithmetic	Konno & Ohmachi	20	Cos
75	0.5	1.5	20	0.5	Geometric	Linear	30	Box
100	0.75	2	25	1.0	Quadratic	None	40	-
200	-	2.5	30	5.0	Complex	-	50	-
-	-	-	35	-	-	-	-	-

Table 4.5 Default values of processing parameters.

Default J-SESAME Parameters used in Experimental Method	
Window Length	50 seconds
Min STA/LTA	0.5
Max STA/LTA	1.5
Merging	Arithmetic
Smoothing	Konno & Ohmachi
Bandwidth	40 Hz
Tapering	Cos
Filter	None
Offset	None

The program J-SESAME was used to process the ambient noise data collected in the Mississippi embayment. J-SESAME was developed as part of a European project SESAME (**S**ite **E**effect**S** assessment using **AM**bient **E**xcitations) and provides a graphical interface for the HVSR technique used in local site effect studies. J-SESAME allows for automatic and manual window selection, several processing options, and a display of processed results. The automatic window is used to select the most stationary parts of ambient vibrations, while avoiding transients. The parameters in J-SESAME tested for this study are displayed in Table 4.4 and the default parameters for variables that were used when not being studied are listed in Table 4.5. All of the default parameters were selected in accordance with the recommended procedures and guidelines set forth by the SESAME workshops (SESAME 2004). The purpose of varying the processing parameters was to evaluate the consistency of the frequency peaks estimated from the HVSR processing under different processing conditions. The following subsections discuss in more detail the processing parameters that were examined.

Window Length: The window length (l_w) parameter refers to the length of time in seconds used to calculate individual HVSR curves. Two criteria need to be met to ensure a reliable measurement:

$$f_0 > \frac{10}{l_w} \tag{4.11}$$

$$l_w \cdot n_w \cdot f_0 > 200 \tag{4.12}$$

where, n_w is the number of windows. Eq. 4.12, can be expressed in terms of significant cycles (n_c) per measurement as:

$$n_c = l_w \cdot n_w \cdot f_0 \tag{4.13}$$

According to SESAME (2004), Eq. 4.11 and 4.12 are meant to ensure that at least 10 significant cycles of the fundamental frequency (f_0) occur in each window, and that there is an adequate amount of significant cycles (200) in the overall measurement, respectively.

Table 4.6 presents the recommended window lengths, based on J-SESAME (2004) user guidelines for different expected values of f_0. For the Mississippi embayment, the expected f_0 value for the soil/bedrock interface is between 0.2 and 0.4 Hz. The number of windows (n_w) recommended for all cases is ten or greater. In order to ensure a minimum of n_w = 10 with a HVSR frequency peak of 0.2 Hz, fifty seconds was the default value of l_w used in this study. The effect of varying l_w was examined by using window lengths from 50 to 200 seconds. The HVSR frequency values with less than the recommended n_w value of ten are demarcated with ($^+$) in the corresponding tables. Results from the analysis are presented in Section 5.3.1 of Chapter 5.

Table 4.6 Recommended processing parameters and recording duration (SESAME 2004).

f_0 [Hz]	**Minimum value for l_w [s]**	**Minimum number of significant cycles [n_c]**	**Minimum number of windows [n_w]**	**Minimum useful signal duration [s]**	**Recommended minimum record duration [min]**
0.2	50	200	10	1000	30
0.5	20	200	10	400	20
1	10	200	10	200	10
2	5	200	10	100	5
5	5	200	10	40	3
10	5	200	10	20	2

Transient Thresholds: Transients are short-duration disturbances that are often caused by footsteps, traffic, etc. The HVSR analysis performs best when transients are removed from the noise recordings. J-SESAME removes transients by using an anti-trigger window selection to keep only the most stationary parts of ambient vibrations. This process uses a comparison between the short-term average (STA) and the long-term average (LTA) of signal amplitude. Default values used in this study for STA and LTA, are 1.0 and 25 seconds, respectively, as recommend by SESAME (2004). Also, default values of the minimum and maximum STA/LTA ratio are 0.5 and 1.5, respectively, as shown in Table 4.5. The effect of varying the minimum and maximum STA/LTA thresholds on the frequency peaks was examined. The parameters used for the threshold values are listed in Table 4.4.

Merging: The merging parameter pertains to the method of combining horizontal components before dividing by the vertical component. The merging parameters in J-SESAME can combine the horizontal components in one of four ways: geometric mean, arithmetic mean, quadratic, and complex. The effect of using different merging methods on the frequency peak was examined. Results are presented in Section 5.3.3 of Chapter 5.

Smoothing: The raw HVSR spectra obtained from the analyses are typically smoothed to remove sharp frequency peaks from the spectra. This portion of the study examined the different smoothing options in J-SESAME, namely: Konno & Ohmachi, linear, and none (no smoothing). The Konno & Ohmachi smoothing parameter is recommended by SESAME (2004) and was the default smoothing parameter used in this study.

Bandwidth of Smoothing Function: The bandwidth is a function of the smoothing parameter and should be adjusted depending on the circumstances. The J-SESAME guidelines recommend decreasing the smoothing bandwidth when a broad frequency peak is present to allow for a possible frequency peak to emerge. Also, when multiple frequency peaks are present, it is recommended to increase the smoothing bandwidth to allow for a dominate frequency peak to present itself. For this study, the bandwidth was adjusted from 20 to 50 (Hz) for the Konno & Ohmachi smoothing parameter (see Table 4.4) while holding the other parameters to the default values, as shown in Table 4.5. A small bandwidth value will lead to a strong smoothing, while a large value will lead to a low smoothing of the Fourier spectra (Wathelet 2006). The recommended and typical bandwidth value is 40 Hz.

Tapering: The tapering parameter is used to minimize the border effects due to the windowing of the Fourier amplitude spectra. The tapering parameter options are either a cosine or box. SESAME (2004) gave no recommendation on which tapering parameter to use. In this study, the cosine parameter was the default.

Filter: The purpose of the filter is to remove known artificial, erroneous frequency components before the windows are processed. The high pass filter removes all frequency components below a frequency threshold; whereas, the low pass filter removes all frequency components above a frequency threshold. SESAME (2004) recommends applying a filter when the spurious frequency of industrial origin coincides with, or is not far from, the true site frequency. The filter should eliminate the artifact and its effects on the HVSR curve. Since most of the sites in this study were in quiet, rural areas, no filters

were set as default values. In this study the parameters were varied from 15 to 35 Hz for the low pass filter and 0.25 to 5.0 Hz for the high pass filter while holding the other parameters to the default values shown in Table 4.5.

4.4 Comparison of Experimental to Simulated Results for Sites in the Mississippi Embayment

The approach in this portion of the study was to compare the experimental results (frequency and estimated $V_{S,AVG}$) to simulated results using the best available information for the V_S profile at each of the eleven measurement sites. In the previous study of Bodin et al. (2001), no information was available on the subsurface profile conditions at their sites. Therefore, many of their conclusions were based on speculation of the subsurface conditions. In this study, full-depth V_S profiles were developed by combining V_S profiles from active-source surface wave measurements at the eleven sites (Bailey 2008) with deeper information from the reference profile of Romero and Rix (2005). Comparisons were made between the experimental and simulated results. Details of the methodology used are presented below.

4.4.1 Development of Site V_S Profiles for Simulation Studies

Shear wave velocity profiles for each of the eleven sites were created by combining V_S profiles to depths of about 250 m from surface wave measurements (Bailey 2008) with deeper V_S information from the reference profile of Romero and Rix (2001). Bailey (2008) developed V_S profiles for each site by inversion of surface wave dispersion measurements. The V_S profiles generally reached depths of 200 to 250 m. Bailey (2008) developed the V_S profile using a generic profile layering with no prior knowledge of the

soil lithology at the site. These profiles are shown for each site in Figure 3.17 and Figure 3.18 of Chapter 3.

Romero and Rix (2005) developed a reference V_S profile for the full depth of the embayment by combining measured V_S data for the top seventy meters (Romero and Rix 2001) with deeper information from multiple sources including: sonic logs, correlations, and models (discussed in greater depth in Section 2.4.2). Due to a lack of information below 250 m at these eleven sites, the deep portion of Romero and Rix (2005) profile was merged with the site-specific profile above 250 m to create an estimate of the V_S profile conditions at each site, as shown for Site 1 in Figure 4.5. The halfspace V_S value of 2500 m/s is consistent with estimated velocity for the Knox Dolomite (2000 to 3400 m/s) in the Mississippi embayment (Cramer 2006). The water table at sites in the embayment is relatively high (within 3-5 m of surface) when compared to the full depth of the soil column, leading to the decision to assume the V_S profiles were fully saturated.

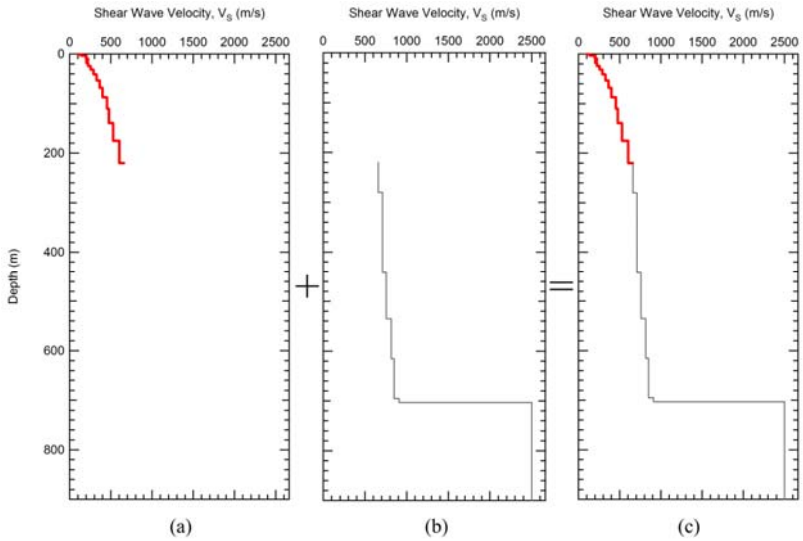

Figure 4.5 The V_S profile of Site 1 measured from surface waves (Bailey 2008) (a) is combined with a reference profile (b) (Romero and Rix 2005) to produce an estimated site V_S profile from the ground surface to bedrock (c).

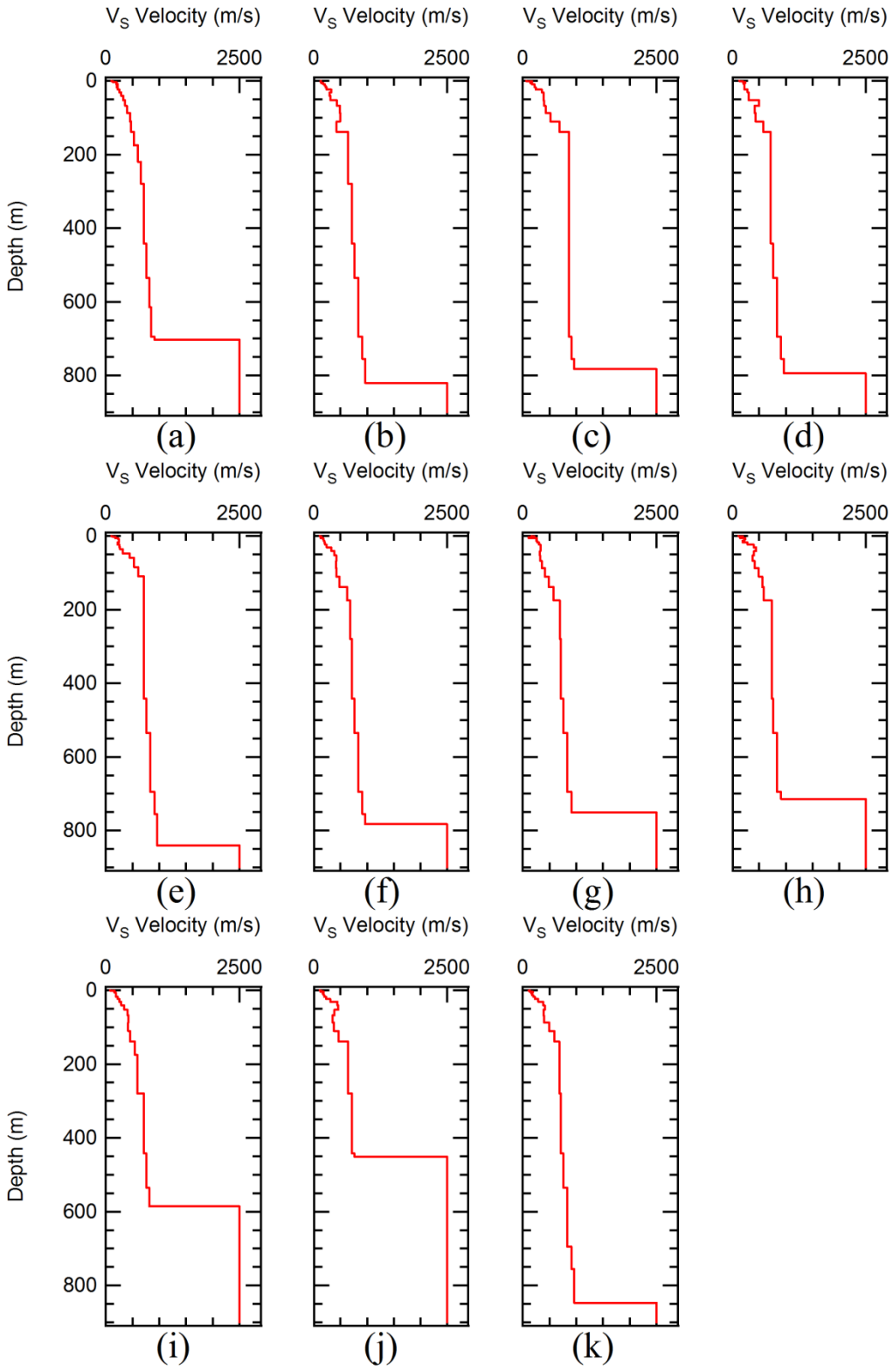

Figure 4.6 Estimated shear wave velocity profiles extended to bedrock for: Sites 1 through 11, (a) through (k) respectively.

Table 4.7 Average shear wave velocities calculated from estimated V_S profiles using Eq. 4.9 for the eleven sites.

Average Shear Wave Velocities from Estimated V_S Profiles			
Site	**$V_{S,AVG}$ (m/s)**	**Site**	**$V_{S,AVG}$ (m/s)**
1	582	7	613
2	625	8	629
3	706	9	542
4	641	10	509
5	672	11	649
6	612		

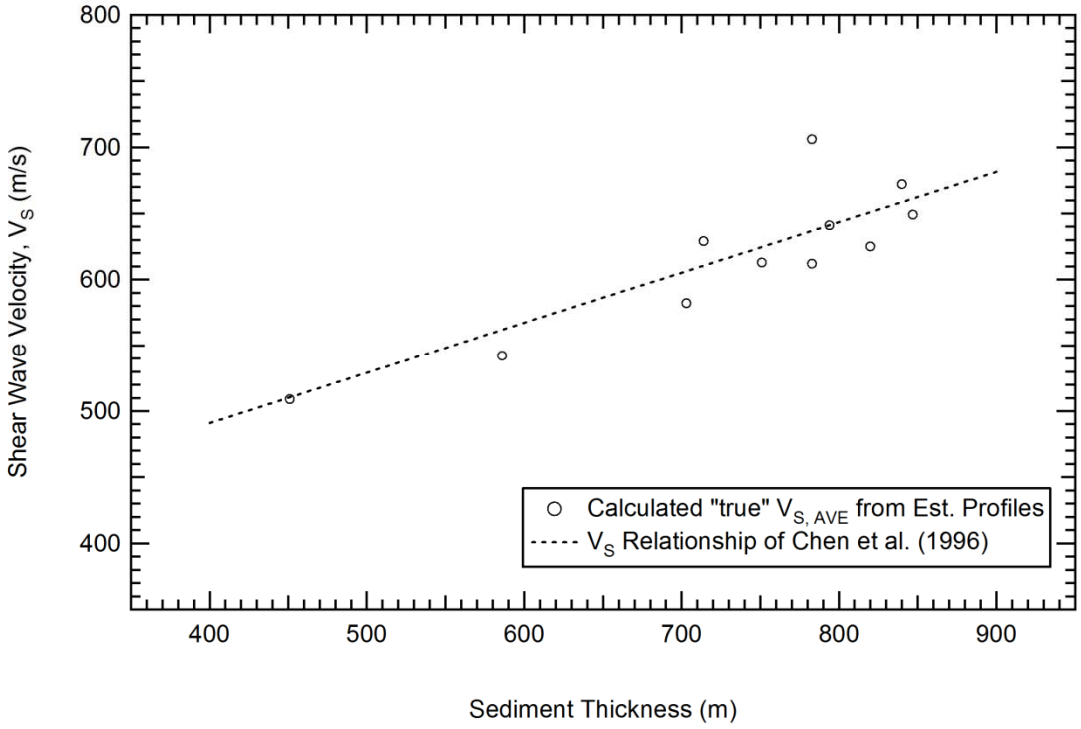

Figure 4.7 Plot showing the comparison between the $V_{S,AVG}$ calculated from estimated full-depth V_S profiles to relationship for $V_{S,AVG}$ in the Mississippi embayment developed by Chen et al. (1996).

In some instances, the V_S measurements from Bailey (2008) were higher than the corresponding V_S measurements of Romero and Rix (2005) at the same depth. In these

instances, the higher V_S measurement from Bailey (2008) was continued to greater depths until overtaken by the reference profile. The thickness of the soil deposits at each site was provided by Professor Roy Van Arsdale from the University of Memphis using interpolated values based on nearby wells, as discussed in Section 3.3.1. The merged V_S profiles, developed for each site, are presented in Figure 4.6. Table 4.7 presents the average V_S values for each profile calculated using Eq. 4.9. It is interesting to note that the $V_{S,AVG}$ values calculated for each of these sites agree with the independently developed $V_{S,AVG}$-sediment thickness relationship of Chen et al. (1996), as shown in Figure 4.7.

4.4.2 Examination of Fundamental Frequency Estimated from HVSR Frequency Peak

An examination of the reliability of the estimate of the fundamental frequency from the HVSR frequency peak was made by entering the V_S profiles for each site (Figure 4.6) into the computer programs mentioned earlier in Section 4.2 (DEEPSOIL and Mat_ Disperse). Typical values used in DEEPSOIL and Mat_Disperse are shown in Table 4.8. Interpretation of the results was aided by results from the parametric study performed on the synthetic profiles (described in Section 4.2.2). The fundamental site frequency estimates identified by each method were compared to the experimental HVSR frequency peak developed from the field measurements. Results are presented in Section 5.4 of Chapter 5.

Table 4.8 Typical values used in DEEPSOIL and Mat-Disperse.

Typical Values used in DEEPSOIL and Mat_Disperse		
	Soil	**Bedrock**
Damping (%)	2	2
Unit Weight (kN/m^3)	18.6	24.3
Range of V_S (m/s)	64 - 910	2500
Range of V_P (m/s)	111 - 1800	4545
Range of ν	0.25 - 0.49	0.28

4.4.3 Average Velocity Comparison using HVSR Frequency Peaks

The approximate method described in Eq. 2.2 of Section 2.4.2 was used to calculate an estimated value of $V_{S,AVG}$ for the full profile depth using the fundamental frequencies obtained from DEEPSOIL and Mat_Disperse. These average velocity estimates $\left(V_{S,AVG_{"Est"}}\right)$ were compared to the "true" $V_{S,AVG}$ values (calculated directly from the V_S profile using Eq. 4.9) for the sites listed in Table 4.7. Results of these comparisons are presented in Section 5.4.3 of Chapter 5.

4.4.4 Examination of Second Frequency Peak in Experimental HVSR Data

The examination of the higher experimental HVSR frequency peak (f_1) was made in a similar fashion to the examination for the lowest frequency peak (f_0). The second frequency peaks obtained from the V_S profiles extended to bedrock were compared to the second frequency peaks from the actual HVSR experimental data.

In addition, to examine the possibility of the second frequency peak being caused by a strong shallow contrast, simulations were performed using only the V_S profile in the top 200 to 250 m (surface wave analysis profiles) without the extension to bedrock. The strong contrast of the deep soil/rock interface was removed in the portion of the analysis to prevent higher modes of shear wave resonance from masking contributions from shallow interfaces. The frequency peak identified from the shallow profile was compared to the second frequency peak from the actual HVSR experimental curve for each site. Results are presented in Section 5.4.4 of Chapter 5.

4.5 Summary

This chapter presented the methods used to perform numerical simulations and experimental analyses for this research. Two computer programs for determining the transfer function and the surface wave HVSR frequency peak of a site were described. The development of synthetic V_S profiles for the analytical study was also presented. Processing parameters used for developing experimental HVSR results were discussed. Lastly, the methodology used to develop representative V_S profiles for the eleven experimental sites was discussed, along with the analysis procedures used to meet the objectives of this study.

5. RESULTS AND ANALYSIS

5.1 Introduction

In this chapter, results from the three studies described in Chapter 4 are presented. The first is a parametric study of variables affecting the frequency peaks in HVSR measurements. This study was performed using simulated surface wave data for a variety of subsurface conditions, and examines the influence of: Poisson's ratio, V_S contrast, and V_S distribution with depth. The second study is an examination of the influence of HVSR processing parameters on the frequency peaks derived from HVSR processing of the experimental data. Variables that were examined for the purpose of verifying the consistency of the frequency estimates included: window length, transient removal method, filtering, merging of horizontal components, spectral smoothing method, smoothing bandwidth, and window tapering. The third and final study provides results from simulations of surface wave and body wave propagation for expected site conditions (V_S profiles) at the eleven experimental sites. These results are used along with the experimental results and results from the parametric studies to meet the two main objectives of this research, namely to explain: (1) the reason for the inconsistent V_S estimate from HVSR measurements in the Mississippi embayment and (2) the origin of the second frequency peak observed in HVSR plots of the Mississippi embayment.

5.2 Study of Variables Affecting HVSR Measurements

Surface and body wave propagation were simulated for different conditions of velocity contrast and Poisson's ratio for seven sites, each with an $V_{S,AVG}$ of 500 m/s, as

presented in Section 4.2.2. The purpose is to compare the HVSR frequency peak (f_{HVSR}) from HVSR processing of the surface waves to the fundamental frequency peak (f_0) obtained from the propagation of SH waves. In addition, this section of the study examined the effectiveness of the method (Eq. 2.2) used to estimate $V_{S,AVG}$ of the profile from the frequency values. Average shear wave velocities calculated from f_0 and f_{HVSR} were compared to the "true" $V_{S,AVG}$ (Eq. 4.9) calculated from the known V_S profiles. The results are presented in the next three subsections followed by a summary section on the findings from this portion of the study.

5.2.1 Effect of V_S Contrast

Fundamental Frequency Estimate: In this section, the effect of V_S contrast between soil and rock layers on the fundamental frequency estimate from the HVSR frequency peak is studied. For each profile condition discussed in Chapter 4, vertical and horizontal displacements of surface wave motions were calculated using the MATLAB program "Mat_Disperse." In addition, the transfer function from horizontally polarized shear waves was calculated using DEEPSOIL, as described in Section 4.2.1. The f_{HVSR} value from the surface wave simulation was compared to the f_0 from the transfer function obtained from DEEPSOIL for each of the seven cases, with V_S ratios ranging from about two to six.

The site frequency from DEEPSOIL (f_0) is what would be obtained if V_S information were known at the site, and is therefore, considered here to be the "true" value of the site resonant frequency. The frequency obtained from the surface wave simulation (f_{HVSR}) is

an estimate of the resonant frequency that would be obtained from HVSR analyses of Rayleigh waves, with no a priori knowledge of the V_S profile. As can be seen in Figure 5.1, the HVSR measurements provide a good estimate of site fundamental frequency (within an average of 3.6%) for cases where the V_S ratio exceeds about 3.5. For large V_S ratios, the best agreement was observed for the uniform profile of Case 1, where the error in the frequency estimate was only 2.2%. In other cases, the frequency was underestimated by 2.0% to 4.7% at large V_S ratios using the HVSR approach. In cases where the velocity ratio was less than 3, the f_{HVSR} value was as much as 30 to 70% higher than the "true" value of the fundamental frequency. These results are consistent with past studies of the HVSR method that recommended V_S contrasts of greater than 4 to obtain reliable results (Bonnefoy-Claudet et al. 2008; SESAME 2004).

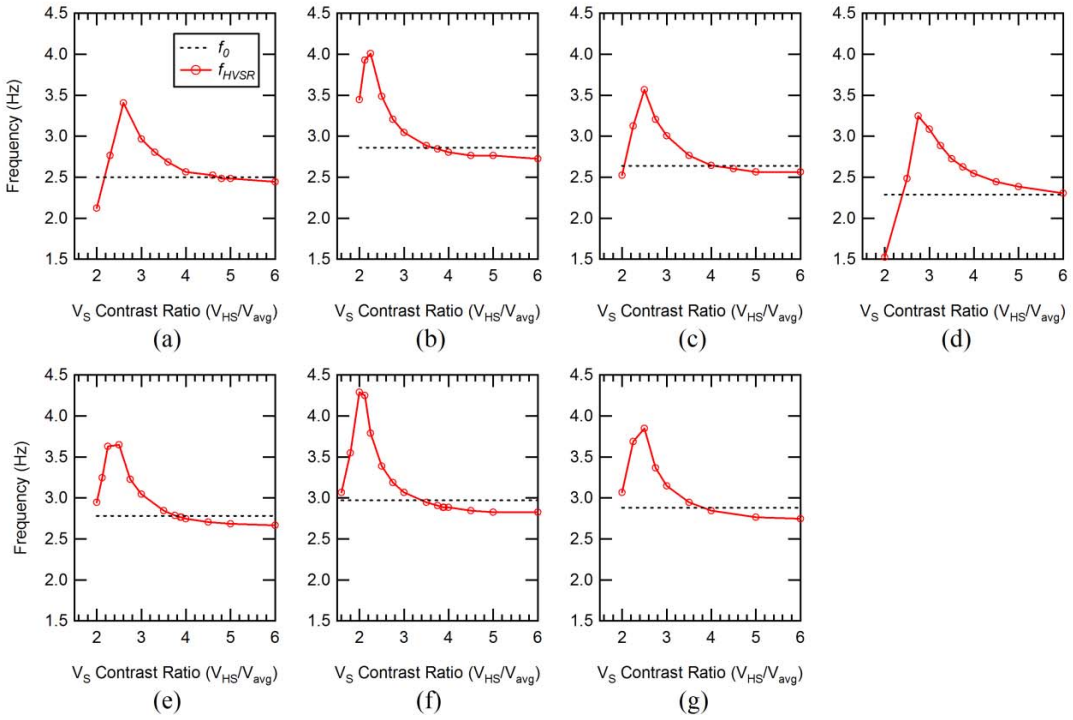

Figure 5.1 Peak frequencies for saturated conditions of Cases 1 through 7, (a) through (g), respectively.

Average Velocity Estimate: The $V_{S,AVG}$ for each profile condition (Cases 1 through 7) was calculated from the site frequency estimates (f_0 and f_{HVSR}) and bedrock depth (50 m) using the common $V_{S,AVG_{"Est"}}$ approximation as described in Section 2.4.2. The average velocity estimate from the approximate method was compared to the "true" value using a normalized velocity, V_n, calculated as:

$$V_n = \frac{V_{S,AVG\ "Est"}}{V_{S,AVG_{"True"}}} \tag{5.1}$$

where, $V_{S,AVG_{"Est"}}$ is the V_S calculated from the approximation of Eq. 2.2 and $V_{S_{"True"}}$ is the value calculated directly from wave travel times (Eq. 4.9). As can be observed in Figure 5.2, for the simple case of a homogeneous layer over the stiff halfspace (Case 1), Eq. 2.2 provides identical results to the true average velocity of the profile when f_0 is used. However, for more complex profiles, where V_S values change with depth, the average velocity estimate can be significantly in error using this simple relationship. For the other six cases examined in this study the approximate method typically produced an over-estimation of the average velocity of 5.6 to 18.8%, depending on the profile (for Case 4 the average velocity was underestimated by 8.4%).

The results from these simulations show that for simple profiles (Case 1) and high velocity contrasts (greater than 3.5), the HVSR method combined with the approximate method to calculate $V_{S,AVG}$ provides a very good estimate of average velocity of the profile. However, for conditions that deviate from this simple case, the frequency estimate and average velocity estimate can differ significantly from the true values.

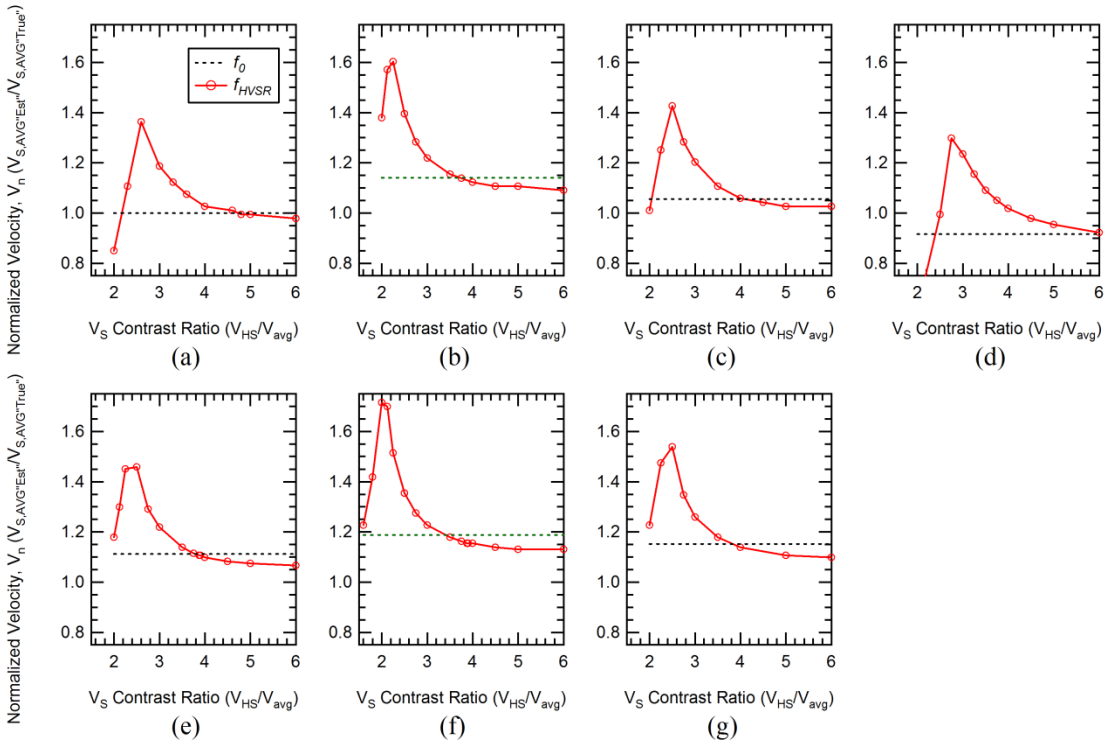

Figure 5.2 Normalized velocities for Cases 1 through 7, (a) through (g), respectively.

5.2.2 Poisson's Ratio

In the simulations presented above, Poisson's ratio (ν) was calculated based on the assumption that the profile was submerged (water table at the surface). In this portion of the study, the surface wave HVSR measurements were simulated using values of ν that represent unsaturated or partially saturated conditions, as described in Section 4.2.3 of Chapter 4. To isolate the influence of ν, the V_S ratio was held constant at a high value of 4. The HVSR measurements provide a good estimate of site fundamental frequency (within an average of 5.1%) for saturated cases where ν is equal to 0.49. Figure 5.3 shows the change in the normalized velocity (Eq. 5.1) with changes in Poisson's ratio. The best estimates were obtained with high values of ν (submerged case). As ν

decreased, the error in the average velocity estimate from the HVSR method increases. Typical conditions for dry soils (Poisson's ratio of 0.2 to 0.33) produce an average velocity value that is significantly overestimated. For the case of continuously increasing velocity with depth (Case 7) the error is as much as 35 % at low values of Poisson's ratio.

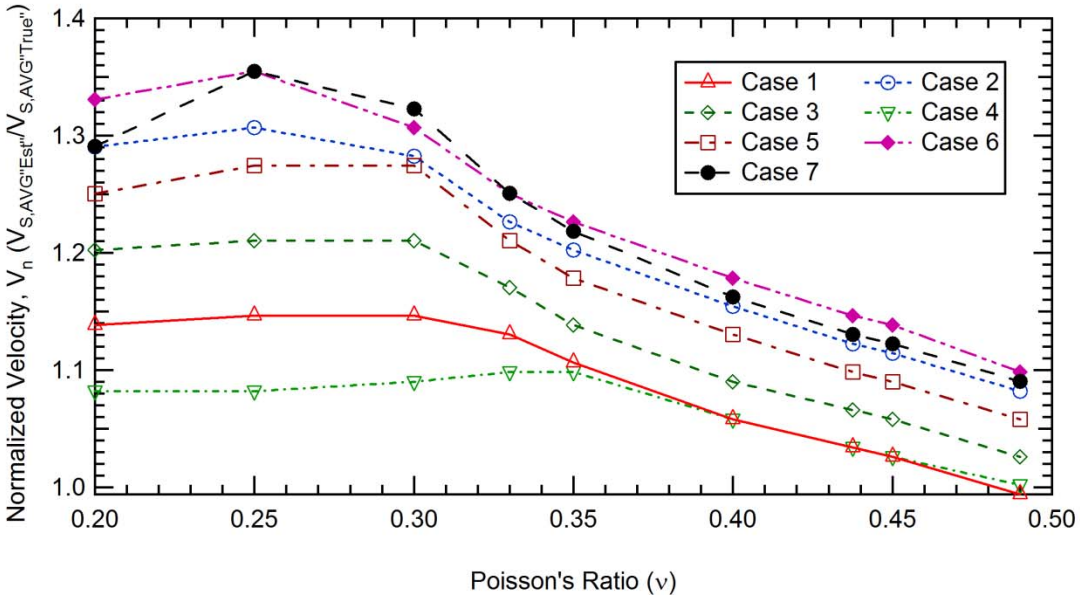

Figure 5.3 Changes in normalized velocity (calculated using f_{HVSR}) with changes in Poisson's ratio for all cases 1-7.

These results demonstrate that the HVSR method may not provide reliable velocity estimates for cases where the soil is unsaturated or partially saturated (deep water table).

5.2.3 Summary of Findings from Simulation Study

The following conclusions can be drawn from the studies performed using simulated profiles:

(1) Reliable fundamental frequency estimates from HVSR required V_S contrasts of about 3.5 or greater. For high V_S contrast, HVSR frequency estimates were lower in most cases but within 3.6% of true values. These findings are in

agreement with past studies and recommendations (Bonnefoy-Claudet et al. 2008; SESAME 2004).

(2) Poisson's ratio has a significant effect on results obtained using the HVSR method with Rayleigh wave propagation. Percent errors increase as ν decreases leading to the conclusion that high values of ν provide more accurate results. For high values of ν, HVSR frequency estimates were lower in most cases but within 5.1% of true values.

(3) Although frequency can be reliably estimated from the HVSR method, the approximate method used for estimating $V_{S,AVG}$ deviates from the true $V_{S,AVG}$ when V_S profiles become more complicated than a simple, uniform material.

These results will have implications on the interpretation of experimental HVSR results in the Mississippi embayment, as discussed in Section 5.4.

5.3 Study of the Influence of Processing Parameters on HVSR Results

The parameters used to process the experimental HVSR measurements are discussed in Section 4.3 of the Chapter 4. The purpose of this portion of the study is to investigate the variability in frequency values produced by changing parameters used in the processing of the HVSR data. The processing parameters that were used are listed in Table 4.4 of Chapter 4. The default values of these parameters, which are consistent with values recommended by SESAME (2004), are presented in Table 4.5. In addition, the recording durations (Table 3.2) that were used to collect the data are also consistent with these recommendations. Results presented in this section were produced by varying each parameter while keeping other values fixed at the default values.

5.3.1 Window Length

The window length parameter, as described in Section 4.3.1, is the length of time from which individual HVSR curves are created before being averaged into a final HVSR curve. The four window length parameters used were 50, 75, 100, and 200 seconds. Sample window lengths for Site 1 are shown in Figure 5.4. From Table 4.6, the number of windows (n_w) recommended for all cases is ten or greater. However, this recommendation was not able to be met for many of the longer window lengths tested due to the fixed recording time. A symbol ($^+$) is placed by the f_0 peaks that failed to meet this requirement, as shown in Table 5.1. A discussion about the influence of the processing parameters is located at the end of this section.

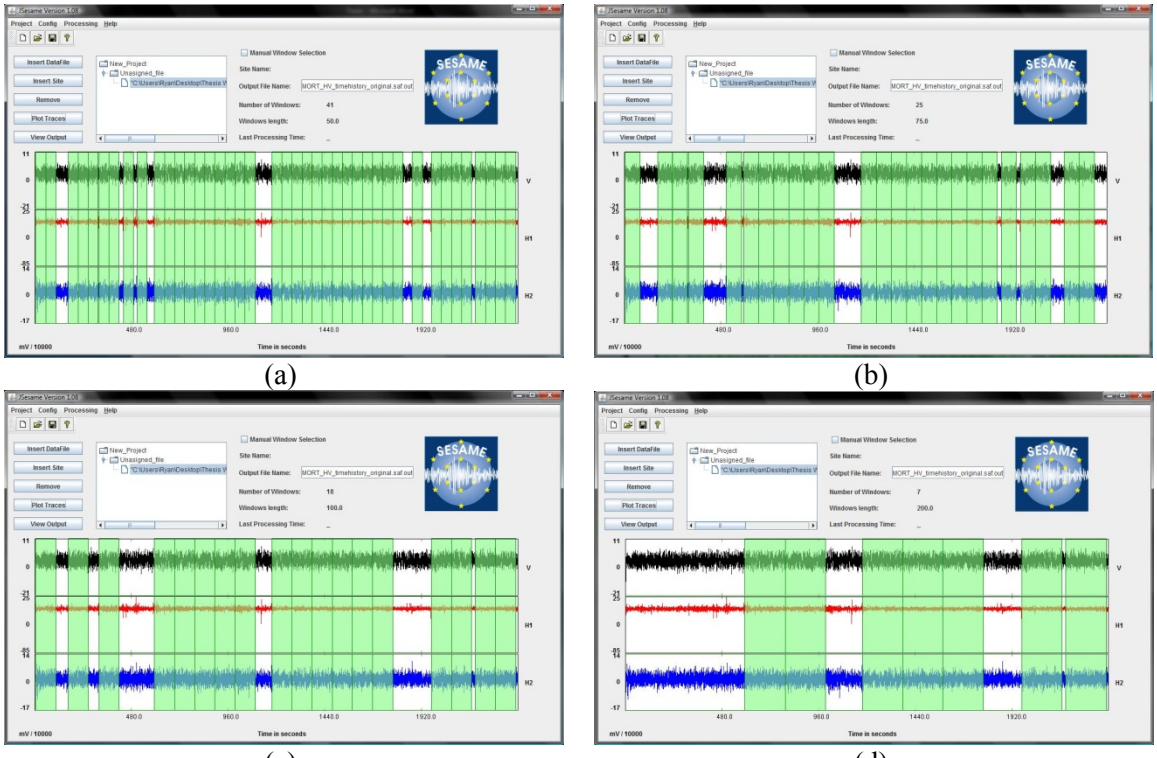

Figure 5.4 The four different values of window length: 50, 75, 100, and 200 seconds, (a) through (d), respectively, applied to Site 1. The windows used in the analysis are shaded in the figure.

Table 5.1 First and second frequency peaks identified for different window lengths tested. ($^{+}$ indicates data were processed with less than the minimum recommended number of windows and "–" indicates that either no frequency peak could be identified or no windows could be developed using the window length parameter)

Site	First Peak Frequency (Hz)				Second Peak Frequency (Hz)			
	Window Length (sec)				Window Length (sec)			
	50	75	100	200	50	75	100	200
1	0.240	0.253	0.260	0.255^{+}	0.720	0.720	0.710	0.710^{+}
2	0.220	0.227	0.230	0.235^{+}	0.760	0.813	0.750	0.525^{+}
3	0.240	0.240^{+}	0.240^{+}	0.245^{+}	0.680	0.693^{+}	0.660^{+}	0.665^{+}
4	0.260	0.253^{+}	0.280^{+}	-	0.680	0.653^{+}	0.730^{+}	-
5	0.240	0.240	0.240^{+}	-	1.020	1.000	0.990^{+}	-
6	0.260	0.253	0.260^{+}	-	0.680	0.640	0.660^{+}	-
7	0.260	0.267	0.270	0.270^{+}	0.700	0.693	0.690	0.690^{+}
8	0.280	0.267^{+}	0.290^{+}	-	-	-	-	-
9	0.280	0.280	0.290	0.290^{+}	-	-	-	-
10	0.380	0.347^{+}	0.340^{+}	-	-	-	-	-
11	0.240	0.240^{+}	0.250^{+}	0.295^{+}	0.660	0.653^{+}	0.630^{+}	0.675^{+}

5.3.2 Transients

The ratio between the STA and LTA is the variable examined in this section (explained in Section 4.3.1). In order to select windows without unwanted energetic transients, a maximum threshold was set for the STA/LTA ratio. Likewise, a minimum threshold was established to avoid ambient vibration windows with abnormally low amplitudes. The default values for this study were 0.5 and 1.5 for the minimum and maximum thresholds. Figure 5.5 shows the change in windows selected for Site 2 when

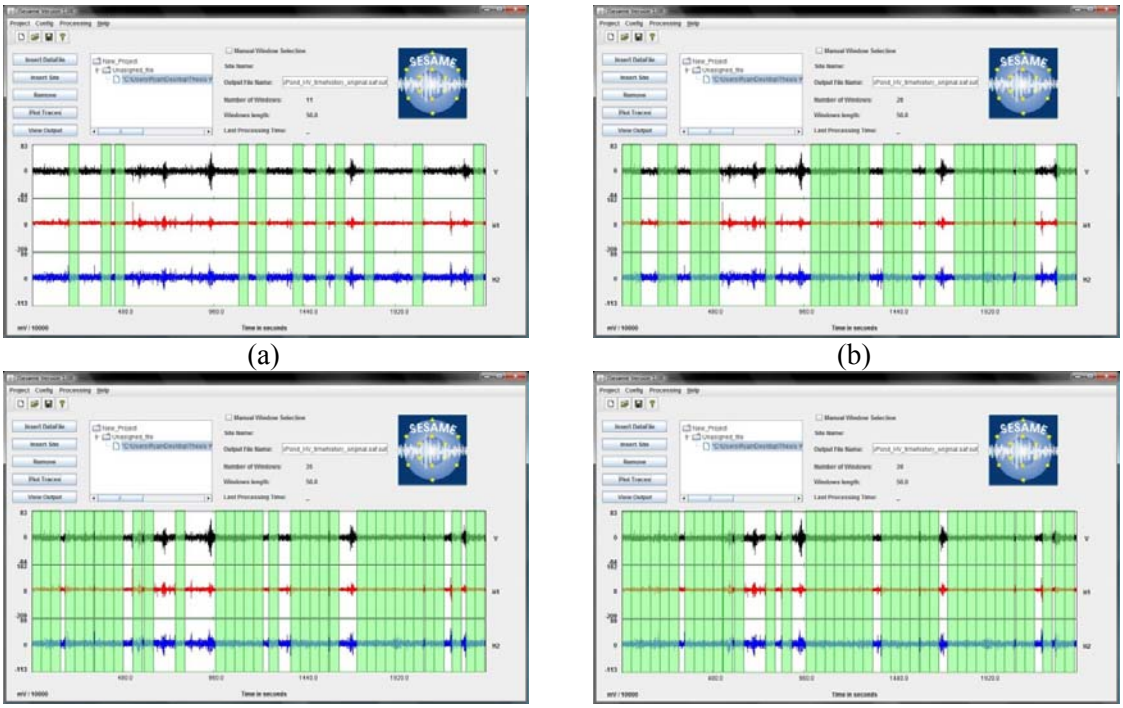

Figure 5.5 The effect of changing the maximum STA/LTA ratio of 1.25, 1.5, 2, and 2.5, (a) through (d) respectively, on the time records for Site 2. The windows are shaded in the figure.

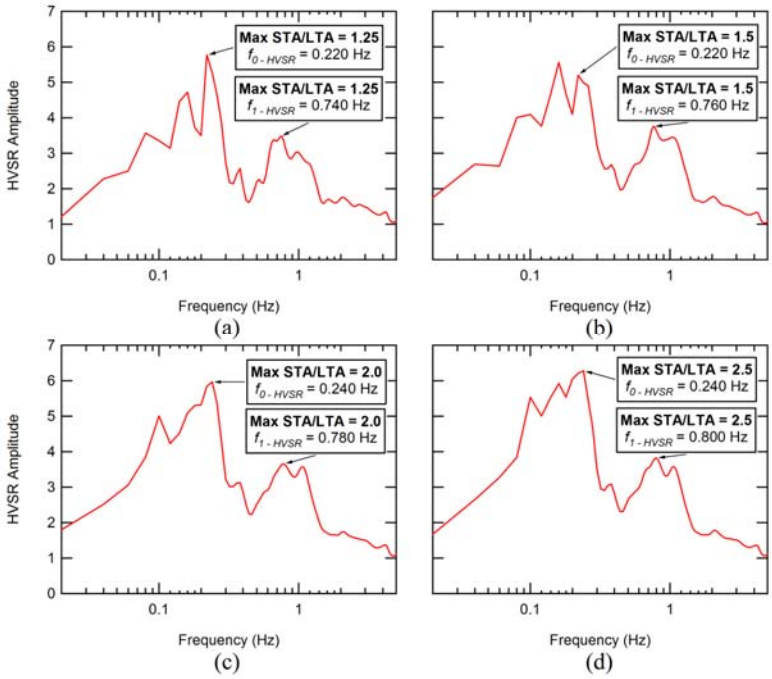

Figure 5.6 HVSR plots for Site 2 of the four maximum STA/LTA ratios of 1.25, 1.5, 2.0, and 2.5, (a) through (d). respectively

the maximum threshold is varied from 1.25 to 2.5 (while holding the minimum value at 0.5). Figure 5.6 shows the resulting HVSR plots from processing these records. A similar analysis was performed by varying the minimum ratio from 0.25 to 0.75, while holding a maximum fixed at 1.5. The first and second frequencies peaks identified using different values of the maximum and minimum thresholds are presented in Table 5.2 and Table 5.3, respectively. Cases when the number of windows (n_w) fell below the recommended values are again indicated with ($^+$) in Tables 5.2 and 5.3.

Table 5.2 First and second frequency peaks for different values of maximum threshold tested while holding minimum threshold at 0.5. ($^+$ indicates data were processed with less than the minimum recommended number of windows and "–" indicates that either no frequency peak could be identified or no windows could be developed using this value of parameter)

Site	First Peak Frequency (Hz)				Second Peak Frequency (Hz)			
	Max STA/LTA				Max STA/LTA			
	1.25	1.5	2.0	2.5	1.25	1.5	2.0	2.5
1	0.240	0.240	0.240	0.259	0.720	0.720	0.720	0.720
2	0.220	0.220	0.240	0.240	0.740	0.760	0.780	0.800
3	0.220$^+$	0.240	0.240	0.240	0.660$^+$	0.680	0.740	0.720
4	-	0.260	0.240	0.240	-	0.680	0.720	0.720
5	0.200$^+$	0.240	0.240	0.240	1.000$^+$	1.020	1.020	1.020
6	-	0.260	0.260	0.260	-	0.680	0.660	0.660
7	0.260	0.260	0.260	0.260	0.680	0.700	0.700	0.700
8	0.280	0.280	0.280	0.280	0.860	-	-	-
9	0.280	0.280	0.280	0.280	-	-	-	-
10	-	0.380	0.380	0.380	-	-	-	-
11	0.220$^+$	0.240	0.220	0.220	0.720$^+$	0.660	0.620	0.640

Table 5.3 First and second frequency peaks for different values of minimum threshold tested while holding maximum threshold at 1.5. (+ indicates data were processed with less than the minimum recommended number of windows and "–" indicates that either no frequency peak could be identified or no windows could be developed using this value of parameter)

Site	First Peak Frequency (Hz)			Second Peak Frequency (Hz)		
	Min STA/LTA			Min STA/LTA		
	0.25	0.5	0.75	0.25	0.5	0.75
1	0.240	0.240	0.240	0.720	0.720	0.720
2	0.220	0.220	0.260	0.760	0.760	0.760
3	0.240	0.240	0.260	0.680	0.680	0.680
4	0.260	0.260	0.280+	0.700	0.680	0.660+
5	0.240	0.240	0.220+	1.020	1.020	1.020+
6	0.260	0.260	-	0.680	0.680	-
7	0.260	0.260	0.260	0.700	0.700	0.700
8	0.280	0.280	0.280	-	-	-
9	0.280	0.280	0.280	-	-	-
10	0.380	0.380	-	-	-	-
11	0.240	0.240	0.220	0.660	0.660	0.620

5.3.3 Merging

Merging refers to the method of combining the two horizontal components before being divided by the vertical component, as discussed in Section 4.3.1. The first and second frequency peaks obtained for every site using different methods of merging are listed in Table 5.4.

Table 5.4 First and second frequency peaks for different merging parameters tested. ("–" indicates that no frequency peak could be identified using this value of parameter)

Site	First Peak Frequency (Hz)				Second Peak Frequency (Hz)			
	Merging				Merging			
	Arith.	Geo.	Quad.	Comp.	Arith.	Geo.	Quad.	Comp.
1	0.240	0.240	0.240	0.240	0.712	0.712	0.712	0.712
2	0.212	0.212	0.212	0.212	0.760	0.760	0.760	0.760
3	0.240	0.240	0.240	0.260	0.680	0.680	0.680	0.680
4	0.260	0.260	0.260	0.220	0.680	0.680	0.700	0.720
5	0.240	0.240	0.240	0.240	1.020	1.020	1.020	1.020
6	0.260	0.260	0.260	0.260	0.680	0.680	0.680	0.660
7	0.260	0.260	0.260	0.280	0.700	0.700	0.700	0.680
8	0.280	0.280	0.280	0.280	-	-	-	-
9	0.280	0.280	0.280	0.280	-	-	-	-
10	0.380	0.380	0.380	0.340	-	-	-	-
11	0.240	0.240	0.240	0.240	0.660	0.660	0.660	0.660

(Arith. = Arithmetic, Geo. = Geometric, Quad. = Quadratic, Comp. = Complex)

5.3.4 Smoothing

Smoothing, as mentioned in Section 4.3.1, is performed after the HVSR plot has been processed in order to remove sharp spikes in the HVSR plot. The first and second frequency peaks for every site are listed in Table 5.5.

Table 5.5 First and second frequency peaks for different smoothing parameters tested. ("–" indicates that no frequency peak could be identified using this value of parameter)

Site	First Peak Frequency (Hz)			Second Peak Frequency (Hz)		
	Smoothing			Smoothing		
	Konno & Ohmachi	Linear	None	Konno & Ohmachi	Linear	None
1	0.240	0.240	0.240	0.720	0.720	0.720
2	0.220	0.180	0.220	0.760	0.780	0.780
3	0.240	0.220	0.240	0.680	0.700	0.760
4	0.260	0.240	0.220	0.680	0.700	0.660
5	0.240	0.220	0.240	1.020	1.000	1.040
6	0.260	0.260	0.260	0.680	0.680	0.780
7	0.260	0.260	0.280	0.700	0.700	0.740
8	0.280	0.300	0.280	-	-	-
9	0.280	0.260	0.280	-	-	-
10	0.380	0.340	0.380	-	-	-
11	0.240	0.220	0.300	0.660	0.680	0.700

5.3.5 Bandwidth of Smoothing Function

The bandwidth parameter affects the smoothing function and is explained in Section 4.3.1. When clear frequency peaks are not visible from the HVSR curve, it is recommended to adjust the smoothing bandwidth. The first and second frequency peaks obtained using different values of the smoothing bandwidth for each site are listed in Table 5.6.

Table 5.6 First and second frequency peaks for different bandwidth parameters tested. ("–" indicates that no frequency peak could be identified using this value of parameter)

Site	First Peak Frequency (Hz)				Second Peak Frequency (Hz)			
	Bandwidth of Smoothing Function (Hz)				Bandwidth of Smoothing Function (Hz)			
	20	30	40	50	20	30	40	50
1	0.240	0.240	0.240	0.240	0.740	0.720	0.720	0.720
2	0.240	0.240	0.220	0.220	0.780	0.760	0.760	0.760
3	0.240	0.240	0.240	0.240	0.700	0.700	0.680	0.680
4	0.240	0.260	0.260	0.220	0.680	0.680	0.680	0.660
5	0.240	0.240	0.240	0.240	0.980	1.000	1.020	1.020
6	0.260	0.260	0.260	0.260	0.680	0.680	0.680	0.680
7	0.260	0.260	0.260	0.260	0.680	0.700	0.700	0.700
8	0.280	0.280	0.280	0.280	-	-	-	-
9	0.280	0.280	0.280	0.280	-	-	-	-
10	0.340	0.320	0.380	0.380	-	-	-	-
11	0.240	0.240	0.240	0.240	0.660	0.660	0.660	0.680

5.3.6 Tapering

As described in Section 4.3.1, the tapering function minimizes the border effects due to the windowing of the Fourier amplitude spectra. The first and second frequency peaks for each site obtained using different tapering functions are listed in Table 5.7.

Table 5.7 First and second frequency peaks for different tapering parameters tested. ("–" indicates that no frequency peak could be identified using this value of parameter)

Site	First Peak Frequency (Hz)		Second Peak Frequency (Hz)	
	Tapering		Tapering	
	Cos	Box	Cos	Box
1	0.240	0.260	0.720	0.720
2	0.220	0.220	0.760	0.780
3	0.240	0.240	0.680	0.680
4	0.260	0.240	0.680	0.680
5	0.240	0.240	1.020	1.020
6	0.260	0.260	0.680	0.680
7	0.260	0.260	0.700	0.700
8	0.280	0.280	-	-
9	0.280	0.300	-	-
10	0.380	0.380	-	-
11	0.240	0.240	0.660	0.680

5.3.7 Filter

The filter parameter is used to remove known artificial or erroneous frequency components before the individual data windows are processed, as discussed in Section 4.3.1. Most of the sites examined in this study were located in rural, quiet environments not producing artificial or erroneous frequencies. For this reason, no filters were used for the default settings. The first and second frequency peaks for each site using different filtering parameters are presented in Table 5.8 and Table 5.9 for the high pass and low

pass filter, respectively. While examining the effect of the low pass filter, a second frequency peak was detected at Site 8 at a frequency of 0.84 to 0.9 Hz.

Table 5.8 First and second frequency peaks for different high pass filter parameters tested. ($^+$ indicates data were processed with less than the minimum recommended number of windows and "–" indicates that no frequency peak could be identified using this value of parameter)

Site	First Peak Frequency (Hz)				Second Peak Frequency (Hz)			
	Filter - High Pass (Hz)				Filter - High Pass (Hz)			
	0.25	0.5	1.0	5.0	0.25	0.5	1.0	5.0
1	0.240	0.240	0.240	0.240	0.720	0.720	0.720	0.720
2	0.220	0.220	0.220	0.240	0.760	0.760	0.760	0.760
3	0.240	0.240	0.240	0.240	0.700	0.700	0.700	0.700
4	0.260	0.220	0.260$^+$	0.240$^+$	0.680	0.700	0.700$^+$	0.640$^+$
5	0.240	0.240	0.240	0.240	1.020	1.020	1.020	1.020
6	0.260	0.260	0.260	0.280	0.680	0.680	0.660	0.640
7	0.260	0.260	0.260	0.260	0.700	0.700	0.700	0.700
8	0.280	0.280	0.280	0.280	-	-	-	-
9	0.280	0.280	0.280	0.300	-	-	-	-
10	0.380	0.380	0.380	0.380	-	-	-	-
11	0.240	0.240	0.240	0.240	0.660	0.660	0.640	0.640

As shown in Table 5.9, there were no acceptable low pass filter parameters that met the minimum requirement of windows for Site 11, however for the default settings, this was not the case.

Table 5.9 First and second frequency peaks for different low pass filter parameters tested. (+ indicates data were processed with less than the minimum recommended number of windows and "–" indicates that no frequency peak could be identified using this value of parameter)

Site	First Peak Frequency (Hz)					Second Peak Frequency				
	Filter - Low Pass (Hz)					Filter - Low Pass (Hz)				
	15	20	25	30	35	15	20	25	30	35
1	0.260	0.260	0.260	0.240	0.260	0.700	0.720	0.700	0.720	0.720
2	0.220	0.220	0.220	0.220	0.220	0.800	0.780	0.760	0.760	0.760
3	0.260+	0.260	0.260	0.260	0.260	0.700+	0.680	0.680	0.680	0.700
4	0.260	0.260	0.260	0.260	0.260	0.640	0.640	0.640	0.660	0.640
5	0.240	0.240	0.240	0.240	0.240	1.020	1.020	1.020	1.020	1.020
6	0.260	0.260	0.260	0.260	0.260	0.680	0.680	0.660	0.660	0.680
7	0.260	0.260	0.260	0.260	0.260	0.700	0.680	0.700	0.680	0.680
8	0.280	0.280	0.260	0.260	0.260	0.900	0.860	0.860	0.840	0.840
9	0.280	0.280	0.280	0.280	0.280	-	-	-	-	-
10	0.320+	0.320+	0.320	0.320	0.320	-	-	-	-	-
11	0.280+	0.280+	0.280+	0.280+	0.280+	0.620+	0.620+	0.620+	0.660+	0.660+

5.3.8 Discussion of Results from the Influence of Processing Parameters

The purpose of this portion of the study was to investigate the possibility that variability in f_{HVSR} due to the HVSR processing method could explain the higher $V_{S,AVG}$ values from HVSR measurements. As shown in Tables 5.1 to 5.12, the results generally showed that the frequency peaks in the HVSR plots remained stable with changes from the default processing parameters. The effect of using different merging, filtering, and tapering methods were negligible in nearly all cases. Changes in the smoothing method,

transient removal method, and window length produced slightly more variability in the frequency estimate. In some cases the frequency peak changed by 5 to 10 %. However, as will be discussed in greater detail in the next section this variability is not sufficient to explain the systematically higher average velocity estimates from the HVSR method, as compared to other methods. The experimental data presented in the following section were developed using the default parameters listed in Table 4.5.

5.4 Comparison of Experimental and Simulated Results for Mississippi Embayment Sites

5.4.1 Introduction

This section presents comparisons of frequency and average velocity values derived from experimental and simulated HVSR data for each test site. Shear wave velocity profiles for each site were created, as described in Section 4.4, and simulations of SH and surface waves were performed using the computer programs, DEEPSOIL and Mat_Disperse, described in Section 4.2.1.

5.4.2 Experimental HVSR Results

The experimental HVSR results, presented and analyzed in Section 5.3, were created using the J-SESAME software using the processing parameters presented in Table 4.5. The HVSR plots for each site are presented in Figure 5.7(a)-(k). As can be observed in these plots, a strong low frequency peak (0.22 to 0.38 Hz) was detected at each of these sites. At most sites, a second frequency peak was detected in the frequency range of 0.66 to 1.02 Hz, although at three sites only one HVSR frequency peak was detected. The

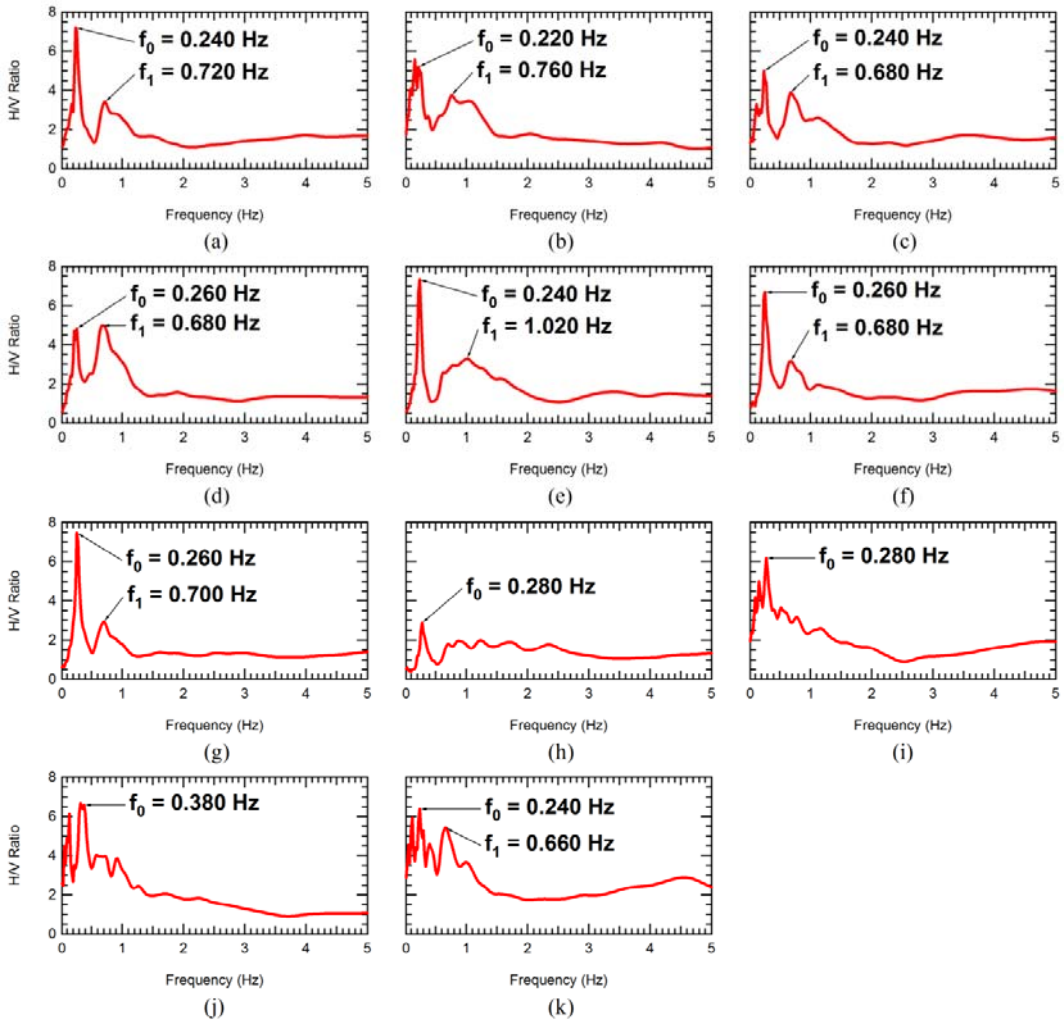

Figure 5.7 HVSR curves with fundamental frequencies peaks indentified for Sites 1 through 11 or (a) through (k), respectively.

lack of a second frequency peak at these three sites could be due to the sites being located closer to the boundaries of the Mississippi embayment (Guillier et al. 2006). The periods of the first and second frequency peaks from this study compare well to values presented in Bodin et al. (2001), as shown in Figure 5.8. Also, the variability observed in the experimental data is consistent with the scatter observed in the Bodin et al. (2001) data (Figure 2.7).

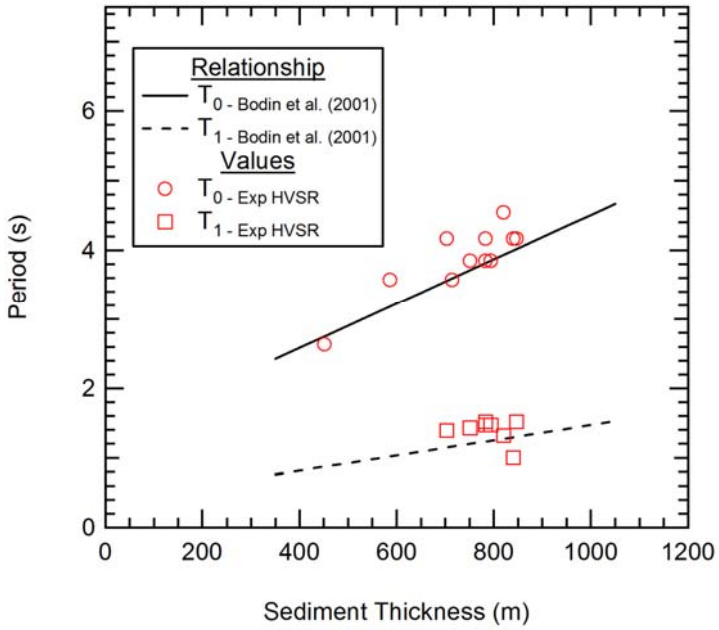

Figure 5.8 Comparison of peak periods from experimental results from this study and relationship developed by Bodin et al. (2001) in the Mississippi embayment.

5.4.3 Simulated HVSR Results for Full Depth of the Profile

Using V_S profiles in the top 250 m from Bailey (2008) and the deeper profile from Romero and Rix (2005), representative V_S profiles were developed for each site. The generation of these profiles is explained in more detail in Section 4.4 of Chapter 4. These V_S profiles represent the best estimate of conditions at each of the measurement sites. All of the full depth profiles are presented in Figure 4.6 of Chapter 4.

Transfer functions from SH propagation (using DEEPSOIL) and HVSR plots due to surface wave propagation (using Mat_Disperse) were calculated for each profile. Figure 5.9 shows an example of these plots developed for Site 1. These same analyses were performed at each site to compare the measured frequency peaks to simulated results using the estimated V_S profiles.

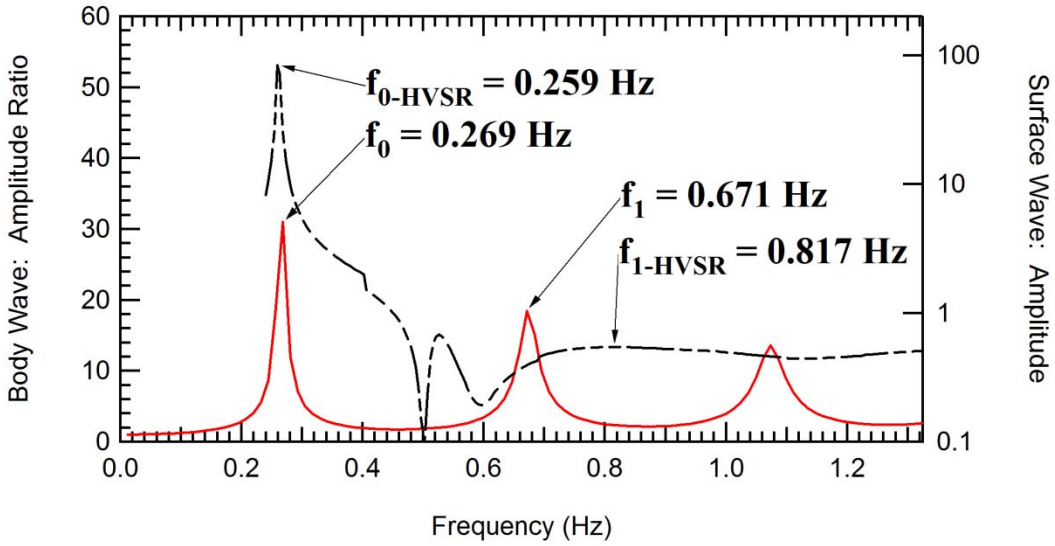

Figure 5.9 Calculated transfer function of SH waves (solid line) and HVSR plot from surface waves (broken line) for Site 1 using estimated V_S profile to bedrock.

Table 5.10 Comparison of simulated to measured frequency values and corresponding percent errors for Sites 1 to 11. (^ indicates that no HVSR peak could be determined)

Site	Experimental	Simulation - SH Transfer Function		Simulation - HVSR Surface Wave	
	$f_{0\text{-Exp HVSR}}$ (Hz)	f_0 (Hz)	% Error	$f_{0\text{-HVSR}}$ (Hz)	% Error
1	0.240	0.269	11.9%	0.259	7.9%
2	0.220	0.244	11.0%	0.254	15.3%
3	0.240	0.281	17.0%	^	^
4	0.260	0.256	1.4%	0.258	0.9%
5	0.240	0.244	1.7%	0.257	7.0%
6	0.260	0.256	1.4%	0.251	3.7%
7	0.260	0.256	1.4%	0.257	1.2%
8	0.280	0.269	4.1%	0.282	0.6%
9	0.280	0.293	4.6%	^	^
10	0.380	0.366	3.6%	0.350	7.9%
11	0.240	0.244	1.7%	0.251	4.4%

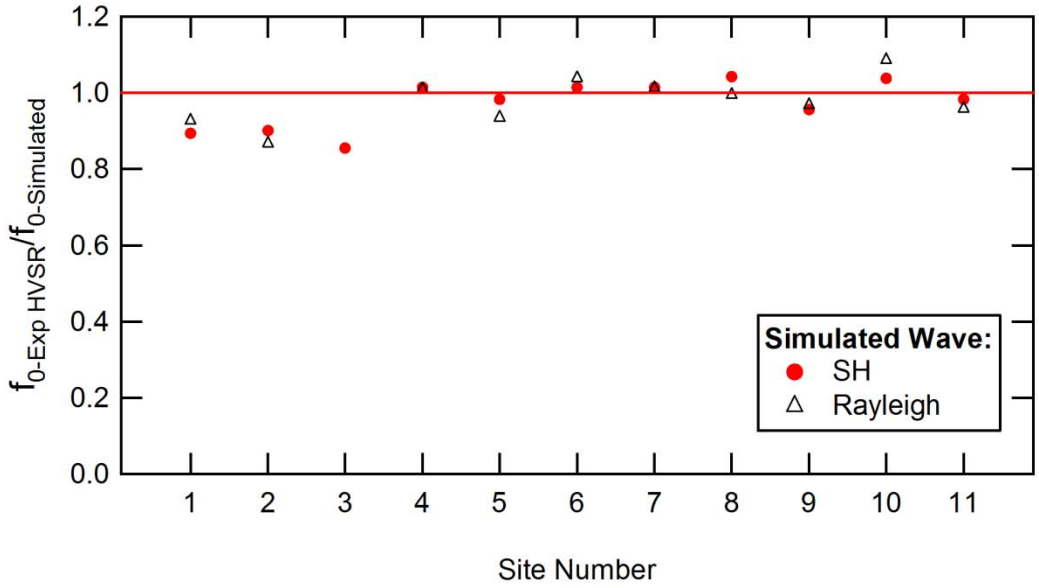

Figure 5.10 Plot relating the experimentally measured first peak frequency to the simulated first peak frequency for each of the eleven sites.

Table 5.10 presents the values of the fundamental frequency (1st peak) from the simulations and the experimental values for each site, along with the percent difference. The results are shown graphically in Figure 5.10 by plotting the ratio of the measured to simulated frequency peak frequency values.

In regard to the first frequency peak (as seen in Figure 5.10 and Table 5.10), both the SH and surface wave simulations produced values that were in good agreement with the experimental values at most sites. At eight of the eleven sites the SH values were within 5% of the measured values. The generally good agreement between the experimental and simulated results provides support for the validity of the V_S profiles developed for each site. At Sites 1, 2, and 3, the larger difference between the simulated and actual values may be due to errors in the estimated V_S profile or the estimated depth to bedrock.

Table 5.11 Comparison of simulated to measured second frequency peak values and corresponding percent errors. ("–" indicates that no frequency peak could be identified)

Site	Experimental	Simulation - SH Transfer Function		Simulation – HVSR Surface Wave	
	$f_{1\text{-Exp HVSR}}$ (Hz)	f_1 (Hz)	% Error	$f_{1\text{-HVSR}}$ (Hz)	% Error
1	0.720	0.671	6.8%	0.817	13.4%
2	0.760	0.635	16.5%	0.936	23.1%
3	0.680	0.769	13.1%	1.029	51.3%
4	0.680	0.684	0.5%	0.943	38.7%
5	1.020	0.684	31.6%	1.213	21.3%
6	0.660	0.659	0.1%	0.882	33.6%
7	0.700	0.659	5.8%	0.773	10.5%
8	-	0.720	-	0.884	-
9	-	0.745	-	1.610	-
10	-	0.879	-	1.798	-
11	0.660	0.647	2.0%	0.977	48.1%

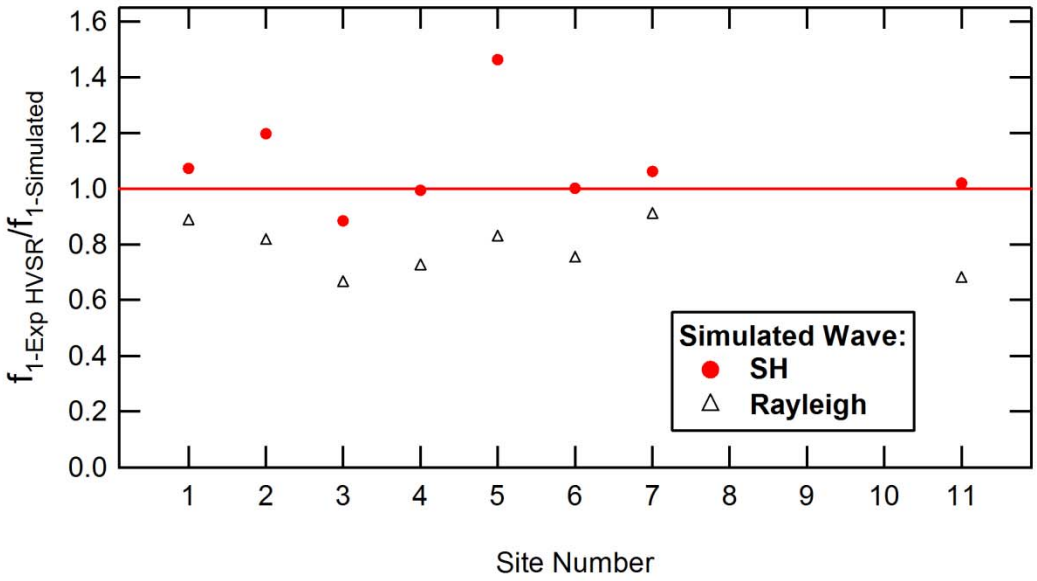

Figure 5.11 Plot relating the experimentally measured second frequency peak to the simulated second frequency peak for each of the eleven sites.

Figure 5.10 also shows good agreement between the frequency peak from the SH simulation and the surface wave simulation. This indicates that the frequency peak observed in the experimental HVSR data could be due to either ambient body waves or ambient surface waves. This result is consistent with the findings from the parametric study of profile conditions (Section 5.2) which showed a good estimate of fundamental frequency from surface wave HVSR when the velocity contrast is greater than 3.5 and the site is saturated; both of these conditions were met at these sites.

Comparisons between the frequency of the second peak obtained from the experimental and simulated results are shown in Table 5.11 and Figure 5.11. In this case, the second frequency peak of the transfer function is in generally good agreement with the experimental results (<10% at most sites), except at Site 5 where the measured value was much higher (31.6%). The second frequency peak developed from the simulated surface wave HVSR was significantly lower in most cases and did not agree well with the measured values. These results suggest that the second frequency peak observed in the experimental data may be explained as a second mode of SH resonance of the full depth of the soil profile. This is the interpretation that was made by Bodin et al. (2001). Another interpretation is examined in Section 5.4.4 to follow.

Average Velocity Values: The lowest frequency peak from the experimental and simulated data (both transfer function and surface wave HVSR) at each site were used to calculate the $V_{S,AVG}$ value for the full profile depth using the approximate relationship of Eq. 2.2. This procedure was performed to replicate the methods used by Bodin et al.

(2001) to obtain average velocity values. The "true" average velocity for each site profile was

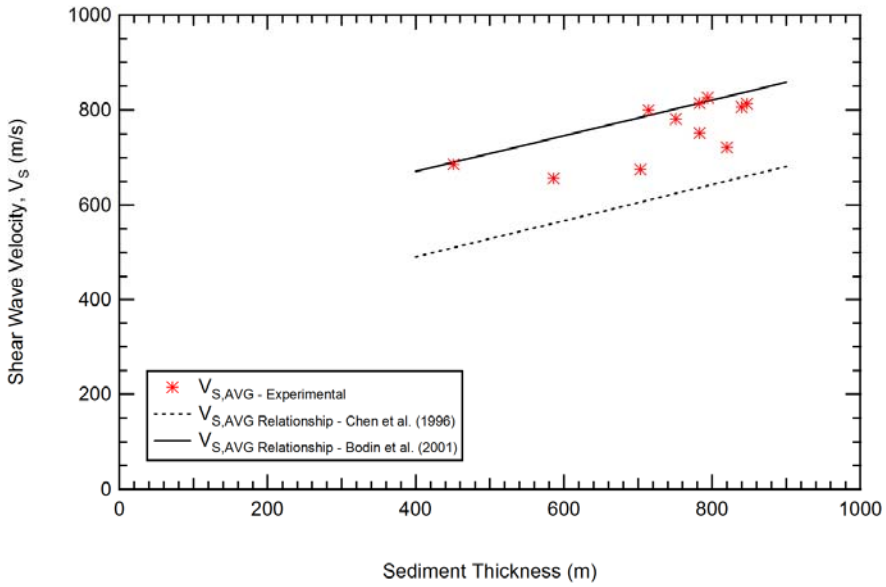

Figure 5.12 Experimental V_S developed from the HVSR data. Also shown are V_S-sediment thickness relationships from Bodin et al. (2001) and Chen et al. (1996).

also calculated, using Eq. 4.9. The experimental and simulated velocity values are plotted versus depth to bedrock (sediment thickness) in Figure 5.12 and Figure 5.13, respectively. Also shown on Figures 5.12 and 5.13 are the velocity relationships developed by Chen et al. (1996) and Bodin et al. (2001). The experimental $V_{S,AVG}$ values in Figure 5.12 correlated well with Bodin et al. (2001); however, it should be noted that the consistency of results does not verify the validity of Bodin et al. (2001), only that the results are reproducible using Eq. 2.2. The first observation from Figure 5.13 is that the true average velocity values based on the site V_S profiles (developed from Bailey 2008; Romero and Rix 2005) are in very good agreement with the values predicted by Chen's (1996) relationship. However, when the fundamental frequency peaks derived from the

site profiles (from either the SH transfer function or the surface wave HVSR values) are used to calculate the average

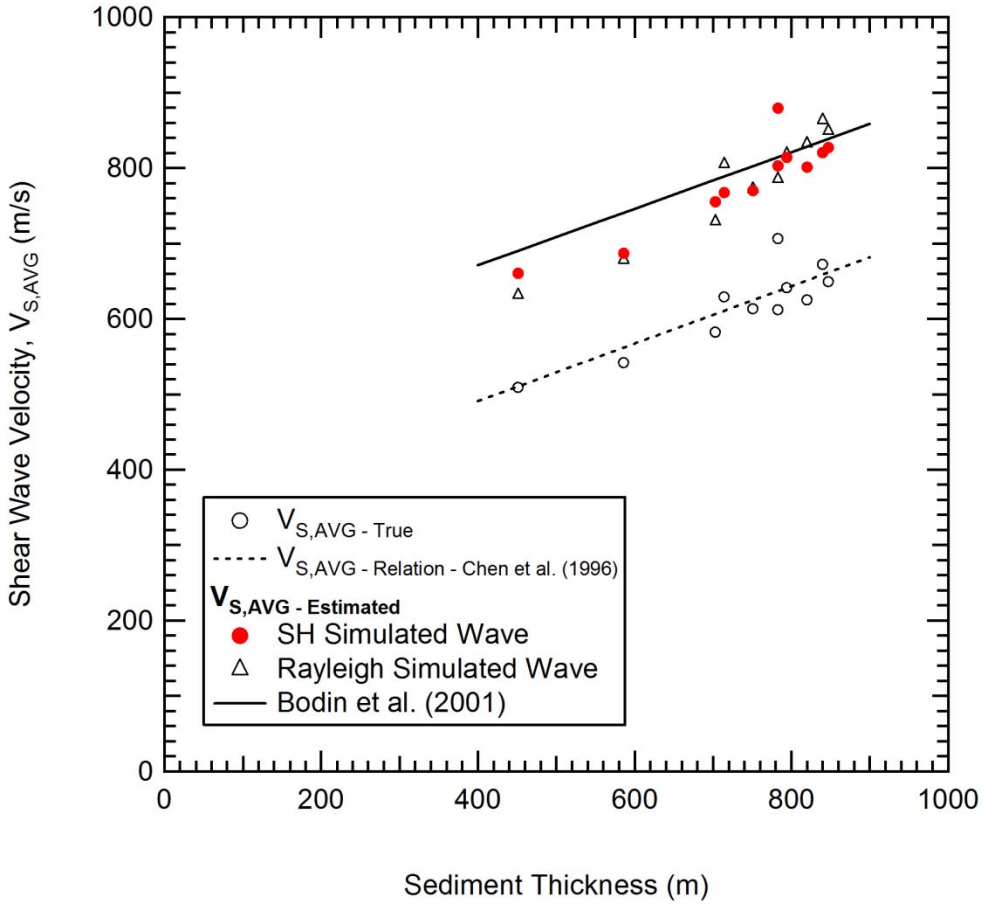

Figure 5.13 Shear wave velocities for "true" and estimated $V_{S,AVG}$ values as a function of sediment thickness for the eleven sites. Also shown are V_S-sediment thickness relationships from Bodin et al. (2001) and Chen et al. (1996).

velocity using Eq. 2.2 (shown as solid markers in Figure 5.13), the velocity values that are determined are significantly higher. In fact, these erroneously high average velocity values are very consistent with the relationship Bodin et al. (2001) developed for the Mississippi embayment. Table 5.12 presents a comparison between the "true" values and the "estimated" $V_{S,AVG}$ values, along with the percent error. Figure 5.14 shows a plot of

the simulated and experimental "estimated" velocities for each site plotted versus the true velocity values, along with the percentage error. The experimental data is consistent with the simulated results, both showing an overestimated of the average velocity by 20 to 30%.

These results demonstrate that although the HVSR method provided a good estimate of the fundamental frequency, the use of the approximation method to calculate $V_{S,AVG}$ produced an overestimate of $V_{S,AVG}$ by 20-25%. Therefore, it can be concluded that the relationship developed by Bodin et al. (2001) using this approach is erroneous.

Table 5.12 Shear wave velocities developed from surface wave V_S profiles with corresponding percent errors for the eleven sites. (^ indicates that no HVSR frequency peak could be determined)

Site	$V_{S,AVG}$ "True" (m/s)	$V_{S,AVG}$ "Estimated" (m/s)			
		SH Simulated Wave	% Error	Rayleigh Simulated Wave	% Error
1	581.5	755	28.2%	729	25.3%
2	625.4	801	27.2%	832	33.0%
3	705.9	879	23.1%	^	^
4	641	814	23.9%	818	27.7%
5	672.1	820	21.2%	863	28.4%
6	611.5	803	28.1%	785	28.3%
7	612.9	770	26.2%	772	25.9%
8	629.5	767	22.5%	805	27.8%
9	541.5	687	28.8%	^	^
10	509.4	661	29.3%	631	23.9%
11	648.7	827	25.3%	849	30.8%

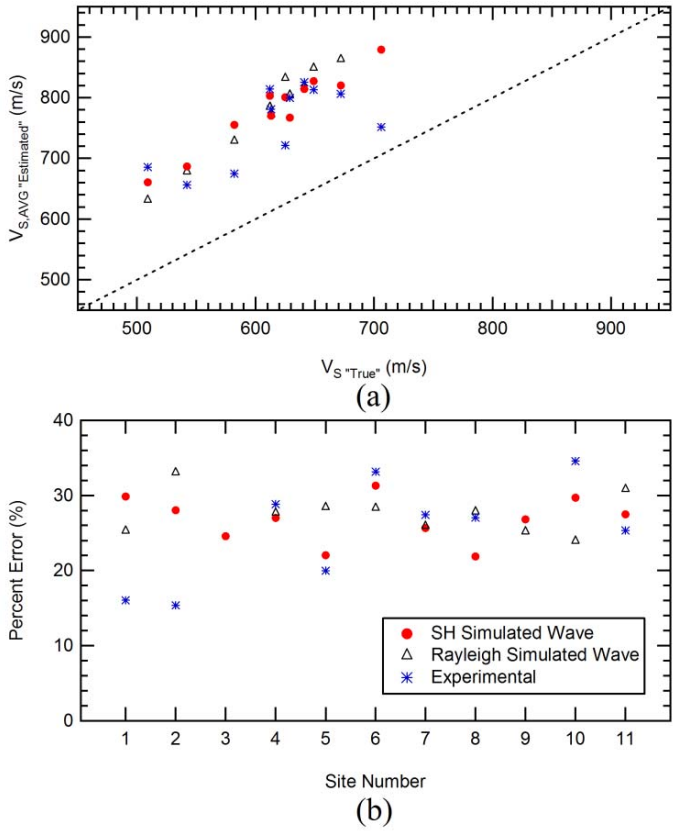

Figure 5.14 The simulated and experimental V_S compared to the "true" V_S for the eleven sites (a) and the corresponding percent error (b).

5.4.4 Simulated HVSR Results for Shallow Profiles

Another possible explanation for the origin of the second frequency peak in the experimental HVSR plots is that it is due to interactions of body and/or surface waves with a strong shallow velocity contrast within the sediment layers. In the work of Bodin et al. (2001), no knowledge of the subsurface conditions at the measurements sites was available, so they were only able to speculate on possible origins of the second frequency peak. In this work, V_S profile information is available at each site in the top 200 m from the surface wave measurements of Bailey (2008).

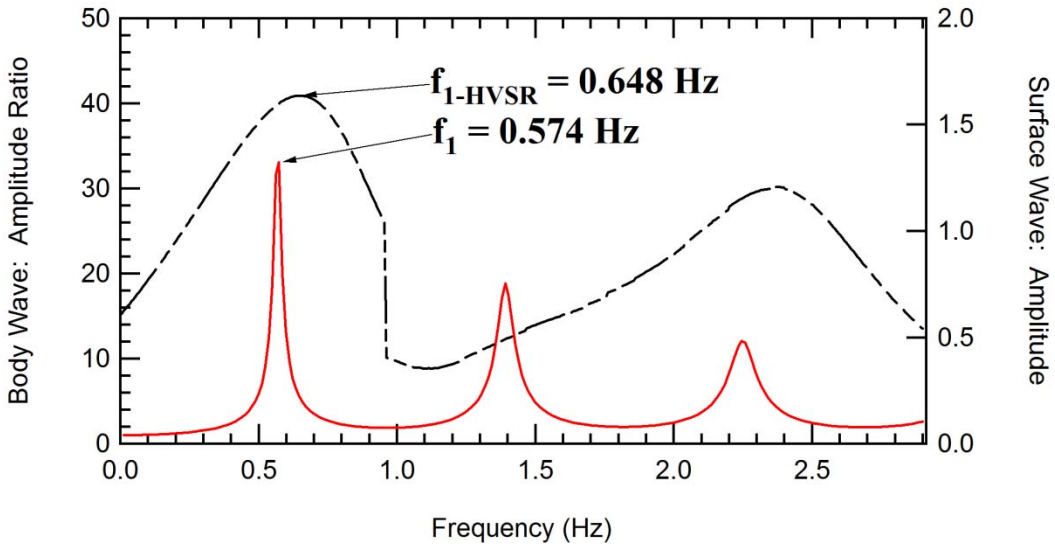

Figure 5.15 Calculated transfer function of SH waves (solid line) and HVSR plot from surface waves (broken line) for Site 1 using shallow V_S profiles.

Table 5.13 Shallow profile comparison of simulated to measured frequency peak results and corresponding percent errors. ("–" indicates that no frequency peak could be identified)

Site	Experimental	Simulation – SH Transfer Function		Simulation - HVSR Surface Wave	
	$f_{1\text{-Exp HVSR}}$ (Hz)	f_1 (Hz)	% Error	$f_{1\text{-HVSR}}$ (Hz)	% Error
1	0.720	0.574	20.3%	0.648	10.1%
2	0.760	0.684	10.1%	0.808	6.3%
3	0.680	0.830	22.1%	1.268	86.4%
4	0.680	0.720	5.9%	1.002	47.4%
5	1.020	0.891	10.9%	1.343	34.3%
6	0.660	0.610	7.5%	0.802	21.5%
7	0.700	0.586	16.3%	0.671	4.1%
8	-	0.647	-	0.872	-
9	-	0.647	-	0.700	-
10	-	0.647	-	0.631	-
11	0.660	0.769	16.5%	1.022	54.9%

To examine this possibility, SH transfer functions and surface wave simulations were performed using only the shallow (top 250 m) V_S profile information obtained from the surface wave measurements, as shown in Figure 3.17 and Figure 3.18. The frequencies of peaks developed from the transfer function and HVSR plots were compared to the values of the second frequency peak from the experimental data. Figure 5.15 shows an example of the plots developed for Site 1. Table 5.13 and Figure 5.16 present a comparison between the experimentally determined and simulated frequency peaks from SH and Rayleigh waves for the shallow profiles.

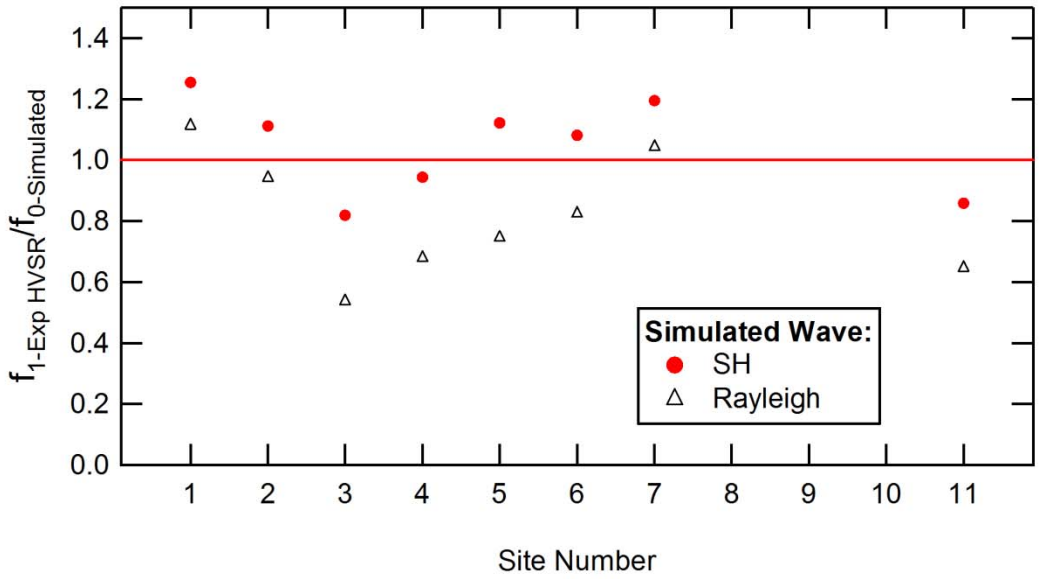

Figure 5.16 Comparison of simulated shallow profiles to measured frequency values for the eleven sites.

As seen in Table 5.13, the transfer function frequency peaks are in reasonably good agreement with experimental values although not quite as good as the agreement seen with the second frequency peak of the full depth profile (Table 5.11 and Figure 5.11). However, for Site 5, the transfer function of the shallow profile provided a much better

prediction of the frequency values than from the second frequency peak of the full depth profile. Surface wave simulated results did not compare well to the experimental frequencies.

It was theorized that the V_S contrast at the top of various geologic formations could be strong enough to be the source of the second frequency peak. The Memphis Sand interface is one possible boundary within the profile with a strong V_S contrast. Past studies (Gomberg et al. 2003) and the V_S profiles from Bailey (2008) show an increase in V_S at depths consistent with the top of the Memphis Sand. If this boundary is the cause of the frequency peak, a trend of increasing site period with increasing depth to the top of

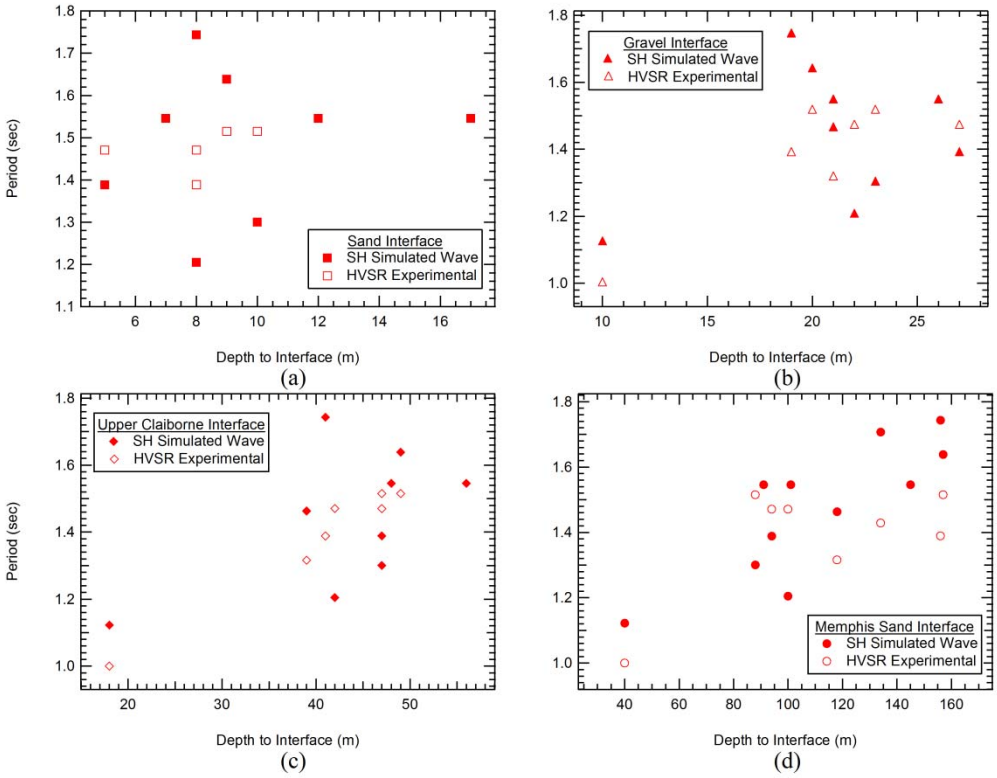

Figure 5.17 Period of experimental and SH simulated waves compared to depth of interfaces for the sand, gravel, Upper Claiborne, and Memphis Sand interfaces, (a)-(d) respectively.

the Memphis Sand is expected. The relationship between the calculated period from simulated V_S profiles and the depth to various formation interfaces is presented in Figure 5.17(a)-(d), along with the HVSR experimental values.

The plots for the Memphis Sand show a relationship of increasing period with the depth to the top of the Memphis Sand, indicating that the velocity contrast at the Memphis Sand interface may be the cause of the second frequency peak observed in the experimental data. When comparing the second frequency peak of the full sediment profile in Figure 5.11 and the frequency peak of the shallow V_S profile in Figure 5.16 to the measured values, it is difficult to strongly prefer one interpretation over the other. However, it appears that the higher-mode body wave interpretation may be a better explanation based on slightly better agreement with the experimental values.

5.4.5 Discussion of Results from Comparison of Experimental and Simulated Data

The comparison of frequency values from experimental and simulated HVSR data highlighted several valuable relationships that will be discussed in this section. The section discusses the following three issues: (1) estimation of the fundamental frequency from HVSR measurements, (2) reliability of average shear wave velocity values using the approximate method of Eq. 2.2, and (3) origin of the high-frequency HVSR frequency peak.

Low-Frequency HVSR Frequency peak: The experimentally measured HVSR frequency peaks from this study were shown to be very consistent with values from HVSR measurements reported by Bodin et al. (2001), only differing by an average of 5.9%. In

addition, the experimental values of fundamental frequency agreed well (average of within 5.4%) with the simulated values using both shear and Rayleigh waves propagating through the estimated V_S profile at each site. These results indicate that the HVSR method does provide a good estimate of the fundamental frequency when site conditions are ideal (as discussed in Section 5.2), as was the case in the Mississippi embayment. Therefore, it can be concluded that the higher $V_{S,AVG}$ values obtained from the HVSR measurements were not caused by poor estimates of the fundamental frequency.

Average Velocity Values: The results presented in the previous section showed that the experimental data from this study is consistent with results obtained by Bodin et al. (2001). The average velocity of full-depth V_S profiles developed for each site using the best available information yielded values that were consistent (within an average error of 3.2%) with what is predicted by the Chen et al. (1996) relationship. However, when HVSR measurements were simulated for each site, it was found that the $V_{S,AVG}$ value calculated using the approximate relationship of Eq. 2.2 was about 25% higher than the "true" calculated value for each site. These erroneously high values were in very good agreement (average error of about 3.5 %) with the relationship developed by Bodin et al. (2001). Given that the frequency estimate from HVSR appears to be good, it can be concluded that the use of the approximate method to estimate $V_{S,AVG}$ is the source of the over-prediction of $V_{S,AVG}$ values. In other words, the results show that the higher $V_{S,AVG}$ relationship of Bodin et al. (2001) can be replicated using V_S profiles with true $V_{S,AVG}$ values that are consistent with the relationship of Chen et al. (1996). This is an important finding because it demonstrates that the relationship of Bodin et al. (2001) is erroneously

high and should not be used to estimate the velocity structure in the embayment. Secondly, it calls into question the use of the approximate approach to estimate $V_{S,AVG}$ in cases where the V_S profile is not uniform with depth.

High-Frequency HVSR Peak: The results showed that the second frequency peak in the experimental data could be explained by a higher mode of shear wave resonance from the soil/bedrock interface. Experimental values for the second frequency peak agreed within an average of 9.6% with values derived from the transfer function calculated using estimated V_S profiles at each site. This is the interpretation suggested by Bodin et al. (2001) to explain the origin of the second frequency peak.

However, transfer function calculations using only the shallow structure also yielded frequency peaks that were reasonably consistent (within 13.7%) with the frequency peaks observed in the HVSR data and provided much better agreement at some sites (particularly Site 5). The likely cause of the second frequency peak (if due to resonance of a shallow layer) is reflections of body waves from the top of the Memphis Sand Formation.

When comparing the two possible interpretations of the second frequency peak, it is difficult to conclusively favor one explanation over the other. Both explanations have been shown to be plausible; however, the higher-mode resonance of the full depth is slightly preferred due to the better comparison between simulated and experimental frequency values. A more conclusive result could be obtained by examining data from sites with well-constrained values of V_S and soil lithology over the full profile depth.

5.5 Summary

This chapter presented the results from numerical simulations and experimental analyses of HVSR measurements. Three research tasks were performed to meet the objectives of this study. First, synthetic V_S profiles were used to examine the influence of V_S contrast and Poisson's ratio on the consistency of the HVSR frequency and $V_{S,AVG}$ estimates. Second, the effect of HVSR processing parameters on experimental HVSR results was examined. Last, comparisons were presented between experimental results (frequency and estimated $V_{S,AVG}$) and simulated results using the best available information for the V_S profile at each of the eleven measurement sites. A discussion of the findings from each aspect of the study was also presented. Final conclusions as related to the objectives of this research, along with recommendations, are presented in Chapter 6.

6. CONCLUSION

6.1 Summary

The objectives of this research were to investigate: (1) why the shear wave velocity relationships from the HVSR method are inconsistent with other methods in the Mississippi embayment and (2) the origin of the second frequency peak observed in HVSR plots of the Mississippi embayment. A combination of both numerical and experimental studies was performed to meet these stated objectives.

Numerical simulations of wave propagation were performed on seven synthetic cases of V_S profiles with the same average shear wave velocity ($V_{S,AVG}$). The synthetic V_S profiles were entered into computer programs to simulate shear wave propagation (using DEEPSOIL) and Rayleigh wave propagation (using Mat_Disperse). The effect of varying the V_S contrast between the soil and halfspace (rock) on the value of the fundamental frequency peaks was examined for each case. Also, the effect of varying Poisson's ratio on the value of the fundamental frequency peaks was examined for each case. In addition, $V_{S,AVG}$ values for each case were calculated using an approximate relationship with the fundamental frequency and bedrock depth. These estimated values were compared to the true $V_{S,AVG}$ values, calculated directly from the V_S profile.

Experimental studies using the HVSR were performed at eleven sites in the upper Mississippi embayment. Experimental ambient noise data were processed using the computer program J-SESAME to generate an HVSR plot for each site. Frequency peaks

in the HVSR plot were used to estimate the fundamental frequency of the site, and to calculate the $V_{S,AVG}$ for the full depth of the sediments. Processing parameters used in J-SESAME were varied to determine the sensitivity of the frequency values to changes in processing parameters. These experimentally measured HVSR frequency peaks were compared to frequency peaks produced from simulated shear and Rayleigh wave propagations using estimated full-depth V_S profiles at each site (Bailey 2008; Romero and Rix 2005). The "true" and estimated $V_{S,AVG}$ values were developed for each site from the known V_S profiles and the approximation of Eq. 2.2, respectively. These $V_{S,AVG}$ values were compared to previous $V_{S,AVG}$ relationships developed for the region by Bodin et al. (2001) and Chen et al. (1996).

6.2 Conclusions

In regard to the first objective, it was found that the higher $V_{S,AVG}$ values could not be attributed to poor estimates of the fundamental site frequency using the HVSR method. Numerical simulations for different profile conditions showed that for cases where the reflecting interface has a high velocity contrast with the soil (3.5 or greater) and the soil is saturated (conditions that are met in the Mississippi embayment), the frequency obtained from HVSR plots, developed from either body wave ambient energy or surface wave ambient energy, yields a reliable estimate (generally within 4%) of the true value. These findings are in agreement with past studies and recommendations (Bonnefoy-Claudet et al. 2008; SESAME 2004). Also, a parametric study of processing parameters showed little impact on the frequency estimates from experimental HVSR measurements. This leads to the conclusion that variability in the estimated fundamental frequency peak

from the HVSR method is not sufficient to explain the higher $V_{S,AVG}$ estimates from the HVSR method.

It was demonstrated that the higher $V_{S,AVG}$ values from the HVSR method can be attributed to use of the approximate method (Eq. 2.2) to estimate $V_{S,AVG}$. The V_S profiles developed for each of the eleven experimental sites had "true" $V_{S,AVG}$ values that were remarkably consistent with values predicted by the relationship of Chen et al. (1996). However, when HVSR measurements were simulated using these site profiles and Eq. 2.2 was used to estimate $V_{S,AVG}$, the values of $V_{S,AVG}$ were about 25% higher than the true values and followed the relationship established by Bodin et al. (2001). In other words, it was possible to replicate the relationship of Bodin et al. (2001) using V_S profiles with average velocities consistent with relationship of Chen et al. (1996). The experimental results at these sites were also in good agreement with the simulated results.

In regard to the second objective, it was found that the second frequency peak observed in the HVSR plots could be attributed to either higher mode resonance of SH waves from the soil/rock interface or SH wave resonance from a shallow velocity contrast within the sediments. Using the estimated site V_S profiles, the second frequency peak of the calculated transfer function compared well, in most cases, with the observed second frequency peak in the experimental data (average error of about 10%). However, when transfer functions were calculated using only the shallow structure (top 220 m) and no bedrock, frequency peaks were observed that were also in general agreement with the experimental data (within about 14%). Although the error was higher, at some sites (particularly Site 5) this approach provided a better match between the experimental and

simulated results. The period of the second frequency peak appeared to correlate well with the expected depth of the top of the Memphis Sand Formation indicating this interface is the likely source of the higher frequency peak (if it is caused by shallow structure). It is difficult to definitively conclude the cause of the second frequency peak, but these results demonstrate that it is plausible that this higher frequency peak could be caused by shallow structure in the embayment.

The primary contribution of this work is that it has demonstrated that the relationship between average shear wave velocity and sediment depth of Bodin et al. (2001) overestimates the shear wave velocity structure in the Mississippi embayment. It was shown that the cause of this overestimation is the use of an approximate method to obtain the average velocity values.

6.3 Recommendations

From the conclusions presented in this thesis, recommendations can be made for applications in the Mississippi embayment and future HVSR studies. It is recommended that the V_S relationship for the Mississippi embayment established by Chen et al. (1996) should be preferred to the relationship of Bodin et al. (2001) to characterize the average velocity structure of the Mississippi embayment sediments. Other studies, such as Julia et al. (2004), also support these lower velocity values. Secondly, it is recommended that the use of the common approximation (Eq. 2.2) to calculate average velocities should only be applied to cases where the velocity structure is known to be nearly uniform with depth.

Appendix

This appendix documents the supplementary information from this Horizontal-to-Vertical Spectral Ratio (HVSR) study. Images are presented along with time records and the individual component spectrums of each site. The number of windows (n_w) for each processing parameter of Section 5.3 is also presented.

A. APPENDIX

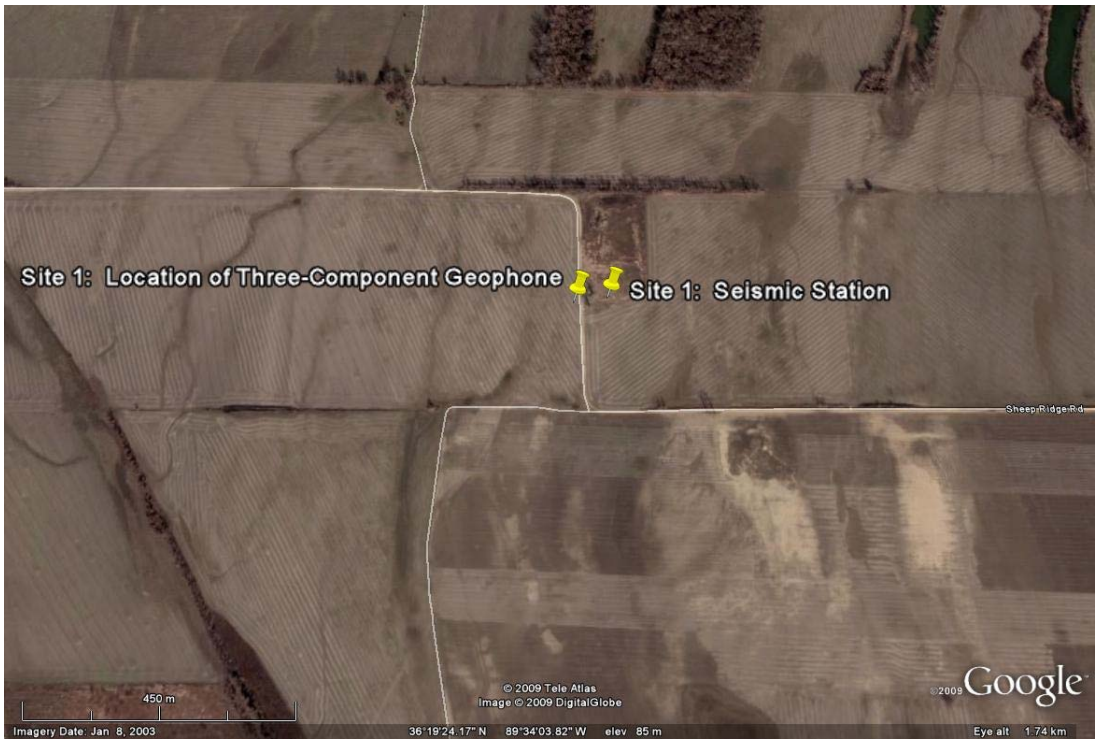

Figure A.1 Image of Site 1 (MORT).

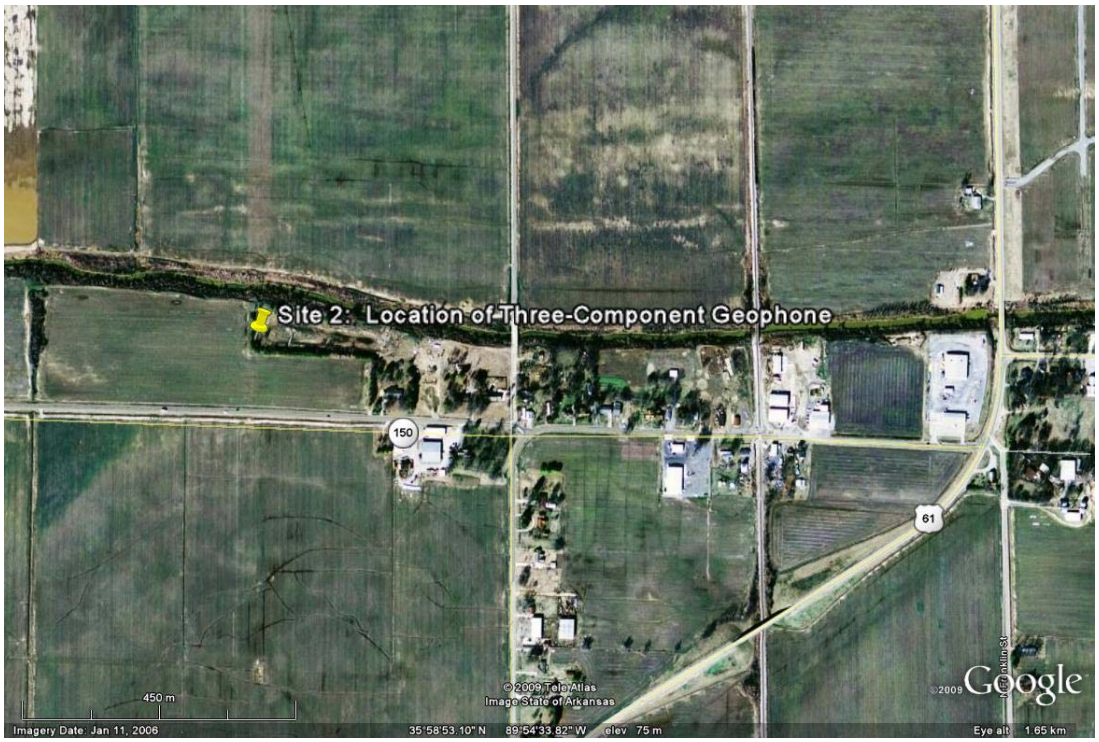

Figure A.2 Image of Site 2 (YARBRO).

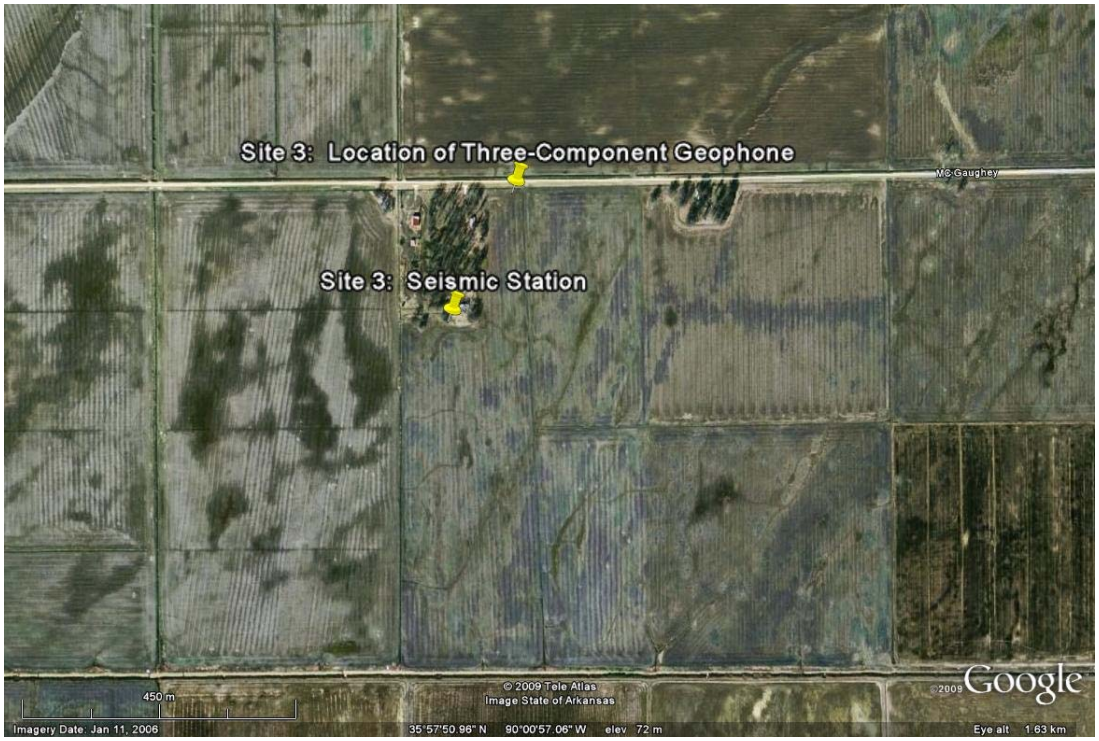

Figure A.3 Image of Site 3 (GNAR).

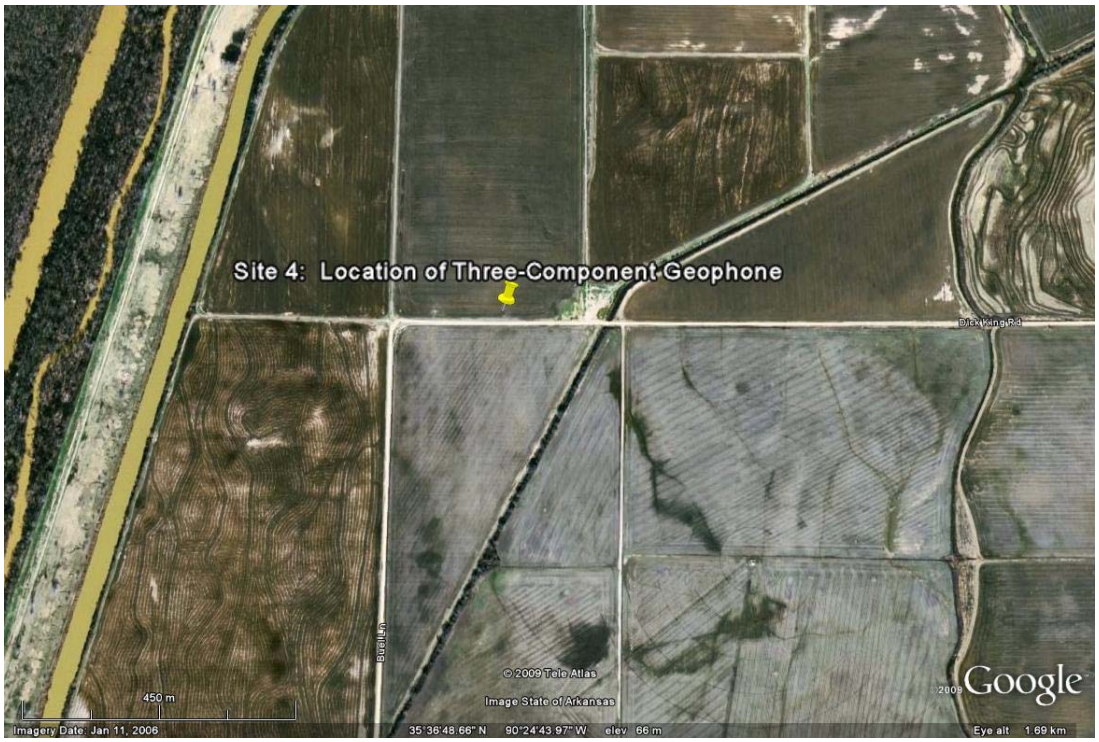

Figure A.4 Image of Site 4 (LEPANTO).

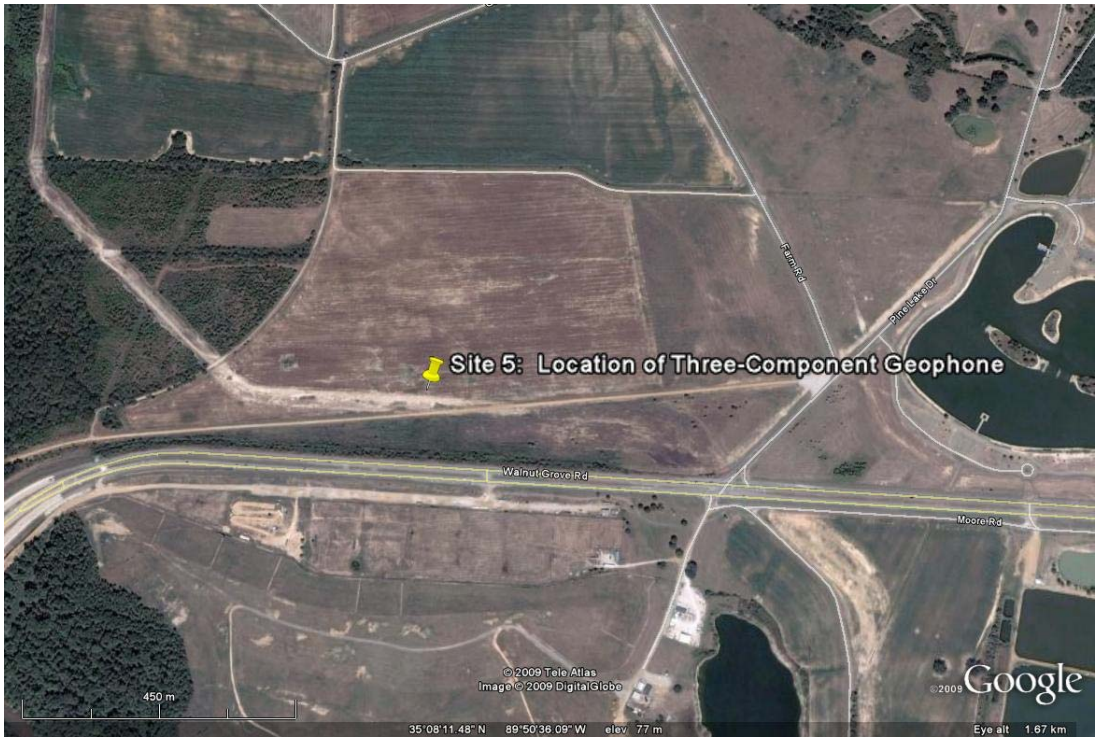

Figure A.5 Image of Site 5 (SHELBY FARMS).

Figure A.6 Image of Site 6 (TNMT).

Figure A.7 Image of Site 7 (GLAT).

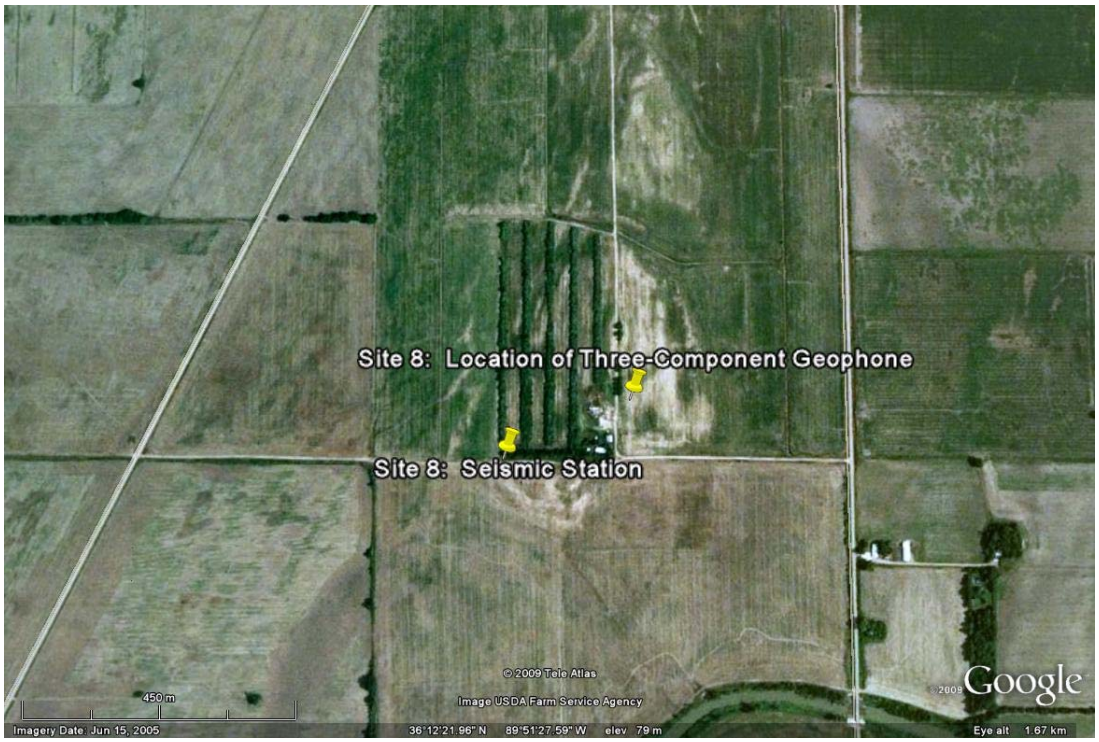

Figure A.8 Image of Site 8 (BRGM).

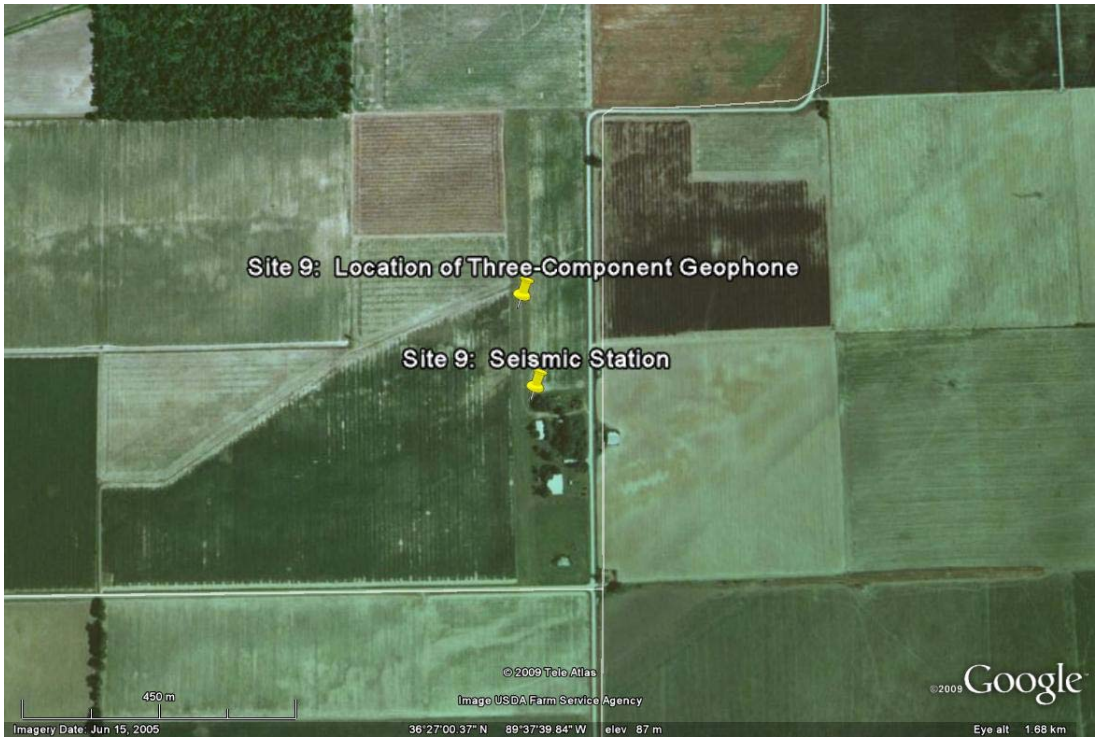

Figure A.9 Image of Site 9 (PENM).

Figure A.10 Image of Site 10 (EPRM).

Figure A.11 Image of Site 11 (MSAR).

B. APPENDIX

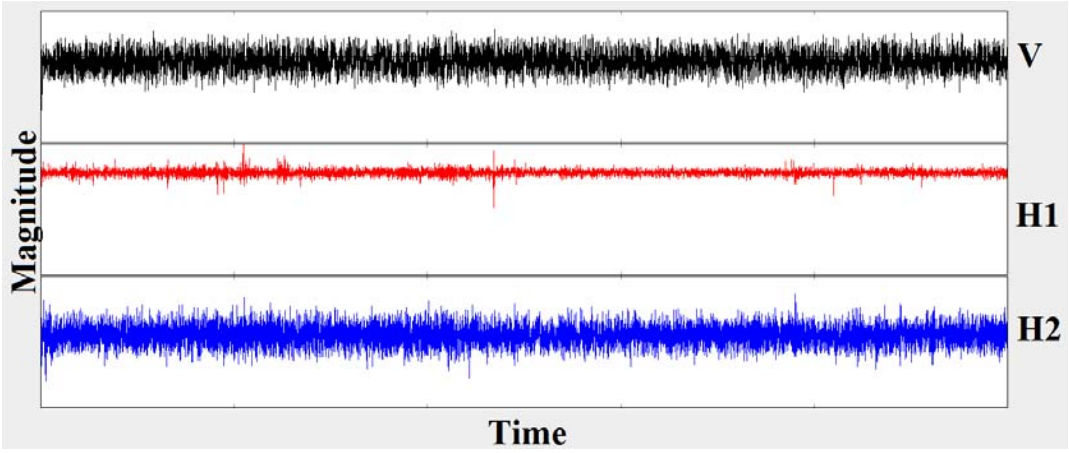

Figure B.1 Time record from the single-station three-component sensor at Site 1.

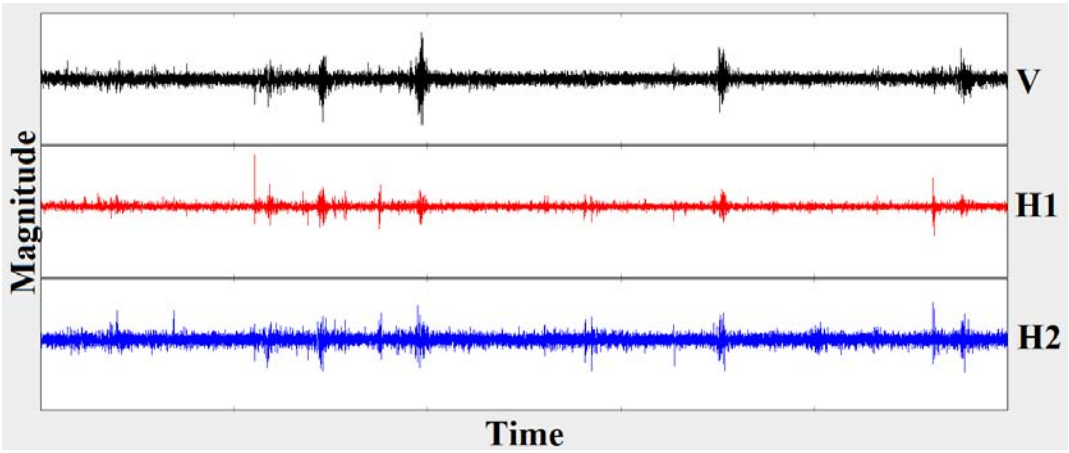

Figure B.2 Time record from the single-station three-component sensor at Site 2.

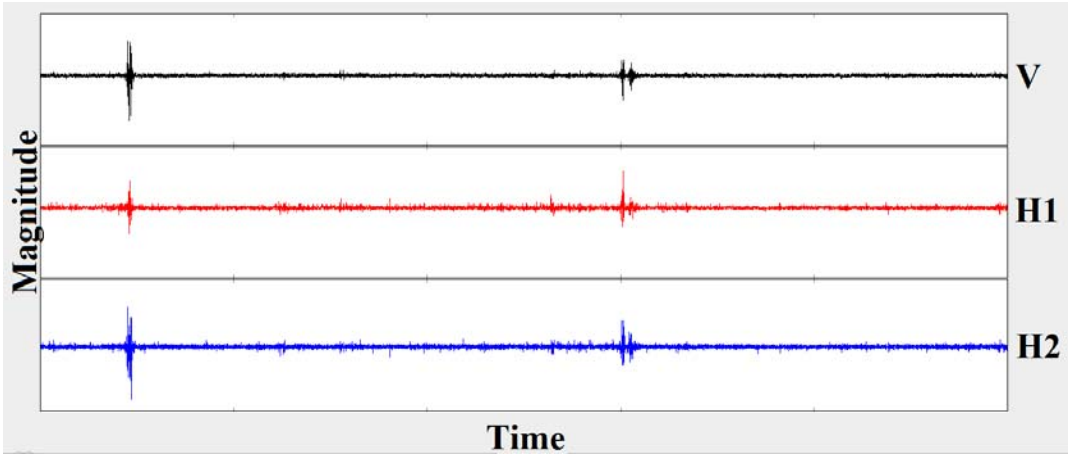

Figure B.3 Time record from the single-station three-component sensor at Site 3.

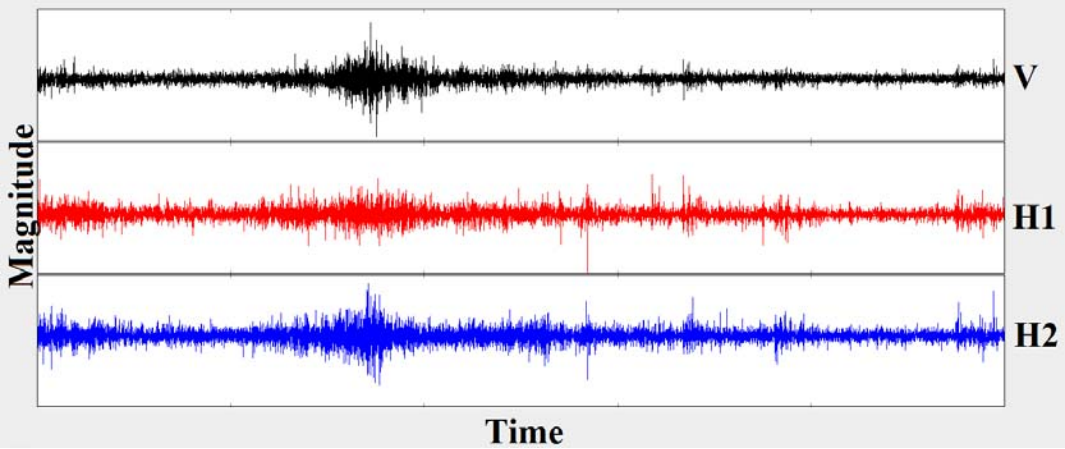

Figure B.4 Time record from the single-station three-component sensor at Site 4.

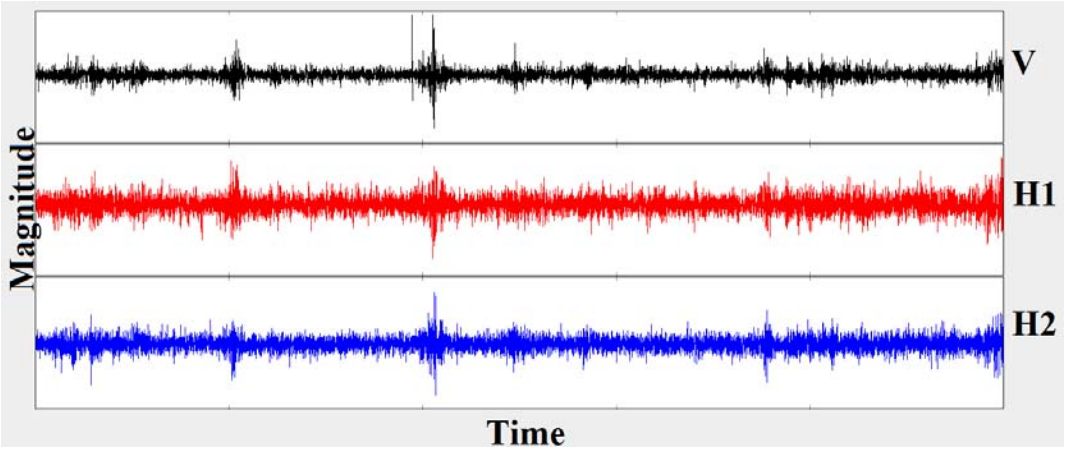

Figure B.5 Time record from the single-station three-component sensor at Site 5.

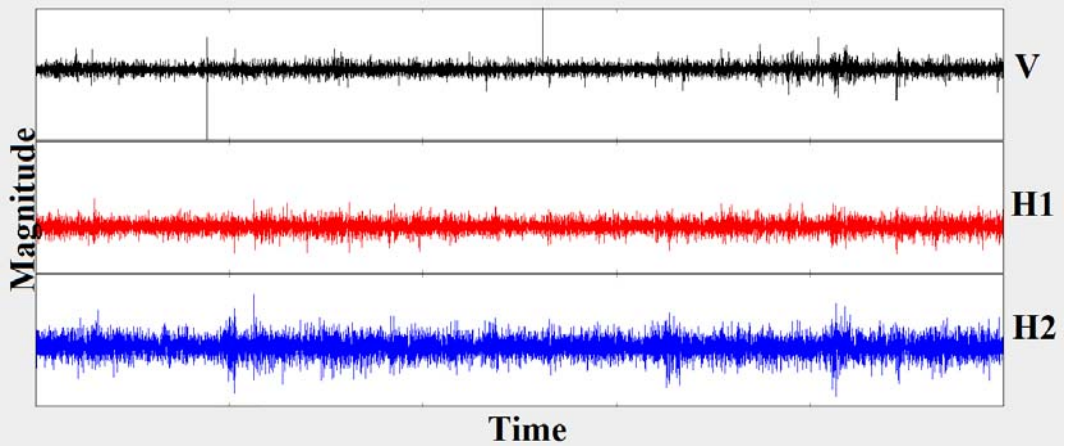

Figure B.6 Time record from the single-station three-component sensor at Site 6.

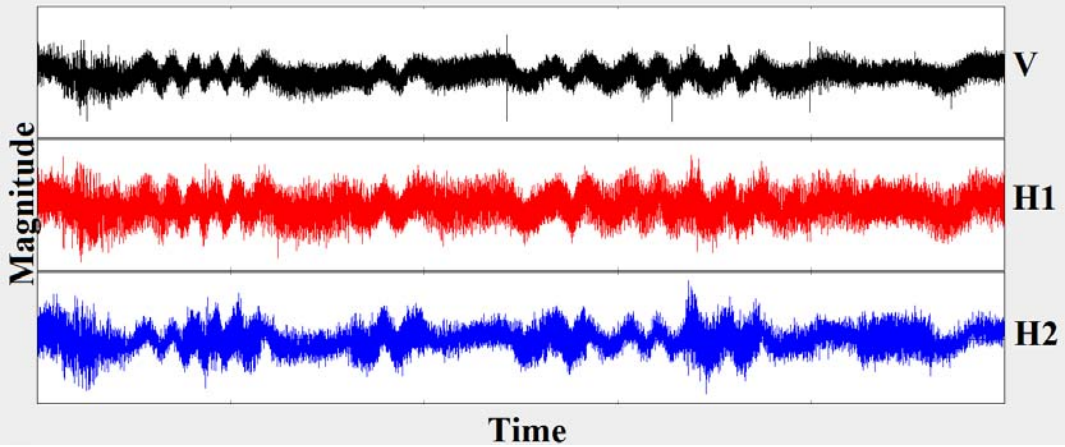

Figure B.7 Time record from the single-station three-component sensor at Site 7.

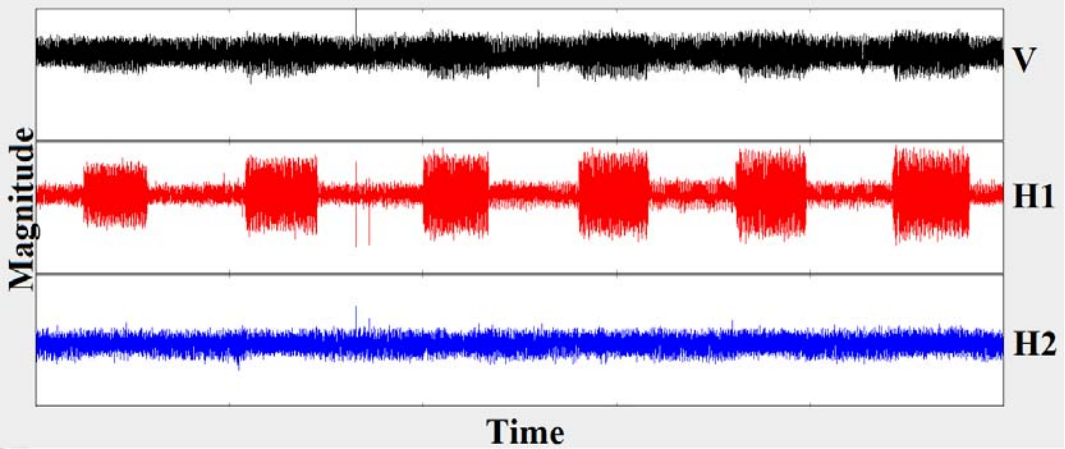

Figure B.8 Time record from the single-station three-component sensor at Site 8.

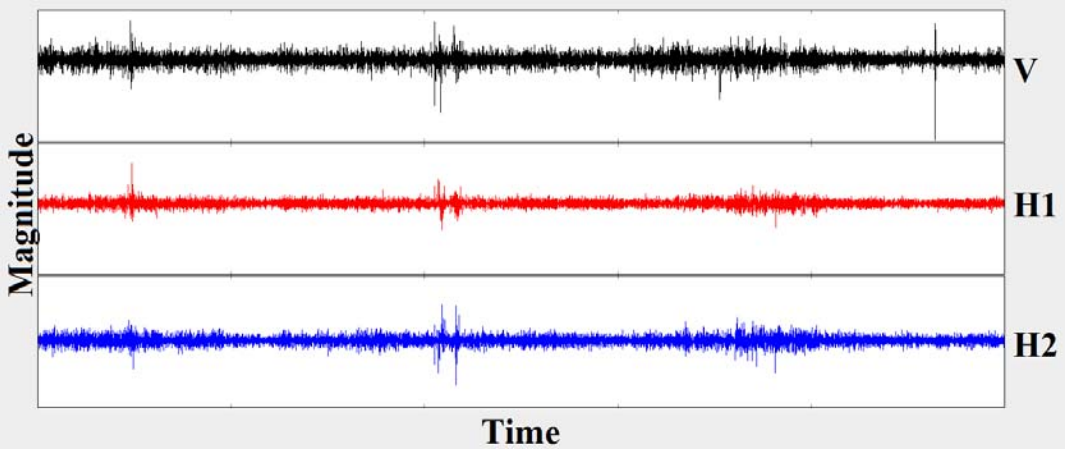

Figure B.9 Time record from the single-station three-component sensor at Site 9.

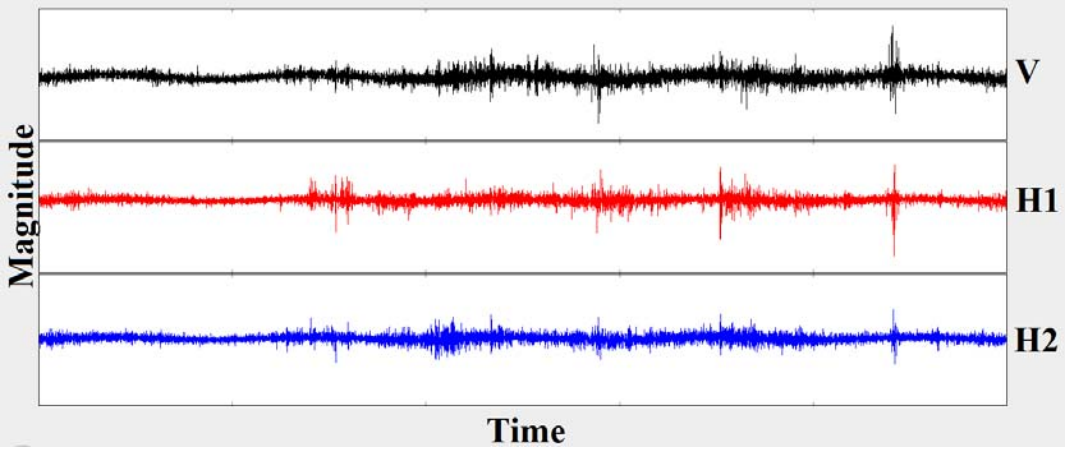

Figure B.10 Time record from the single-station three-component sensor at Site 10.

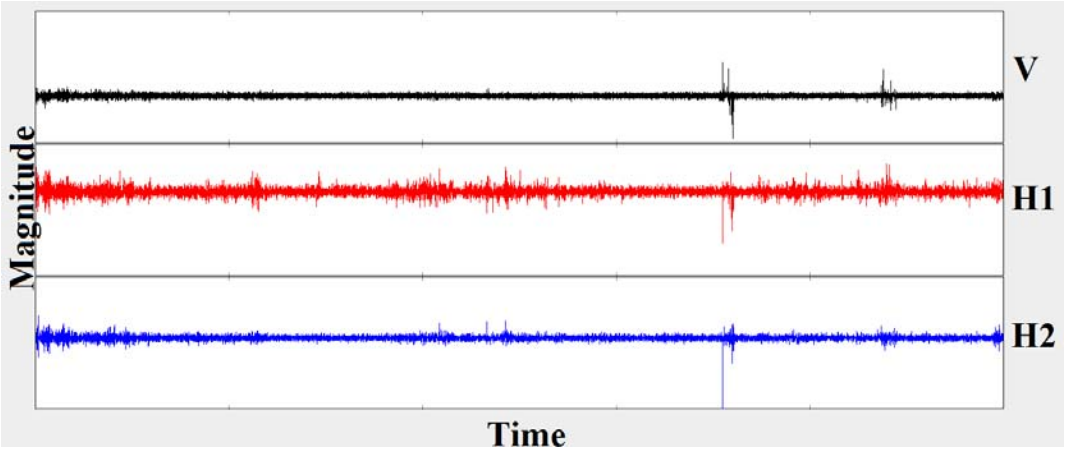

Figure B.11 Time record from the single-station three-component sensor at Site 11.

C. APPENDIX

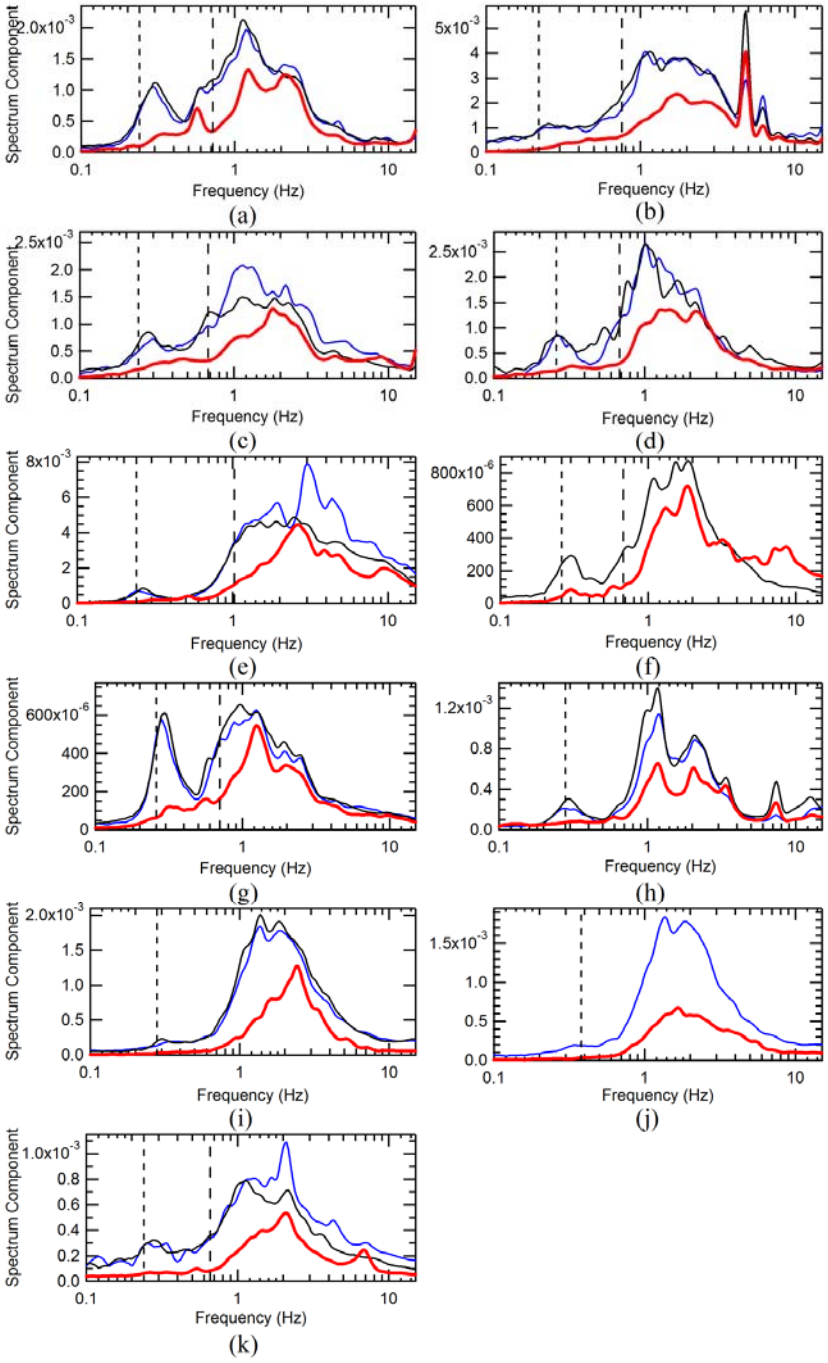

Figure C.1 Three component spectrum for Sites 1-11 corresponding to (a)-(k), respectively. Vertical spectrum is represented by the thicker of the lines and HVSR frequency peaks are shown as dashed vertical lines.

D. APPENDIX

Table D.1 Table displaying the number of windows for each parameter that was used in the experimental processing of data. (Blocks having less than the minimum number of recommended windows are highlighted.)

Site	Number of Windows (n)																				
	Window Length				Min STA/LTA			Max STA/LTA				Filter - Low Pass						Filter - High Pass			
	50 sec	75 sec	100 sec	200 sec	0.25	0.5	0.75	1.25	1.5	2.0	2.5	15	20	25	30	35	0.25	0.5	1.0	5.0
1	41	25	18	7	41	41	40	26	41	46	46	29	38	40	42	43	41	42	43	41
2	28	16	10	1	30	28	24	11	28	35	39	29	28	29	29	29	28	29	29	16
3	18	9	3	1	19	18	15	2	18	41	42	6	12	18	21	26	18	18	18	18
4	15	8	2	-	16	15	2	-	15	38	40	16	20	24	27	26	15	14	9	2
5	23	12	6	-	23	23	2	1	23	44	46	23	23	23	23	23	23	23	24	26
6	25	12	6	-	25	25	-	-	25	45	46	28	27	25	26	25	25	25	27	10
7	28	17	12	6	28	28	27	26	28	29	29	15	20	24	25	24	28	28	29	29
8	17	9	4	-	18	17	12	15	17	19	19	20	13	12	10	11	17	17	17	17
9	30	18	12	3	31	30	20	12	30	33	33	18	19	21	22	23	30	29	29	27
10	11	3	2	-	12	11	-	-	11	22	26	9	9	11	10	10	10	10	11	12
11	18	9	5	1	19	18	12	4	18	33	34	2	2	2	3	3	18	18	18	23

REFERENCES

Andrus, R. D., and Stokoe, K. H. (2000). "Liquefaction Resistance of Soils from Shear-Wave Velocity." *Journal of Geotechnical and Geoenvironmental Engineering*, 126(11), 1015-1025.

Arai, H., and Tokimatsu, K. "Evaluation of Local Site Effects Based on Microtremor H/V Spectra." *The Effects of Surface Geology on Seismic Motion*, Balkema, Rotterdam, 1–3.

Arai, H., and Tokimatsu, K. (2004). "S-Wave Velocity Profiling by Inversion of Microtremor H/V Spectrum." *Bulletin of the Seismological Society of America*, 94(1), 53-63.

Arai, H., and Tokimatsu, K. (2005). "S-Wave Velocity Profiling by Joint Inversion of Microtremor Dispersion Curve and Horizontal-to-Vertical (H/V) Spectrum." *Bulletin of the Seismological Society of America*, 95(5), 1766-1778.

Asten, M. (2003). "Comment on "Microtremor observations of deep sediment resonance in metropolitan Memphis, Tennessee" by Paul Bodin, Kevin Smith, Steve Horton and Howard Hwang." *Engineering Geology*, 72(3-4), 343-349.

Bailey, J. P. (2008). "Development of Shear Wave Velocity Profiles in the Deep Sediments of the Mississippi Embayment using Surface Wave and Spectral Ratio Methods," M.S. Thesis, University of Missouri, Columbia, MO.

Bodin, P., Smith, K., Horton, S., and Hwang, H. (2001). "Microtremor observations of deep sediment resonance in metropolitan Memphis, Tennessee." *Engineering Geology*, 62(1-3), 159-168.

Bonnefoy-Claudet, S., Cornou, C., Bard, P.-Y., Cotton, F., Moczo, P., Kristek, J., and Faeh, D. (2006a). "H/V Ratio: A Tool for Site Effects Evaluation. Results from 1-D Noise Simulations." *Geophysical Journal International*, 167, 827-837.

Bonnefoy-Claudet, S., Cotton, F., and Bard, P.-Y. (2006b). "The Nature of Noise Wavefield and its Applications for Site Effects Studies: A Literature Review." *Earth-Science Reviews*, 79(3-4), 205-227.

Bonnefoy-Claudet, S., Kohler, A., Cornou, C., Wathelet, M., and Bard, P.-Y. (2008). "Effects of Love Waves on Microtremor H/V Ratio." *Bulletin of the Seismological Society of America*, 98(1), 288-300.

Cara, F., Cultrera, G., Azzara, R. M., De Rubeis, V., Di Giulio, G., Giammarinaro, M. S., Tosi, P., Vallone, P., and Rovelli, A. (2007). "Microtremor Measurements in the City of Palermo, Italy: Analysis of the Correlation with Local Geology and Damage." *Bulletin of the Seismological Society of America*.

Chen, K.-C., Chiu, J.-M., and Yang, Y.-T. (1996). "Shear-Wave Velocity of the Sedimentary Basin in the Upper Mississippi Embayment using S-to-P Converted Waves." *Bulletin of the Seismological Society of America*, 86(3), 848-856.

Chen, Q., Liu, L., Wang, W., and Rohrbach, E. (2009). "Site Effects on Earthquake Ground Motion based on Microtremor Measurements for Metropolitan Beijing." *Chinese Science Bulletin*, 54(2), 280-287.

Cramer, C. H. (2006). "Quantifying the Uncertainty in Site Amplification Modeling and Its Effects on Site-Specific Seismic-Hazard Estimation in the Upper Mississippi Embayment and Adjacent Areas." *Bulletin of the Seismological Society of America*, 96(6), 2008-2020.

Crone, A. J., and Russ, D. P. (1979). "Preliminary Report on an Exploratory Drill Hole: New Madrid Test Well 1-X in Southeast Missouri." *79-1216*, US Geological Survey.

Cushing, E. M., Boswell, E. H., and Hosman, R. L. (1964). "General Geology of the Mississippi Embayment." *Professional Paper 448-B*, U.S. Geological Survey.

Delgado, J., López Casado, C., Estévez, A., Giner, J., Cuenca, A., and Molina, S. (2000). "Mapping Soft Soils in the Segura River Valley (SE Spain): A Case Study of Microtremors as an Exploration Tool." *Journal of Applied Geophysics*, 45(1), 19-32.

Dorman, J., and Smalley, R. (1994). "Low-Frequency Seismic Surface Waves in the Upper Mississippi Embayment." *Seismological Research Letters*, 65(2), 137-148.

EduPro Civil Systems, I. (2006). "EduShake." Redmond, Washington.

Fäh, D., Kind, F., and Giardini, D. (2001). "A theoretical investigation of average H/V ratios." *Geophysical Journal International*, 145(2), 535-549.

Fernandez, J. A., and Rix, G. J. "Basin Effects in the Upper Mississippi Embayment." *Geotechnical Earthquake and Engineering and Soil Dynamics IV Congress 2008*, Sacramento, California, 10-10.

García-Jerez, A., Navarro, M., Alcalá, F. J., Luzón, F., Pérez-Ruiz, J. A., Enomoto, T., Vidal, F., and Ocaña, E. (2007). "Shallow Velocity Structure using Joint Inversion of Array and H/V Spectral Ratio of Ambient Noise: The Case of Mula Town (SE of Spain)." *Soil Dynamics and Earthquake Engineering*, 27(10), 907-919.

Ge, J., Pujol, J., Pezeshk, S., and Stovall, S. (2007). "Determination of Shallow Shear-Wave Velocity at Mississippi Embayment Sites Using Vertical Seismic Profiling Data." *Bulletin of the Seismological Society of America*, 97(2), 614-623.

Gomberg, J., Waldron, B., Schweig, E., Hwang, H., Webbers, A., VanArsdale, R., Tucker, K., Williams, R., Street, R., Mayne, P., Stephenson, W., Odum, J., Cramer, C., Updike, R., Hutson, S., and Bradley, M. (2003). "Lithology and Shear-Wave Velocity in Memphis, Tennessee." *Bulletin of the Seismological Society of America*, 93(3), 986-997.

Gosar, A. (2007). "Microtremor HVSR Study for Assessing Site Effects in the Bovec Basin (NW Slovenia) Related to 1998 Mw5.6 and 2004 Mw5.2 Earthquakes." *Engineering Geology*, 91(2-4), 178-193.

Guéguen, P., Chatelain, J. L., Guillier, B., and Yepes, H. (2000). "An indication of the soil topmost layer response in Quito (Ecuador) using noise H/V spectral ratio." *Soil Dynamics and Earthquake Engineering*, 19(2), 127-133.

Guillier, B., Cornou, C., Kristek, J., Moczo, P., Bonnefoy-Claudet, S., Bard, P., and Fäh, D. "Simulation of Seismic Ambient Vibrations: Does the H/V Provide Quantitative Information on 2D–3D Structure?" *Third International Symposium on the Effects of Surface Geology on Seismic Motion*, Grenoble, France.

Hashash, Y., Park, D., and Tsai, C. (2005). "DEEPSOIL." Board of Trustees of University of Illinois at Urbana-Champaign, Urbana-Champaign, IL.
Hashash, Y. M. A. (1999). University of Illinois, Urbana-Champaign, IL, personal communication to Romero and Rix (2005).
Hashash, Y. M. A., and Park, D. (2001). "Non-linear one-dimensional seismic ground motion propagation in the Mississippi embayment." *Engineering Geology*, 62(1-3), 185-206.
Herak, M. (2008). "ModelHVSR--A Matlab® Tool to Model Horizontal-to-Vertical Spectral Ratio of Ambient Noise." *Computers & Geosciences*, 34(11), 1514-1526.
Herrmann, R. B., and Akinci, A. (1999). "Mid-America Ground Motion Models." http://www.eas.slu.edu/People/RBHerrmann/MAEC/maecgnd.html, Department of Earth and Atmospheric Sciences, Saint Louis University, St. Louis, MO.
Hisada, Y. (1994). "An Efficient Method for Computing Green's Functions for a Layered Half-Space with Sources and Receivers at Close Depths." *Bulletin of the Seismological Society of America*, 84(5), 1456-1472.
Hwang, H. H. M. (2000). "Memphis Soil Profiles." http://www.ceri.memphis.edu/~hwang/memphis_soil_profiles/profile1.html.
Ibs-von Seht, M., and Wohlenberg, J. (1999). "Microtremor measurements used to map thickness of soft sediments." *Bulletin of the Seismological Society of America*, 89(1), 250-259.
Johnston, A. C., and Nava, S. J. (1985). "Recurrence Rates and Probability Estimates for the New Madrid Seismic Zone." *J. Geophys. Res.*, 90, 6737-6753.
Julia, J., Herrmann, R. B., Ammon, C. J., and Akinci, A. (2004). "Evaluation of Deep Sediment Velocity Structure in the New Madrid Seismic Zone." *Bulletin of the Seismological Society of America*, 94(1), 334-340.
Kanai, K., and Tanaka, T. (1961). "On microtremors. VIII." *Bull. Earthquake Res. Inst*, 39, 97–114.
Kausel, E., and Assimaki, D. (2001). "Simulation of Dynamic, Inelastic Soil Behavior by Means of Frequency-Dependent Shear Modulus and Damping." *Journal of Engineering Mechanics*, 34-47.
Kerh, T., and Chu, D. (2002). "Neural networks approach and microtremor measurements in estimating peak ground acceleration due to strong motion." *Advances in Engineering Software*, 33(11-12), 733-742.
Konno, K., and Ohmachi, T. (1998). "Ground-motion characteristics estimated from spectral ratio between horizontal and vertical components of microtremor." *Bulletin of the Seismological Society of America*, 88(1), 228-241.
Kramer, S. L. (1996). *Geotechnical Earthquake Engineering*, Prentice Hall, Upper Saddle River, NJ.
Kudo, K. (1995). "Practical Estimates of Site Response: State-of-Art Report " 5th Int. Conf. on Seismic Zonation, Nice, France.
Lachet, C., and Bard, P. Y. (1994). "Numerical and Theoretical Investigations on the Possibilities and Limitations of Nakamura's Technique." *Journal of Physics of the Earth*, 42(4), 377-397.

Lai, C. G., and Rix, G. J. (1998). "Simultaneous Inversion of Rayleigh Phase Velocity and Attenuation for Near-Surface Site Characterization." *GIT-CEE/GEO-98-2*, School of Civil & Environmental Engineering, Georgia Institute of Technology, Atlanta, Georgia.

Lermo, J., and Chavez-Garcia, F. J. (1994). "Are microtremors useful in site response evaluation?" *Bulletin of the Seismological Society of America*, 84(5), 1350-1364.

Li, J. (2008). "Study of Surface Wave Methods for Deep Shear Wave Velocity Profiling Applied in the Upper Mississippi Embayment," Ph.D. Thesis, University of Missouri, Columbia, MO.

Liu, H. P., Yiguang, H., Dorman, J., Chang, T. S., and Chiu, J. M. (1997). "Upper Mississippi Embayment Shallow Seismic Velocities Measured In Situ." *Engineering Geology*, 46, 313-330.

Lunedei, E., and Albarello, D. (2009). "On the Seismic Noise Wavefield in a Weakly Dissipative Layered Earth." *Geophysical Journal International*, 177(3), 1001-1014.

Luzietti, E. A., Kanter, L. R., Schweig, E. S., Shedlock, K. M., and VanArsdale, R. B. (1992). "Shallow Deformation along the Crittenden County Fault Zone near the Southeastern Boundary of the Reelfoot Rift, Northeast Arkansas." *Seismological Research Letters*, 63, 263-295.

Mueller, C. (2000). US Geological Survey, Denver, CO, personal communication to Romero and Rix (2005).

Nakamura, Y. (1989). "A Method for Dynamic Characteristic Estimation of Subsurface using Microtremor on the Ground Surface." *QR Railway Technical Research Institute*, 30(1), 25-33.

Nakamura, Y. "Clear identification of fundamental idea of Nakamura's technique and its applications." *12th World Conference on Earthquake Engineering*.

Nogoshi, M., and Igarashi, T. (1971). "On the amplitude characteristics of microtremor (part 2)." *Jour. Seism. Soc. Japan*, 24, 26-40.

Panou, A. A., Theodulidis, N., Hatzidimitriou, P., Stylianidis, K., and Papazachos, C. B. (2005). "Ambient noise horizontal-to-vertical spectral ratio in site effects estimation and correlation with seismic damage distribution in urban environment: the case of the city of Thessaloniki (Northern Greece)." *Soil Dynamics and Earthquake Engineering*, 25(4), 261-274.

Park, D., and Hashash, Y. M. A. (2004). "Soil Damping Formulation in Nonlinear Time Domain Site Response Analysis." *Journal of Earthquake Engineering*, 8(2), 249-274.

Parolai, S., Bormann, P., and Milkereit, C. (2002). "New Relationships between Vs, Thickness of Sediments, and Resonance Frequency Calculated by the H/V Ratio of Seismic Noise for the Cologne Area (Germany)." *Bulletin of the Seismological Society of America*, 92(6), 2521-2527.

Parolai, S., Richwalski, S., Milkereit, C., and Bormann, P. (2004). "Assessment of the Stability of H/V Spectral Ratios from Ambient Noise and Comparison with Earthquake Data in the Cologne Area (Germany)." *Tectonophysics*, 390(1-4), 57-73.

Powell, C. A., and Withers, M. (2009). "The Effects of Mississippi Embayment Sediments on Local Earthquake Tomography." *Seismological Research Letters*, 80(1), 149-158.
Purser, J. L., and Van Arsdale, R. B. (1998). "Structure of the Lake County Uplift: New Madrid Seismic Zone." *Bulletin of the Seismological Society of America*, 88(5), 1204-1211.
Romero, S. M., and Rix, G. J. (2001). "Regional Variations in Near Surface Shear Wave Velocity in the Greater Memphis Area." *Engineering Geology*, 62(1-3), 137-158.
Romero, S. M., and Rix, G. J. (2005). "Ground Motion Amplification of Soils in the Upper Mississippi Embayment." *GIT-CEE/GEO-01-1*, Mid-America Earthquake Center, University of Illinois at Urbana-Champaign, CD Release 05-01, March.
Schnabel, P. B., Lysmer, J. L., and Seed, H. B. (1972). "SHAKE: A Computer Program for Earthquake Response Analysis of Horizontally Layered Sites." *EERC72-12*, Earthquake Engineering Research Center, Berkeley, CA.
Sen, M. K., and Stoffa, P. L. (1995). *Global Optimization Methods in Geophysical Inversion*, Elsevier New York.
SESAME. (2004). "Guidelines for the Implementation of the H/V Spectral Ratio Technique on Ambient Vibrations: Measurements, Processing, and Interpretation." *WP12 - Deliverable D23.12*, European Commission – Research General Directorate.
Souriau, A., Roulle, A., and Ponsolles, C. (2007). "Site Effects in the City of Lourdes, France, from H/V Measurements: Implications for Seismic-Risk Evaluation." *Bulletin of the Seismological Society of America*, 97(6), 2118-2136.
Steinwachs, M. (1974). "Systematische Untersuchungen der kurzperiodischen seismischen Bodenunruhe in der Bundesrepublik Deutschland." *Geologisches Jahrbuch E3*.
TC4-ISSMGE. (1999). *Manual for Zonation on Seismic Geotechnical Hazard*, Revised edition,Technical Committee for Earthquake Geotechnical Engineering (TC4) of the International Society of Soil Mechanics and Geotechnical Engineering (ISSMGE) 209.
Tokeshi, K., Karkee, M., and Cuadra, C. (2008). "Estimation of Vs profile using its natural frequency and Rayleigh-wave dispersion characteristics." *Advances in Geosciences*, 14, 75-77.
Tokimatsu, K., Tamura, S., and Kojima, H. (1992). "Effects of Multiple Modes on Rayleigh Wave Dispersion Characteristics." *Journal of Geotechnical Engineering*, 118(10), 1529-1543.
Van Arsdale, R. B., and TenBrink, R. K. (2000). "Late Cretaceous and Cenozoic Geology of the New Madrid Seismic Zone." *Bulletin of the Seismological Society of America*, 90(2), 345-356.
Walling, M. Y., Mohanty, W. K., Nath, S. K., Mitra, S., and John, A. (2009). "Microtremor Survey in Talchir, India to Ascertain its Basin Characteristics in Terms of Predominant Frequency by Nakamura's Ratio Technique." *Engineering Geology*, 106(3-4), 123-132.
Wathelet, M. (2006). "Geopsy Manual." Sesarray, SESAME European research project.

Wen, Y. K. (1999). University of Illinois, Urbana-Champaign, IL, personal communication to Romero and Rix (2005).
Williams, R. A., Stephenson, W. J., and Odum, J. K. (2003). "Comparison of P- and S-wave Velocity Profiles Obtained from Surface Seismic Refraction/Reflection and Downhole Data." *Tectonophysics*, 368, 71-88.
Woolery, E. W., and Street, R. (2002). "Quaternary Fault Reactivation in the Fluorspar Area Fault Complex of Western Kentucky: Evidence from Shallow SH-wave Reflection Profiles." *Seismological Research Letters*, 73(5), 628-639.